PCA R&D SN2969

The Thermal and Radiative Characteristics of Concrete Pavements in Mitigating Urban Heat Island Effects

by Kamil E. Kaloush, Joby D. Carlson,
Jay S. Golden, and Patrick E. Phelan

The Thermal and Radiative Characteristics of
Concrete Pavements in Mitigating Urban Heat Island Effects

Final Report

Kamil E. Kaloush
Associate Professor
Department of Civil and Environmental Engineering

Joby D. Carlson
Assistant Research Technologist
Global Institute of Sustainability

Jay S. Golden
Assistant Professor
School of Sustainability

Patrick E. Phelan
Professor
Department of Mechanical and Aerospace Engineering

The Thermal and Radiative Characteristics of Concrete Pavements in Mitigating Urban Heat Island Effects

Final Report

March 2008

Submitted to

American Concrete Pavement Association
Market Development Group
1130 Connecticut Ave, NW Suite 1250
Washington, DC 20036

Submitted by

**National Center of Excellence on
Sustainable Material and Renewable Technology (SMART) Innovations**
Global Institute of Sustainability / Ira A. Fulton School of Engineering

Arizona State University
Tempe, Arizona, USA 85287-3211
Phone: (480) 727-9124, Fax: (480) 727-9123
Email: kaloush@asu.ed

KEYWORDS

Pavement Temperatures, Thermal Properties, Urban Heat Island Mitigation

ABSTRACT

The main objective of this research study was to provide understanding, supporting documentation, and tools on how pavement designs and materials selection contribute to surface and subsurface temperature fluctuations. This objective was achieved through two focus areas that outlined the scope of work of this research: thermal properties and reflectance evaluation, and heat absorption and transfer modeling.

In the first focus area, the reflectance "albedo" characteristics of various concrete pavement surfaces / mix types were identified. Surface and in-depth pavement temperatures of several field sections were collected to help validate modeling efforts. Perhaps one of the most notable accomplishments in this focus area was the development of a simplified laboratory test procedure to measure the thermal conductivity of paving materials using cylindrical specimens. Laboratory tests were also conducted to measure key thermal properties of the different paving materials. These properties were used as input parameters for the pavement heat absorption and transfer model.

In the second focus area, a pavement heat absorption and transfer model was developed and validated. This fundamental model accounts for the surface rates of solar radiation absorption and heat transmission of various pavements designs. It can be used for comparative evaluation for the different pavements designs in mitigating the Urban Heat Island Effect.

The outcome of the two focus areas outlined above are envisioned to play a key role aiding future decision makers and designers when choosing appropriate pavement materials for their particular application. It will provide further awareness of urban heat island, and drives further municipal ordinances and building codes that incorporate environmentally appropriate materials into development and rehabilitation projects.

REFERENCE

Kaloush, Kamil E.; Carlson, Joby D.; Golden, Jay S., and Phelan, Patrick E., *The Thermal and Radiative Characteristics of Concrete Pavements in Mitigating Urban Heat Island Effects*,**SN2969, Portland Cement Association, Skokie, Illinois, USA, 2008, 136 pages.**

TABLE OF CONTENTS

FIGURES

TABLES

ACKNOWLEDGMENTS

NOTATIONS

The following symbols are used in this paper

c	=	specific heat capacity
CFL	=	Courant-Friedrichs-Lewy
$\dfrac{dT}{dx}$	=	temperature gradient within pavement
$\dfrac{\partial T}{\partial t}$	=	rate of change of temperature
$\dfrac{\partial T_{max,\ min}}{\partial (property\ )}$	=	change in temp. (max/min) with respect to thermophysical prop.
h_{rad}	=	radiative heat transfer coefficient
h_∞	=	convective heat transfer coefficient
k	=	thermal conductivity
k_∞	=	thermal conductivity of air
l	=	thickness of pavement layer
(p) or (p+1)	=	time-step
Pr_∞	=	Prandtl Number
q''_{cond}	=	conduction heat transfer
q''_{conv}	=	convection heat transfer
q''_{int}	=	heat flux through interface
q''_{rad}	=	infrared radiation heat transfer
q''_s	=	solar radiation heat transfer
R_c	=	contact resistance
Δt	=	time-step spacing
T_{b1}	=	first temperature node in lower layer
T_{dew}	=	dew-point temperature
$T_{layer\ i,int}$	=	interfacial temperature at layer i
T_n	=	last temperature node in upper layer
$T_{ref(max,min)}$	=	reference temperature, $T_{ref(max,min)}$,
T_s	=	pavement surface temperature
T_{sky}	=	sky temperature
T_∞	=	atmospheric dry-bulb temperature
U_∞	=	wind velocity
x	=	ground depth
Δx	=	nodal spacing within pavement

Greek symbols

ã	=	albedo
α	=	thermal diffusivity
δ	=	penetration depth
ε	=	emissivity

ν_∞	=	kinematic viscosity of air
ρ	=	density
ρc	=	volumetric heat capacity
σ	=	Stefan-Boltzmann constant (5.68×10^{-8} W m^{-2} $^{\circ}$C^{-4})
σ_s	=	standard deviation
ψ_{sky}	=	sky view factor

Chapter 1: Introduction

Rapid urbanization, which is transitioning native vegetation to man-made engineered surfaces, is taking place on a global scale. In 1950 approximately 30% of the world population lived in urban areas and, by 2030 that number is projected to be at 60%. As an example, by 2004, Phoenix had over 80% of Arizona residents residing in its urban area. Phoenix exploded in growth to become the nation's 5th largest city in population and larger in geographical terms than the City of Los Angeles. The added volume of paved surfaces and engineered materials during this time of growth has contributed to Phoenix experiencing one of the worlds strongest Urban Heat Island effects (UHI) at a 0.86ºF/decade-warming rate during the last century (Golden 2004).

Paved surfaces (roads, highways, and parking lots) comprise 29% to 45% of the urban fabric. Because the demand and resulting climatic impacts of pavements will continue to increase, a combined research initiative comprising laboratory, field experimentation, and heat transfer modeling, need to be undertaken. The results of such research will help to better understand how pavement designs and materials selection contribute to surface and subsurface temperature fluctuations.

Task 15 of the 2005 ACPA Concrete Pavement Research and Development program addresses the need to quantify the reflectance, absorption and emittance – of different concrete pavement surface materials, including the effects of color and texture over time, as a means of mitigating UHI. As urban centers continue to expand and/or are being rehabilitated, there is a growing concern over local temperature increases due to solar absorption and associated heat emission. The problem is focused on the extensive network of dark colored horizontal structures (roof and pavement) in the built environment. These increases are exacerbated by the loss of vegetation and trees in and around our cities due to urban and suburban growth patterns and practices.

In an effort to mitigate the effect of UHI, the US Environmental Protection Agency and the US Green Building Council through its Leadership in Environmental and Energy Design, LEED™ Rating Systems are working to develop a variety of techniques and processes through which temperature reductions can be achieved and the overall impact of heat absorption and transfer can be reduced.

The EPA calls for three techniques to help mitigate the extreme temperature increases experienced in and around cities:
1.) Design and material selection for roof structures and surfaces
2.) Design and material selection for pavement surfaces
3.) The incorporation of more trees, planting and landscaping elements in our communities.

To date, research has focused on roof structures with innovation resulting in a variety of new designs and roofing materials and improved impact through landscaping strategies. Little however has been done to consider or evaluate the impact and opportunities of design, material selection and innovation related to pavement surfaces.

Objective and Scope

The main objective of this research study was to provide understanding, supporting documentation, and tools on how pavement designs and materials selection contribute to surface and subsurface temperature fluctuations. This objective was achieved through two focus areas

that outline the scope of work of this research: thermal properties and reflectance evaluation, and heat absorption and transfer modeling. These are outlined as follows:

Part I – Measuring Reflectance, Thermal Properties, and Data Collection

A. Determine constituent materials that help deliver resultant surfaces and demonstrate the highest reflectance characteristics. Establish a list of these materials/combinations related to mix designs to comply with current LEED™ criteria for reflectance.

B. Determine the reflectance "albedo" characteristics of various concrete pavement surfaces / mix types.

C. Collect surface and in-depth pavement temperatures of several field sections to help validate modeling efforts in Part II of the study.

D. Conduct laboratory tests to measure the thermal properties of the different paving materials / design. This effort is also needed to provide input parameters for the pavement model(s) developed in Part II of the study.

Part II – Modeling of Pavement Heat Absorption and Transfer

E. Develop fundamental model(s) that can account for the surface rates of solar radiation absorption and heat transmission (re-radiation) of various pavements designs; and to also allow for comparative evaluation and what-if-scenarios for the different pavements designs and types.

F. Determine the levels of heat gain and emittance on ambient air temperatures surrounding each test surface from a comparative point-of-view.

Part III – Evaluating Impact on Energy and Safety
G. Evaluate and estimate the savings in energy use related to reduced lighting standards for using high albedo versus low albedo paving materials, while maintaining the optimum lighting levels for road, intersection, parking lots with regard to pedestrian safety and security.
H. Evaluate and develop recommendations regarding the potential impact related to improved pedestrian and public safety as a result of the high vs. low albedo pavement surfaces.

Significance of the Project

This research project serves to increase the body of knowledge centered on the economic, environmental, and social implications and benefits of concrete pavements. The outcome of the tasks outlined will assist future decision makers and designers when choosing appropriate pavement materials for their particular application. It will provide further awareness of urban heat island, and drives further municipal ordinances and building codes that incorporate environmentally appropriate materials into development and rehabilitation projects.

Organization of the Report

This report is divided into four chapters, including the introduction. Each chapter is based on the work conducted for this research project providing a summary of the major findings. Additional information and details for each chapter are also found in the Appendices. Chapter 2 documents various concrete pavement mix designs along with the corresponding thermal and radiative properties as determined through laboratory and field evaluations. Chapter 3 presents a one-dimensional pavement heat transfer model developed specifically for this project. The model uses material properties and field data presented in Chapter 2 to calibrate a robust model driven by real-world meteorological conditions. Chapter 4 discusses the luminance characteristics of concrete pavements and evaluates the reduction in energy use made possible with high albedo pavement materials. Chapter 5 provides a summary of the work.

Chapter 2: Pavement Reflectance and Data Collection

The radiative and thermal properties of pavement materials are direct indicators of their thermal performance in the outside environment. Environmental rating systems for buildings are beginning to specify certain minimum criteria for pavements in for UHI mitigation and storm water management. Designing concrete pavements with optimal thermal performance while meeting the required engineering and economic performance (strength, durability, safety, and cost) presents a new and interesting challenge for the paving industry. Pavement designers and material suppliers need accurate thermal property data in relation to their mix designs to gauge the thermal performance of the final product.

This chapter serves as a foundation of properties, field trials, and laboratory investigations that support future modeling and the selection of alternative pavement designs. The information is grouped into four sections. The first, *The Reflectance of Pavements,* provides alternative mix designs that increase the reflectance of concrete, a vital aspect of meeting today's environmental rating systems. Next, the section, *Correlating albedo and Maximum Surface Temperature*, presents the result of an experimental field study that provides evidence of the direct correlation between surface temperatures and the radiative properties of pavement. This is followed by *Surface and In-depth Pavement Temperatures,* which reviews the results of a several year long studies of subsurface thermal behaviour of pavements. Lastly, *Thermophysical Properties of Paving Materials* contains a detailed review of the thermophysical properties of pavement materials including definitions, test methodologies, and experimental results for an assortment of conventional and non-conventional pavement materials.

Concrete Pavement Reflectance

Cool pavements are pavements that absorb less solar energy than conventional paving materials under identical environmental conditions. Although there is no industry standard established yet for what constitutes a cool pavement, there are several key elements that indicate a surface's potential for mitigating the Urban Heat Island. The most important of these elements is solar reflectance (see Figure 1), commonly referred to as albedo. The following sections define albedo, discuss the albedos of conventional pavements, and present alternative mix designs and surface treatments that will help designers meet the requirements of the USGBC's LEED™ Rating System for pavements.
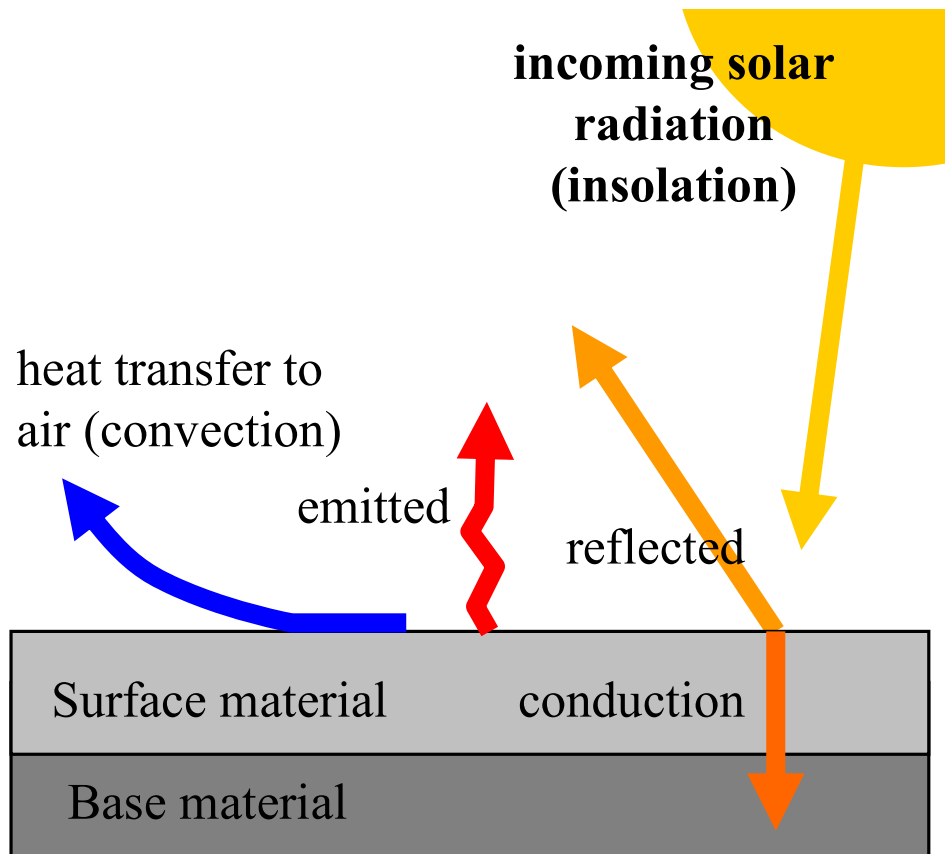
Figure 1 Energy balance at the surface of pavements. Radiation energy from sun is either reflected or absorbed. Absorbed energy is then conducted deeper, emitted as radiation, or transferred to air near the surface by convection.

Solar Reflectance (Albedo) and Thermal Emittance
Albedo is the term given to the amount of solar energy that is reflected by a surface. In opaque surfaces (transmittance =0), albedo is simply (1-α) where α is the absorptivity of the surface. The greater the albedo of a surface, the less solar energy it will absorb. Albedo is the first line of defense a surface has against incoming solar radiation. It is regarded as the most important factor in the mitigation of the urban-heat-island effect in urban centers (Rosenfeld et al. 1995). The value of albedo can range from 0 (perfect absorber) to 1 (perfect reflector). Albedo is the ratio of solar radiation that reflects off of a surface divided by the total incoming radiation. For this reason albedo, is also given as a percentage (e.g., an albedo of 0.75 indicates that 75% of the solar radiation that hits the surface is reflected).
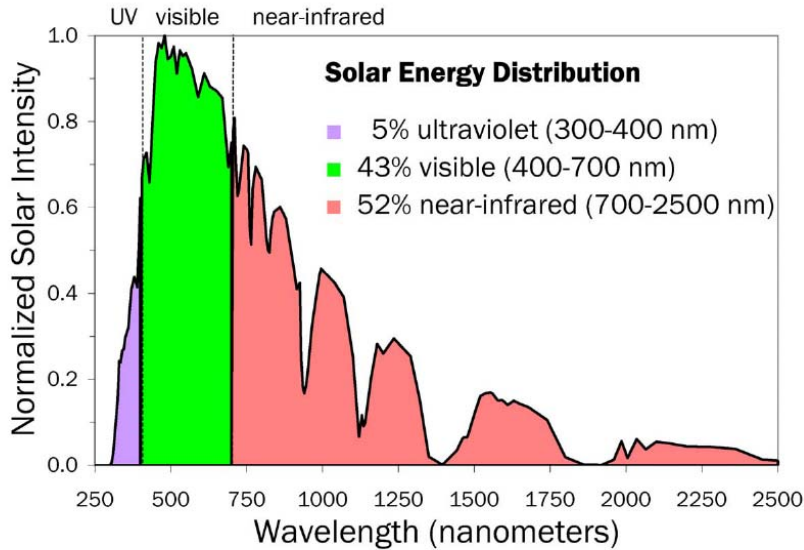
Figure 2 Solar energy intensity versus wavelength, indicating the large amount of energy in the near-infrared portion of the solar spectrum. Original figure created by H. Akbari, Lawrence Berkeley National Laboratory.

Albedo is often related to lighter shades of color (ie. sky blue vs. navy blue). Although this is true to a certain extent, a more thorough analysis is required to determine the true albedo of a given surface. Because solar energy is comprised of 5% ultraviolet, 43% visible, and 52% infrared wavelengths, a large portion of the solar energy cannot be seen (see Figure 2). Color, to the naked eye, is only the visible energy that is reflected by a surface. To accurately determine albedo, one must use a sensor that also detects light in UV, visible, and near infrared wavelengths. The American Society for Testing and Materials (ASTM) describes methods for determining solar reflectance in the following standards; ASTM E 903, ASTM E 1175, and ASTM E 1918. Figure 3 and Figure 4 show typical albedo ranges for common urban surfaces.

A portion of the thermal energy contained within a pavement is constantly being emitted as radiation back into the atmosphere. The property that indicates a surface's ability to emit radiation is its thermal emittance, which can range from 0 (non-emitter) to 1 (perfect emitter).

Most natural and construction materials have relatively high emittance values. The absorptance and emittance of a surface are independent of each other as illustrated in Figure 5.
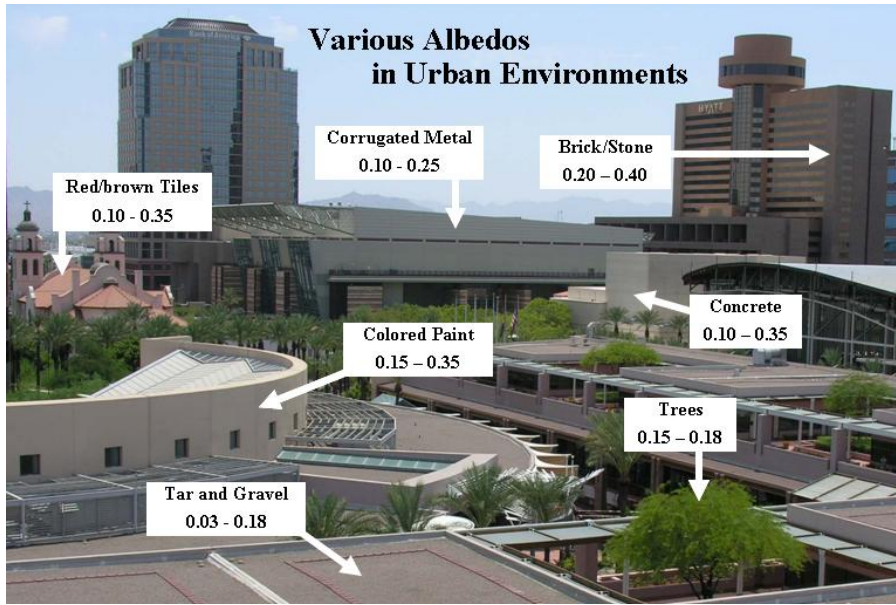
Figure 3 A typical urban area with roof and wall albedo ranges indicated on the different surfaces. Source for albedo ranges: US EPA 1992
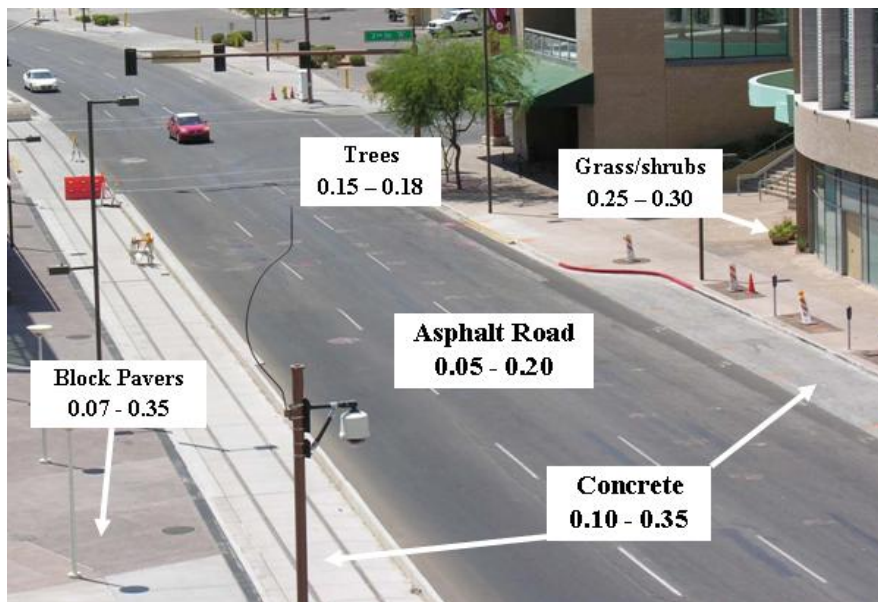
Figure 4 A typical urban area showing various ground-level-material albedo ranges. Source for albedo ranges: US EPA 1992
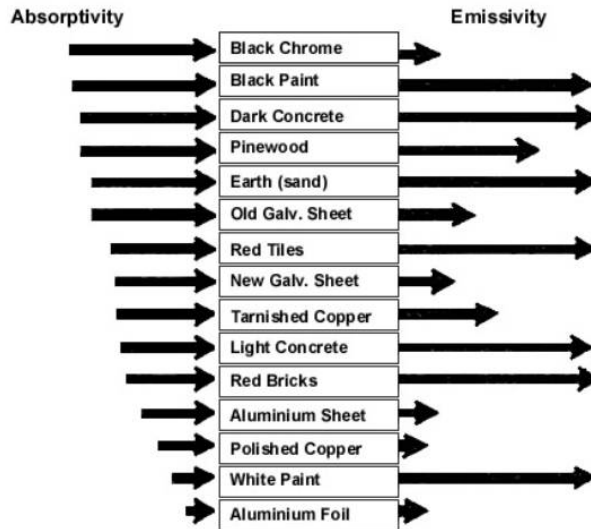
Figure 5 A visual representation of the magnitudes of absorptivity and emissivity for common building materials. Source: Lawrence Berkeley National Laboratory, Urban Heat Island Group.

The thermal emittance of a surface greatly depends on the surface material and its finish. For instance, a polished copper surface will have a very low emittance level close to 0.06, while rough surfaces such as concrete and asphalt have an emittance level above 0.90.

The following section discusses the typical albedo ranges of conventional pavements with particular focus on commercially available pavements with high albedo and emittance characteristics.

Albedo and the LEED™ Rating System

The US Green Building Council (USGBC) offers the LEED™ Rating System for evaluating the environmental, or 'green' aspects of a building's design, construction practices, and operation. LEED™ stands for Leadership in Energy and Environmental Design. LEED™ offers rating systems for a wide range of projects ranging from new construction, to building renovations, health care facilities, homes, and more recently entire neighborhoods. Each project is evaluated based on an extensive list of criteria. By meeting criteria the project can gain points towards a certification. There are four levels of certification; Certified (26-32 points), Silver (33-38 points), Gold (39-51 points), and Platinum (52+ points), all requiring a certain number of total points. The criteria are grouped into five major categories that total 64 points;

Sustainable Sites (14 points)
Water Efficiency (5 points)
Energy and Atmosphere (17 points)
Materials and Resources (13 points)
Indoor Environmental Quality (15 points)

Within the Sustainable Sites category, the *Credit 7: Landscape and Exterior Design to Reduce Heat Islands*, is divided into Non-Roof (7.1) and Roof (7.2) criterion, each worth 1 point. One of the four accepted strategies for meeting this criteria is to use 'high albedo' (>0.30) for a minimum of 30% of the site's non-roof impervious surfaces. This literally means that 30% of all

paved surfaces on the property (sidewalks, parking areas, driveways, etc) need to be made of a high-albedo material. This single rating criteria can cause major concern among building designers because one point can make a lot of difference when the minimum requirement is 26 points for the most base Certification and 52 points for Platinum Certification where nearly ever point is needed.

Commercially Available High Albedo Pavements

Portland Cement Concrete: Particles that form a bond when mixed with water are referred to as hydraulic cements. The most common of these in the construction industry is Portland cement. Portland cement is made by mixing calcareous materials with argillaceous (clay) materials (Brantley and Brantley 1996). The raw materials of lime, silica, aluminum oxide, and iron oxide are mixed in specific proportions. The mixture is then sent to a kiln, where temperatures close to 2700^oF (1482^oC) drive a chemical process that produces hard pellets of a material referred to as clinker, which are ground into Portland cement powder. Portland cement, when mixed with fine aggregate, coarse aggregate, air, and water is the basis of Portland cement concrete (PCC). PCC is initially a plastic material, perfect for casting or molding, that solidifies by a chemical reaction (Brantley and Brantley 1996). Portland concrete provides engineers with a low cost, easy to place, strong, and durable material.

New roads made of PCC are usually at least eight inches thick and can have lifetimes of over 35 years. PCC typically has a high albedo of 0.35 to 0.40 when first constructed. Dirt residues can lower its albedo to 0.25 or less overtime. By using lighter cement, lighter aggregate, and lighter sand, PCC can attain initial albedo of 0.40 to 0.80. An example of a large commercial Parking lot made entirely of PCC can be seen in Figure 6.

Figure 6 Portland cement concrete parking lot in Tempe, Arizona. Photo courtesy of National Center of Excellence, Arizona State University.

White Cement

9

White cement is made using the same process as regular cement, but kaolin is substituted for ordinary clay. The iron oxide in clay is responsible for the gray color of cement. Albedo as high as 0.80 is possible with the use of white cement (see Figure 7).

**Figure 7 Albedos of white and grey cement with identical aggregate proportions.
Source: Levinson and Akbari, 2001**

White Topping

White topping is an industry term for a layer of conventional Portland cement concrete laid over new or existing asphalt pavement. Thin white topping is a similar term used but for a PCC layer thickness being in the range of 4 to 7 inches. The surface radiative properties are the same as those of cement, with albedo ranging from 0.25 to 0.40 (Figure 8).

Ultra-thin white topping (UTW) is a fiber reinforced cement concrete layer only 2-to-4-inches thick. It has been successfully implemented at asphalt concrete intersections that suffers from frequent distortions. UTW are also hypothesized to lower the elevated surface temperatures at these intersections. As a result of high surface temperatures and slow moving loads, asphalt pavements at intersections suffer from rutting, shoving, and cracking.

Figure 8 A thin white topping project in Phoenix: (a) grinding down the existing asphalt base, and (b) curing the final surface. Photos courtesy of National Center of Excellence, Arizona State University.

Increasing the Albedo of Concrete Pavements

If direct sun exposure is unavoidable, the next best opportunity to limit the heat gain of pavements is by reflecting it. Increasing the albedo of surface pavements has been shown to reduce the surface temperature and heat retention of pavement more than any other material property. In fact, a 10% increase in albedo of a pavement reduced the surface temperature by 7.2°F (4°C) (Pomerantz et al., 2000). A decrease in surface temperature can also greatly reduce

the temperature gradient within a pavement. This gradient causes stresses within the pavement layers that can result in cracking and greatly reduce the pavement's useful life. Solar reflectance is not customary included in pavement requirements, but perhaps it should be.

Specifying a minimum albedo for concretes is not of high priority for most pavement engineers involved with standard construction projects. It is however, becoming a priority for those who are working on projects attempting to meet LEED™ and other environmental design guides relating to Urban Heat Islands and thermal comfort. The problem facing the pavement industry is that there are no accepted specifications for how to increase the albedo of conventional pavements to meet minimum requirements.

There are essentially two types of methods for increasing the albedo of concrete pavements; those that describe Alternative Mix Designs; and those that modify the surface of conventional mix designs, referred to as Surface Treatments. This section reviews the latest research findings on both methods.

Alternative Mix Designs

Modifying the types and percentage of cement as well as the size and types of aggregates used can affect the albedo of the final surface. A study conducted at Lawrence Berkeley National Labs sought to determine which components of concrete contribute to the surface albedo (R. Levinson & Akbari, 2002). The researchers tested 32 concrete mix variations using two different types of cement, four sands, and four aggregates (Figure 9). The samples were laboratory manufactured and compared under two conditions; one unexposed and the others were set outside and exposed to the simulated weathering and soiling for 70 weeks. The base materials and their properties for the concrete mixes are shown below.

The test results showed an average albedo for mature unexposed concretes of 0.35 for grey-cement concrete, 0.54 for white-cement concrete, and 0.45 for all 32 concretes tested (Figure 10). The smoother the concrete surface the higher the average albedo. The highest albedo measured (0.77) were on the surface of 25 week old smooth, unexposed concrete made of Type I White Portland cement and plagioclase and granite rock aggregate.

11
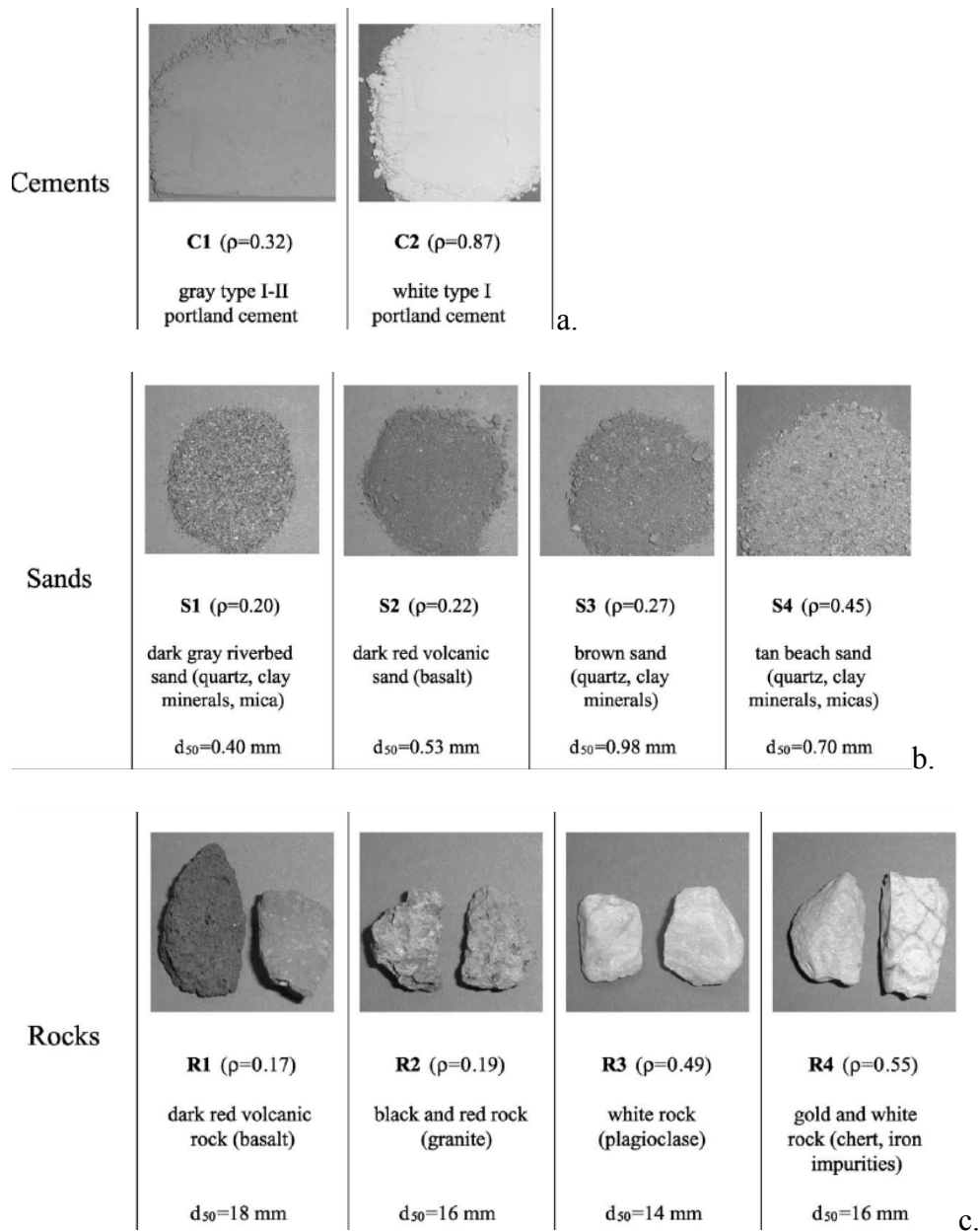
Figure 9 Properties of concrete components used in mix design study. Includes albedo ρ, mass mean diameter d50, composition, and image. There were a) two cements, b) four sands, and c) four rocks used in a total of 32 mix designs. Source: R. Levinson & H. Akbari, 2002.

Unexposed Concrete @ 25 Weeks (*FC2*)

bold = gray-cement concrete
plain = white-cement concrete
shaded = smooth concrete

component albedos

C1	gray cement	0.32
C2	white cement	0.87
S1	riverbed sand	0.20
S2	basalt sand	0.22
S3	brown sand	0.27
S4	beach sand	0.45
R1	basalt rock	0.17
R2	granite rock	0.19
R3	plagioclase rock	0.49
R4	chert rock	0.55

mean concrete albedos

	gray	white	both
smooth	0.45	0.73	0.59
all	0.35	0.54	0.45

(n=8) C1:S4:R4 (0.48)
(n=7) C2:S3:R4 (0.39) | C2:S3:R2 (0.48)
(n=6) C2:S4:R1 (0.59)
C1:S2:R3 (0.38) | C2:S2:R2 (0.47)
(n=5)
C1:S3:R2 (0.29) | C2:S1:R4 (0.38) | C1:S4:R2 (0.44) | C2:S2:R3 (0.57)
C1:S2:R1 (0.27) | C1:S1:R1 (0.34) | C1:S1:R2 (0.44) | C2:S3:R1 (0.54)
(n=3)
C1:S3:R3 (0.25) | C2:S2:R4 (0.33) | C1:S1:R4 (0.43) | C2:S1:R1 (0.54) | C2:S1:R3 (0.69)
(n=2)
C1:S3:R1 (0.24) | C1:S2:R2 (0.33) | C1:S4:R1 (0.41) | C2:S3:R3 (0.54) | C2:S1:R2 (0.68) | C2:S4:R3 (0.77)
(n=1)
C1:S3:R4 (0.19) | C1:S2:R4 (0.22) | C2:S2:R1 (0.32) | C1:S1:R3 (0.41) | C1:S4:R3 (0.52) | C2:S4:R4 (0.60) | C2:S4:R2 (0.77)

Number of Concretes (vertical axis, 0 to 10)
Albedo (horizontal axis, 0.0 to 0.8)

Figure 10 Albedos of mature, unexposed concrete. Source: R. Levinson & H. Akbari, 2002.

The results of the investigation concluded that the concrete albedo correlates mostly with the cement albedo (Figure 11). Over time the albedo of the sand in the mix plays a minor role and only if the surface is abrased does the aggregate have any effect on reflectivity. The albedo of most of the samples decreased when subjected to weathering, soiling, and abrasion. Lastly, they observed an increase in albedo as the concretes cured, however it usually stabilized within six weeks of construction. The researchers did not test the mechanistic properties of the mixes.

The grey color of Portland cement is related to the original material that was mined and used in its manufacture. Sources with higher iron deposits typically result in darker cements. Depending on where the material is obtained, cement can range from very light grey (white) to dark grey. Sources of cement that produce very light or white cement are limited, and making these cements are often more expensive and difficult to obtain than normal grey cement. It is therefore very useful to find methods of removing iron content or finding cement additives or replacements that result in higher albedo. The challenge is to find materials that are readily available nationwide, inexpensive, maintain strength requirements, and that are acceptable admixtures by the concrete industry.
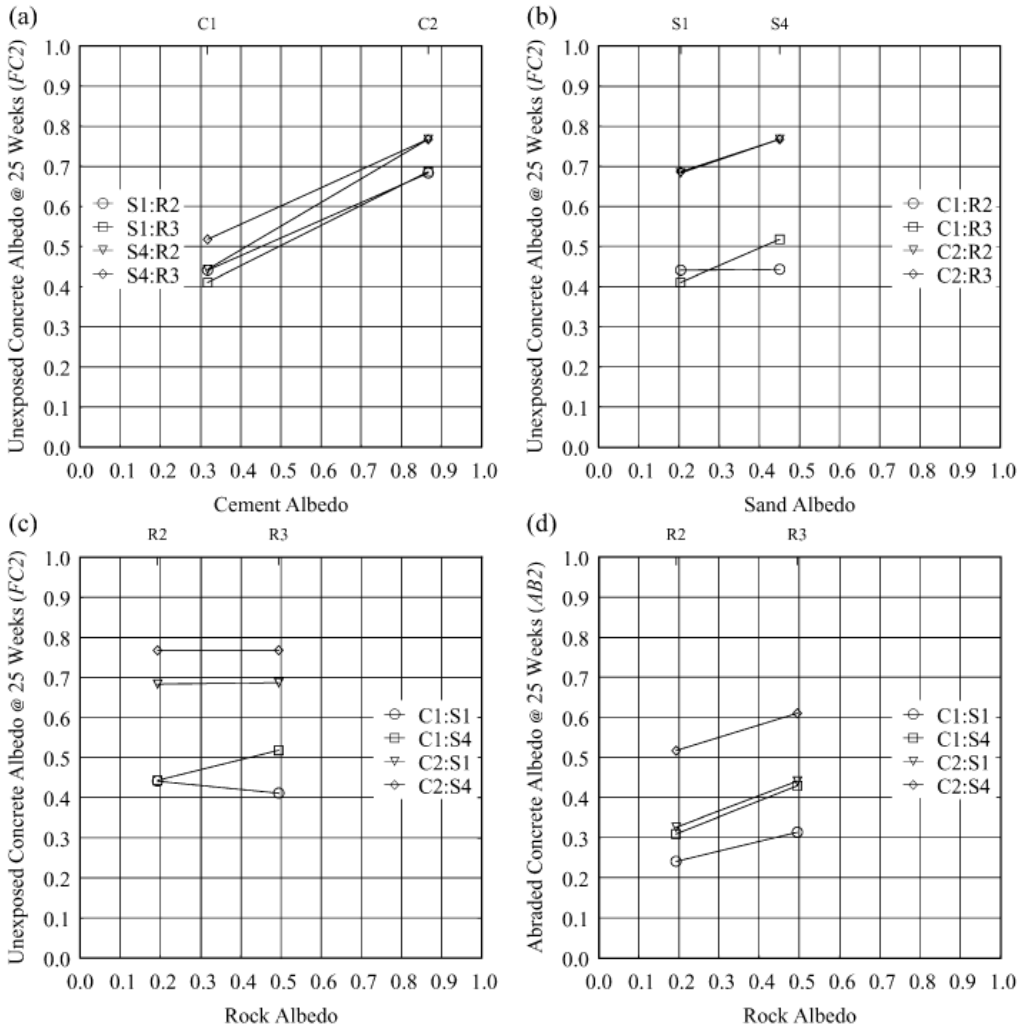
Figure 11 Mature, smooth concrete albedo vs. composition. Source: R. Levinson & H. Akbari, 2002.

Flyash (FA) and ground granulated blast furnace slag are often used in concrete to replace a portion of the total cement (Figure 12). Both of these materials are the waste products of industrial processes, FA is formed during the combustion of powdered coal in power plant boilers, and slag is the remains after the production of iron from ore. Slag cement is manufactured from slag. FA and slag cement are used in concretes to enhance the performance of concrete including increases in strength, reduced permeability, reduced shrinkage, and increased durability (Federal Highway Administration; National Slag Association). The color of FA can range from tan to grey. Slag cement can also vary in color however it is typically a few shade lighter than that of flyash. Because both of these materials are considered diverted resources they are awarded points for resource efficiency by the LEED™ rating system when used in concrete for building, parking lots, and other non-roof structures (US Green Building Council 2006).

Researchers at the University of California Irvine and Ohio Northern University determined the albedos of Portland cement concretes comprised of several different proportions of FA and Slag (K. Boriboonsomsin & F. Reza, 2007). This study was conducted in Ohio and followed the specifications of the Ohio Department of Transportation (ODOT) for concrete pavements. Three

14

standard concrete mixes were used as control mixes. The first control mix was conventional design with no substitution of the Portland cement. The second two mixes contained cement replacement materials; 24% FA by weight of the total cementation materials in one and 30% slag in the other. The aggregate used for all test mixes were #8 limestones and ASTM C33 sand. There were 11 mixes tested in total (Figure 13, Table 1). Four samples from each mix were tested for albedo using the procedure defined in ASTM C1549. The final three mix designs did not use FA or slag cement and replaced a fraction of the cement with white sand and Latex as an additional attempt to increase albedo. The results of this experimentation are included in Figure 14.

Figure 12 Three cementatious materials used in concrete. a) Portland cement (cement), b) flyash (FA) c) ground granulated blast furnaces slag (slag).
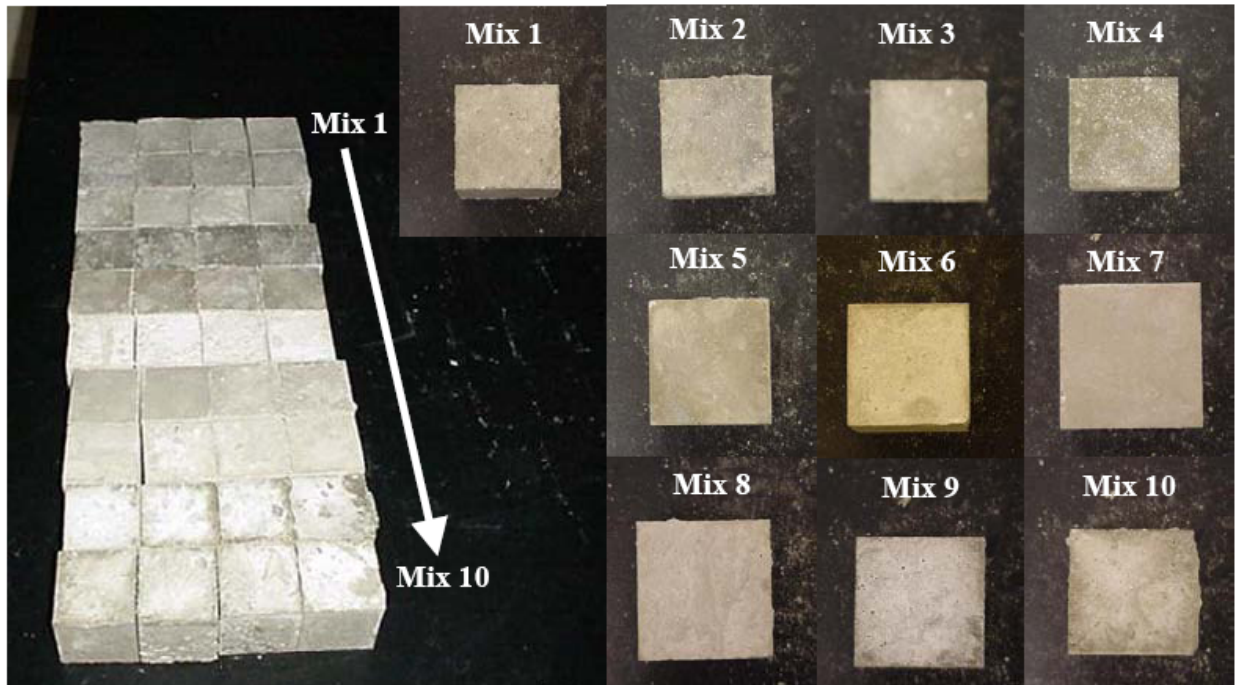
Figure 13 Image of all sample concrete mixes testing (Mix 1-10) using different proportions of cement, FA, and slag. (K. Boriboonsomsin & F. Reza, 2007)

Table 1Concrete mix designs for mixes 1 through 11 used in albedo study.
Table Source: K. Boriboonsomsin & F. Reza, 2007.

Mix #	Description	Portland Cement	Fly Ash	Slag	Water	Coarse Aggregate	Fine Aggregate
1	ODOT base mix	600	0	0	355	1410	1320
2	ODOT high performance concrete 1 (HP1) – 24% fly ash	530	170	0	263	1480	1310
3	ODOT high performance concrete 2 (HP2) – 30% slag	490	0	210	264	1495	1330
4	ODOT HP2 but with 30% fly ash	490	210	0	245	1495	1330
5	ODOT HP1 with 60% fly ash	280	420	0	233	1480	1310
6	ODOT HP2 with 60% slag	280	0	420	258	1495	1330
7	ODOT HP2 with 40% fly ash + 20% slag	280	280	140	233	1495	1330
8	ODOT HP2 with 20% fly ash + 40% slag	280	140	280	245	1495	1330
9	ODOT base mix with white sand	600	0	0	355	1410	1320[b]
10[a]	ODOT base mix with latex	611	0	0	131	1410	1320
11	ODOT HP2 with 70% slag	210	0	490	256	1495	1330

[a]This mix includes 220 lbs of latex (24% solids content); [b]White sand
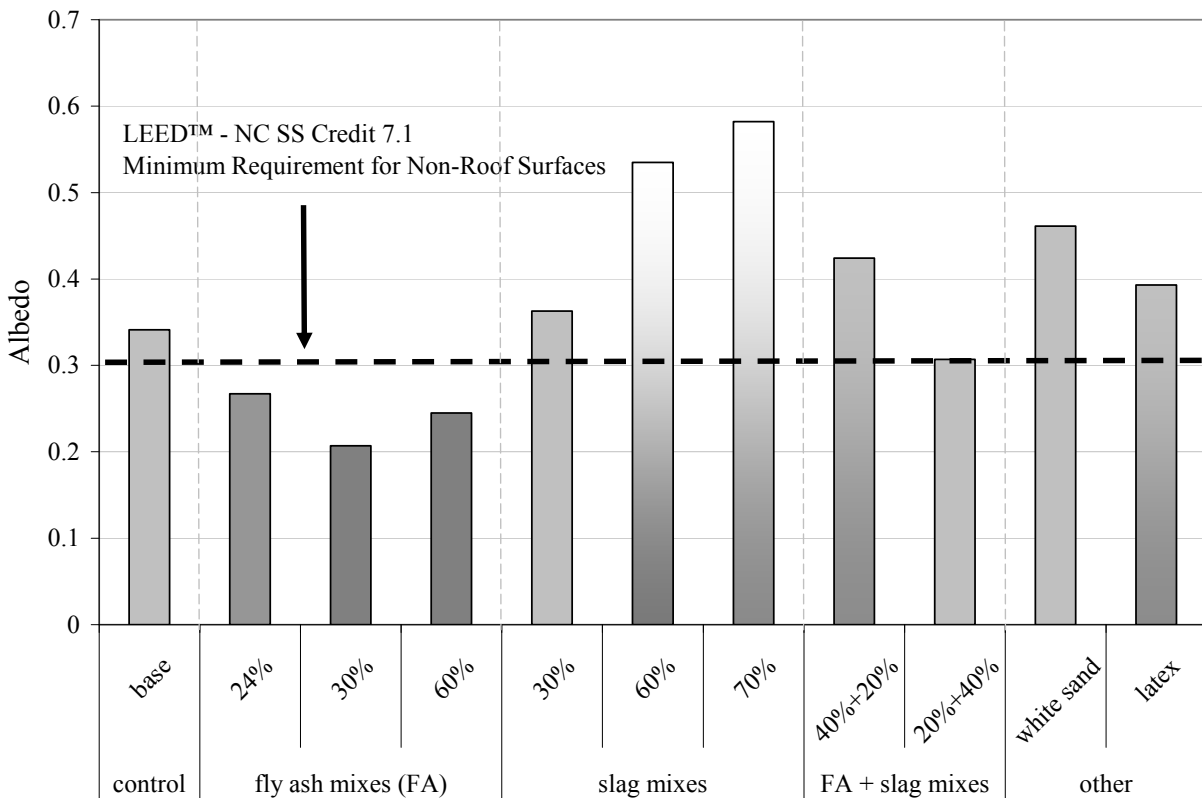
Figure 14 Albedo results for experimental tests of 11 concrete mix designs containing different proportions of fly ash and slag. Data Source: K. Boriboonsomsin & F. Reza.

The study concluded that slag has the greatest potential for increasing albedo of concrete pavements while adding Class C flyash actually decreased the albedo of concrete. Substituting 70% of the cement (by weight) with slag produced an albedo of 0.582 which is 71% greater than the conventional mix (albedo =0.341).   Though mix 11 did produce the greatest albedo, there were six other mix designs that increased the albedo as compared to the conventional control mix. These results also indicated that seven of the mix designs would achieve LEED™ points as they meet the minimum albedo requirement of 0.30.

Correlating Albedo and Maximum Surface Temperature

Conventional pavement materials are often modified to increase their engineering performance. Altering the mix design (types and % of constituents) or construction methods, designers can often improve the strength, durability, sound, surface friction, weight, and many other performance characteristics depending on the application. While the engineering performance of many common pavement variations has been well documented through past research, the thermal and radiative characteristics have not. In the following sections the results of several studies are presented; they quantified the albedo, temperature behavior, and thermal properties of several common pavement types.

The first describes a field experiment in which several materials were constructed and monitored in close proximity and thus were influenced by nearly identical meteorological and subgrade influences. While these surfaces were not under the influence of traffic patterns they are the best comparison of multiple pavement materials to date. Here we measure the albedo and emissivity of the pavement while in the next section we analysis the temperature gradients below the surface over time.

This part of the research was considered to understand how albedo modifications may impact road surface temperatures extremes in the desert region of Phoenix.

The use of an outdoor research facility with experimental pavement test sections was coordinated with the Arizona Department of Transportation (ADOT) in Phoenix.   Figure 15 shows a portion of the layout that was used in this research. Pavement test sections consisted of thick 19cm (7.5in) and thin 3cm (1.2in) sections of conventional dense graded Hot Mix Asphalt (HMA), an asphalt rubber chip seal surface treatment, a thick 19cm (7.4in) and thin 3 cm (1.2in) sections of a gap graded asphalt rubber mixture (typically used in Arizona), thick 30cm (11.8in) and thin 10cm (3.9in) plain Portland Cement Concrete (PCC) pavement sections, and a plain PCC section modified with 4% by volume using crumb rubber. All of these test sections were constructed per standard ADOT specifications.
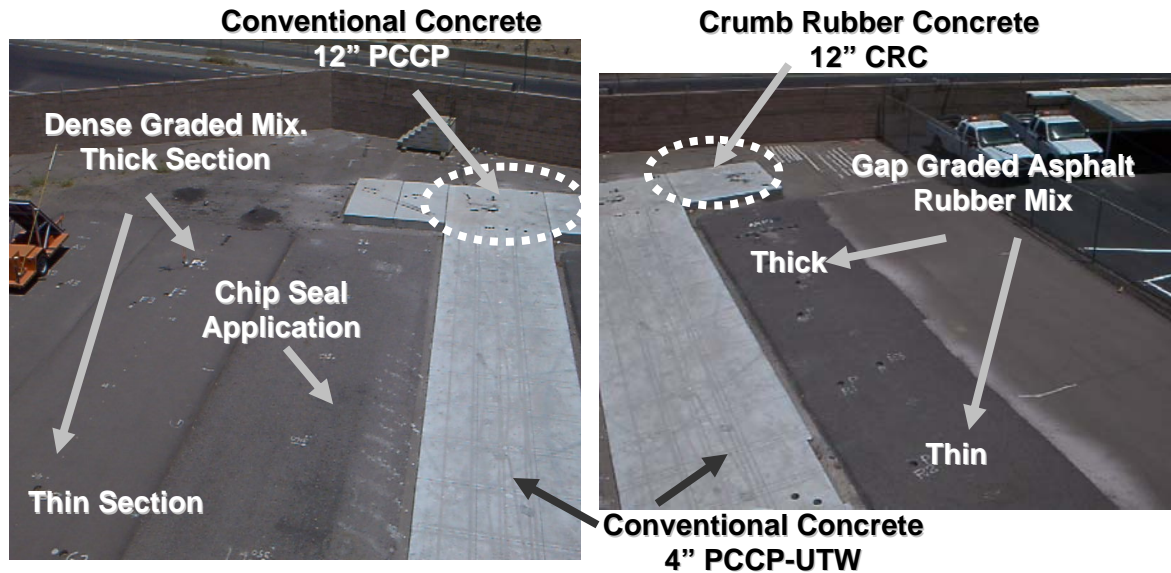
Figure 15 Pavement test sections in Phoenix courtesy of Arizona Department of Transportation.

During July 2004, albedo alterations were made to the above described pavement test sections. The albedo of a road material is the fraction of light incident that is reflected from a surface. Incoming short-wave radiation (K, ↓=incoming, ↑=reflected) is controlled by the zenith (Z) angle of the sun relative to the horizon, with a maximum at the local solar noon [Oke 1987]. Albedo (ά) is not a perfect constant throughout the day however, Q↑ can be expected to be reduced in proportion to Q↓ since the surface is not opaque to short-wave radiation. Therefore, the percent of Q↓ that is not reflected is absorbed Q_{abs}, which can be represented as:

$Q_{abs} = Q{\downarrow} - Q{\uparrow} = Q{\downarrow}(1 - \acute{a})$

A field survey of each pavement material was conducted on a calm, clear day to determine albedo. A pyranometer (wavelength range 250 - 2500nm, Matrix, Inc.) was used to measure the incoming and reflected solar radiation according to the ASTM E 1918-06 *Standard Test Method for Measuring Solar Reflectance of Horizontal and Low-Sloped Surfaces in the Field*. The pyranometer converts radiation energy into a voltage and is calibrated using an Eppley™ precision solar spectrometer.

Table 2 summarizes the albedo measurement for pavements test section for this study. The table also includes results from modifying albedos through the use of application of commercial white paint on some of the test sections. The results show the maximum surface temperatures observed on July 24. These temperatures were captured using a FLIR Systems™ ThermaCAM™ S-60 handheld infrared camera. The S-60 camera consists of a built-in 24° lens, a visual color camera, a laser pointer, and a 10cm (4in) color LCD on a removable control. The unit has a spectral range of 7.5 to 13μm with a thermal sensitivity of 0.06° at 30°C and a focal plane of 320x240 pixels. The unit is equipped with an internal digital camera that can capture a digital image of the IR subject. Images are stored in either an internal memory or with a memory card. The infrared camera was compared with actual thermocouple temperatures and resulted in an average accuracy of approximately ±0.5°C (±0.9°F).

Table 2 Influence of albedo on pavement surfaces, July 24, 2004 – Phoenix, Arizona

Pavement Section	Q↓	Q↑	ά	Maximum Surface Temperature (Observed)	
	Wm⁻²			°C	°F
Hot Mix Asphalt (HMA) Thin	827	167	0.20	63.3	146
*HMA Thin w/ White Paint**	863	220	0.25	58.3	137
Hot Mix Asphalt (HMA) Thick	863	146	0.17	62.8	145
*HMA Thick with White Paint**	863	221	0.26	56.1	133
Asphalt Rubber (AR-OGFC) Thin	862	106	0.12	67.2	153
*Asphalt Rubber Thin with White Paint**	844	105	0.26	65	149
Asphalt Rubber (AR-OGFC) Thick	844	111	0.13	66.7	152
*Asphalt Rubber Thick with White Paint**	862	223	0.26	51.1	124
Asphalt Chip Seal	863	130	0.15	62.8	145
Portland Cement Concrete (PCC) Thick	827	376	0.46	51.1	124
PCC Thin	862	369	0.43	53.9	129
Crumb Rubber PCC (CR-PCC)	845	356	0.42	53.9	129

application of commercial white paint

Emissivity, ε, the radiative property that governs the rate at which thermal radiation is emitted from a surface is also an important characteristic of materials. In most cases pavements, regardless of material (HMA or PCC) are thought to have very high emissivity values for the thermal wavelengths. In order to verify this assumption the emittance was measured for each of the surfaces plus an additional brick surface. The results of these measurements are compared to literature values for the three types of pavement materials (Table 3). These findings indicated an acceptable agreement with the literature values.

Table 3 Field validation of emissivity, ε

Material	Published Emissivity*	Measured Emissivity
Asphalt Paving	0.967-0.970	0.95-0.971
Concrete	0.93-0.97	0.90-0.98
Brick	0.93	0.94

* FLIR Systems ThermaCAM 2003

The results of these measurements (Figure 16) showed that the open graded asphalt rubber concrete-thin (AR OGFC) section had the lowest albedo (0.12) as well as the highest peak surface temperature of 67.2°C (153 °F). This is compared to the PCC test section which had the highest albedo of 0.46 and a maximum surface temperature of 51°C (124°F). The difference in the peak temperature is 16°C (28.8°F). The dependence of the change in temperature on the change in albedo was: $\Delta T_s/\Delta \acute{a}$ = -4.7°C/0.1 (-8.5°F/0.1). This is consistent with prior works including those carried out by Lawrence Berkley National Laboratory which resulted in $\Delta T/\Delta \acute{a}$ ranges of -3.9°C/0.1 (-7°F/0.1) to -7°C/0.1 (12.6 °F/0.1). Of significance were the findings of the asphalt rubber pavements. As presented in Figure 17, the surface temperature of the thick asphalt rubber pavement went from having the second highest surface temperature of 66.7°C to

being equal to the lowest surface temperature for all pavements both flexible and rigid, at 51.1°C with an albedo increase from 0.13 to 0.26.
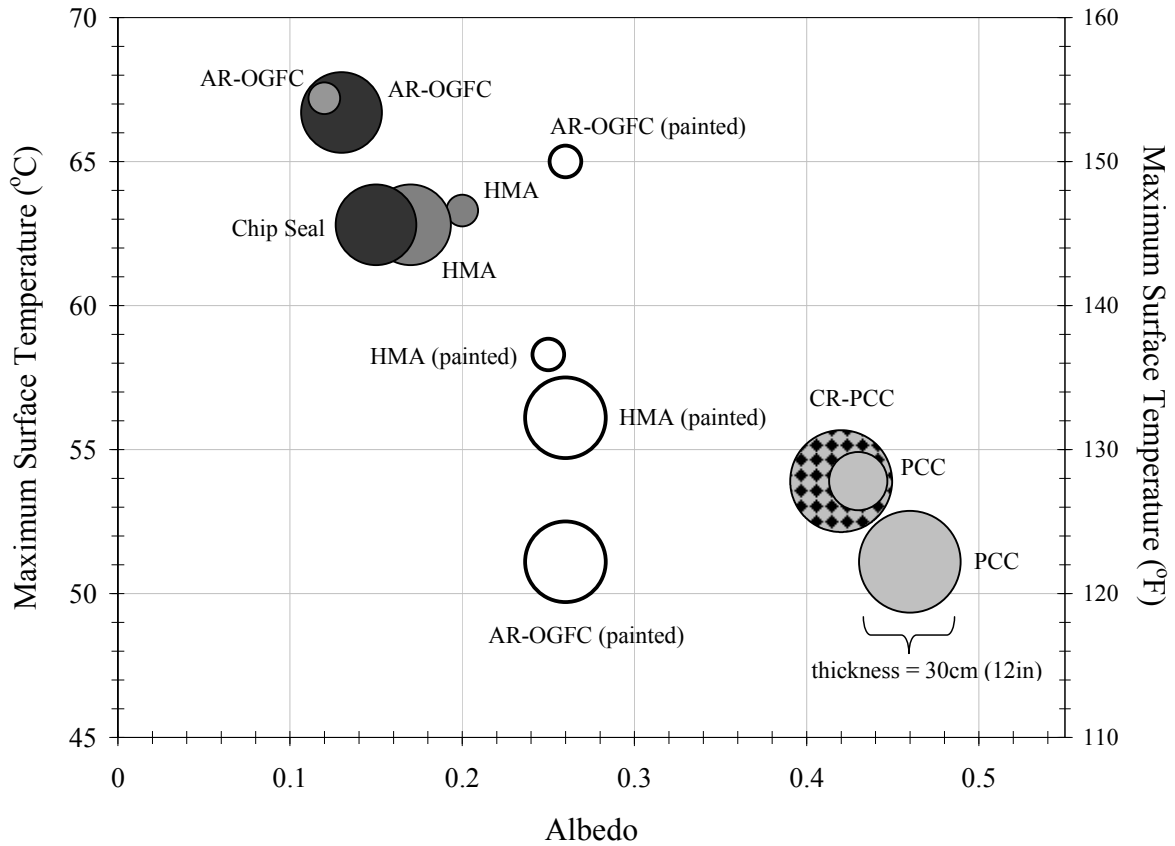
Figure 16 Comparing maximum surface temperature with measured albedo of various concrete mixes. Note: the size of the circle indicates the thickness of the pavement layer.
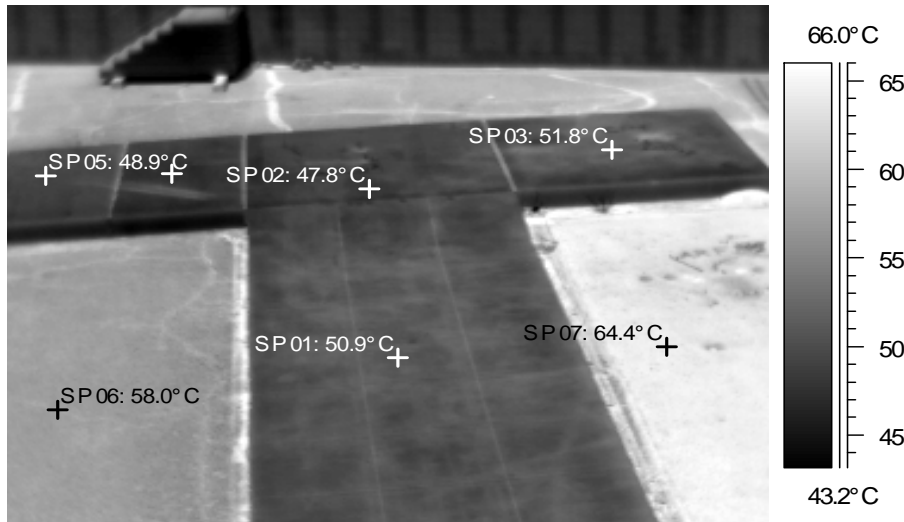
Figure 17 Example of handheld IR thermographic image of pavements.

The dependence of the change in temperature on the change in albedo ($\Delta T_s/\Delta\acute{\alpha}$) was 12.3°C/0.1 (22°F/0.1), is far higher than typical albedo mitigation rates from prior research on conventional pavements. Additionally, while the surface temperature of the painted white gap graded asphalt rubber concrete pavement was the same as the PCC pavement (tied as the overall lowest surface temperatures), the asphalt rubber pavement had a 0.20 lower albedo than the conventional concrete. However, the thickness of the asphalt rubber pavement was almost half of the PCC pavement, and its density is also lower. Therefore, the albedo alone is not the determinative factor in surface temperature. While it is a key player in the energy balance of surfaces, it alone may not be the determinative factor in defining the road surface temperature characteristics through-out the full diurnal cycle. Factors such as a materials density, specific heat, thermal conductivity, pavement thickness, and sky view are all important considerations as will be demonstrated in Chapter 3 of this report. The following section takes a closer look at how energy absorbed by the pavements migrates beneath the surface of pavement structures in the field.

Surface and in-depth pavement temperatures

The transient thermal response of pavement materials can be estimated using reference thermal properties and fundamental energy balance equations; however, this may not always produce accurate and reliable results due to the complex nature of the outdoor environment. Experimental data from actual real world scenarios are vital in calibrating theoretical predictive models. To date, there have been limited research investigations that have monitored the surface to deep ground temperature gradients under pavements in the field. The research team set out to provide a year's worth of subsurface temperature data from near surface to 3m (10 ft) below the surface of various urban materials. This marks the first pavement focused effort of its kind. All data was collected in the metropolitan Phoenix, Arizona over a three year period from 2004 to 2007. The following section describes the methodologies and results of the four subprojects that address the issues of near surface and in-depth temperature gradients of pavements in the field.

Pavement surface and subsurface temperature gradient experiments

The near surface and subsurface temperature measurements presented in this section utilized a unique methodology for sensing and data storage. At each location were temperature readings were measured an array of temperature sensors were either embedded during initial construction or inside of a cylindrical core hole that was back filled with a nearly identical concrete mix as the larger section being analyzed.

The temperature sensors used in these studies offer a temperature monitoring system that includes the temperature sensors and a software tool named COMMAND Center[TM] that is specifically designed for calculating maturity in concrete. The temperature sensors called iButton[TM], are produced by Dallas Semiconductors.

The DS1920 Temperature iButton[TM] is about 1.5 cm in diameter and provides 9-bit temperature readings that indicate the temperature of the device (Dallas Semiconductors, 2005). The data is sent to and from the sensor over a 1-Wire interface. This same wire also provides the power that the device stores as energy on an internal parasite capacitor during periods of time when the sensor is not connected to a data communication line to a computer. This enables the sensors, once activated, to be left alone to collect temperature data periodically without the need for bulky data loggers.

The DS1920 Temperature iButton^{TM} is different than a standard thermocouple or thermistor in that it uses a on-board measurement technique developed by Dallas Semiconductors. This digital temperature measurement technique results in a resolution of +/- 0.5 ^{o}C (0.9^{o}F) over the range of -55°C (131°F) to 100°C (212°F). The sensors were placed at various pavement depths and below the pavement structure. An example is shown in Figure 18.

Figure 18 Example of temperature sensors placement at various depths.

In addition to the embedded temperature sensors, meteorological data such as solar radiation, relative humidity, air temperature and wind speed was also collected on site. In instances where meteorological data was not collected on site this information was obtained from local metrological stations such as those provided by the Arizona Meteorological Network which provides hourly data from stations at various positions in the valley [AZMET]. In some cases infrared handheld thermography is being used to collect large surface area temperature measurements. These activities are designed to provide tremendous value to the validation of the heat transfer models developed in Chapter 3 of this report.

Pavement Test Sections

The data presented here were collected at the outdoor research facility located at a facility owned and operated by the Arizona Department of Transportation (ADOT) in Phoenix. This same location was used in the albedo (reflectance) data collection study discussed in the previous sections. This section presents the subsurface temperature gradients below the surface over a complete diurnal cycle. Data was collected at this location for a 12 months from 2004 to 2005. An air temperature and humidity sensor were posted at a 2 meter height above the pavement section.

Figure 15 showed a portion of the layout that was used in this research. The pavement test sections consisted of thick 19cm (7.5in) and thin 3cm(1.2in) sections of conventional dense graded Hot Mix Asphalt (HMA), an asphalt rubber chip seal surface treatment over 3cm (1.2in) HMA, a thick 19cm (7.4in) and thin 3 cm (1.2in) sections of a open graded asphalt rubber mixture (AR-OGFC), a thick 30cm (11.8in) and thin 10cm (3.9in) plain Portland Cement Concrete (PCC) pavement sections, and a plain PCC section modified with 4% by volume using crumb rubber. All of these test sections were constructed per standard ADOT specifications.

The Ibutton™ temperature sensors were installed post construction by coring and refilling the holes with similar materials after the sensors had been installed at the correct depth. To be consistent, temperature readings sensors were placed at 1cm (0.5in), 3.8-5cm (1.5-2in) for all pavements and additional sensors at 7.6-10cm (3-4in), 15-17.8cm (6-7in), and 20cm (12in) for the thick pavements. The plot in Figure 19 of the near surface (1cm (0.5in) temperatures for June 20 are a good representation of peak temperature profiles during this investigation. Pavement temperature and air temperature were recorded every 20 minutes while solar radiation was every 1 hour. The results are typical for surface temperatures of pavements. The peak temperature usually at about an hour after solar noon. This is followed by the peak air temperature which typically occurs later in the afternoon. And as the solar radiation decreases the temperatures begin to reduce after some time. This lag in temperature is often referred to as a hysteresis lag and is most pronounced in areas where the air temperature remains elevated well into the night.
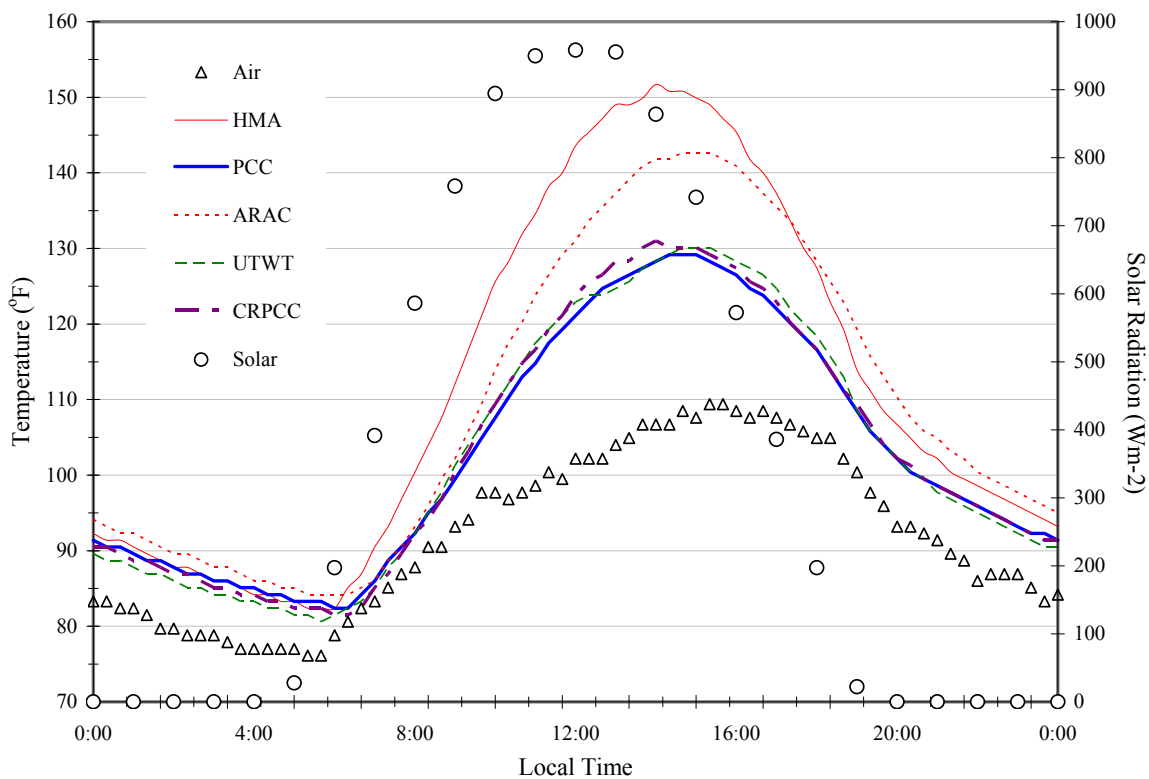
Figure 19 Pavement materials temperature comparison. Near surface (depth=0.5in) temperatures (20 minute intervals) over a 24 hour period on June 20, 2004. HMA – Hot Mix Asphalt, PCC – Portland Cement Concrete, ARAC – Asphalt Rubber Asphalt Concrete, UTWT – Ultra Thin White Topping, CRPCC – Crumb Rubber Portland Cement Concrete. Hourly solar data from Arizona Meteorological (AZMET) Station Mesa, Arizona.

Observations indicated that maximum surface temperature at approximately 1500 hour, and a minimum surface temperature between 0500 and 0600 hours. The Portland cement concrete pavements maximum near surface temperature was in the range of 53.5 to 54.5ºC (128 to 130ºF), and the dense graded hot mix asphalt pavement sections maximum surface temperature was between 60 and 64ºC (140 to 147 ºF) . Furthermore, the gap graded asphalt rubber mixtures had lower maximum near surface temperature 61ºC (142ºF) compared to the conventional dense graded HMA mix 64ºC(147ºF). During the day, the Portland cement concrete pavements are

cooler than the HMA pavements by approximately 6 to 10ºC (10.8 to 18ºF). There were no significant differences in the low temperatures, but the UTWT PCC pavement had the lowest temperature. Figure 20 provides a look at the temperature gradients observed during the same day (June 20) at an average depth of 7.6cm (3in) below the surface of each material. The thinner pavements are not shown on this plot because their thickness was less than 7.6cm (3in). Temperatures follow a similar profile to the surface temperature however they peak at a much lower temperature at about an hour later than the surface. This indicates a relatively low thermal diffusivity for the pavement materials
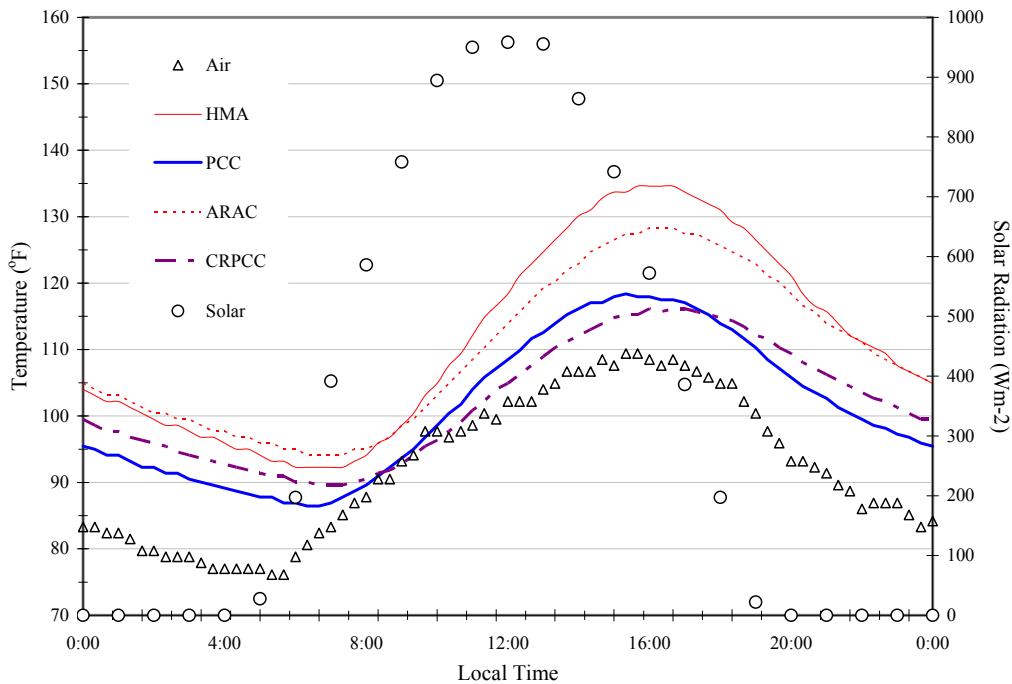
Figure 20 Sub surface paving materials temperature comparison. In depth (depth=3in) temperatures (20 minute intervals) over a 24 hour period on June 20, 2004. HMA – Hot Mix Asphalt, PCC – Portland Cement Concrete, ARAC – Asphalt Rubber Asphalt Concrete, CRPCC – Crumb Rubber Portland Cement Concrete. Hourly solar data from Arizona Meteorological (AZMET) Station Mesa, Arizona.

Pervious concrete subsurface temperature monitoring

While research into the construction methods and longevity of permeable pavements have been assessed [Delatte, N. 2007] and the strength and drainage properties have also been verified, there is a significant lack of research on the overall effectiveness of permeable pavements for storm water mitigation and UHI reduction. Of particular interest in the desert southwest is the application of permeable pavements for reducing UHI formation under normal hot arid conditions. In 2007, the National Center of Excellence on SMART Innovations undertook to research these various system components by designing, constructing, and monitoring a Portland cement pervious concrete (PCPC) surface parking lot on the main campus of Arizona State University in Tempe, Arizona, USA (Figure 21).

Figure 21 Pervious concrete parking lot located at the J. Russell and Bonita Nelson Fine Arts Center on the main campus of Arizona State University in Tempe, Arizona.

The pervious pavement structure comprised of four layers; pervious Portland cement concrete, gravel base, filter fabric, and compacted subgrade. The pavement structure supports common automobile loads with the occasional heavier delivery trucks used for catering and equipment delivery at the front of the center.

The pervious concrete layer was 15.2cm (6in) thick. The mix design specified for this project used a 3/8 inch (9mm) aggregate. This size aggregate was selected for its relative smoothness and visual appeal as compared with other larger aggregate sizes (1/2 inch) also used for PCPC. A representative cylindrical sample of this mix is shown in Figure 22. It was designed and manufactured by CEMEX and consisted of aggregate, cement, flyash, water, and additional proprietary admixtures. The approximate mix design information used is provided in Table 4.

The mix was delivered in multiple seven-ton concrete mix trucks and poured using a shoot. Water was added to the mix in small quantities on site to achieve the desired coating of the aggregate. The quality was verified by a pervious concrete specialist from CEMEX. The concrete was leveled using a hydraulically-driven roller screed and then compacted with a 34kg (75lb) roller both manufactured by Bunyan Industries of Utah. Joints were spaced every 4.5 m (15ft) apart using a wet joint roller with circular flange to form a 4cm (1.5in) creases in the pavement before it cured. Within 20 minutes of laying the mix the surface was covered with a 6-mil thick, semi-clear plastic sheet to prevent moisture from escaping during curing.
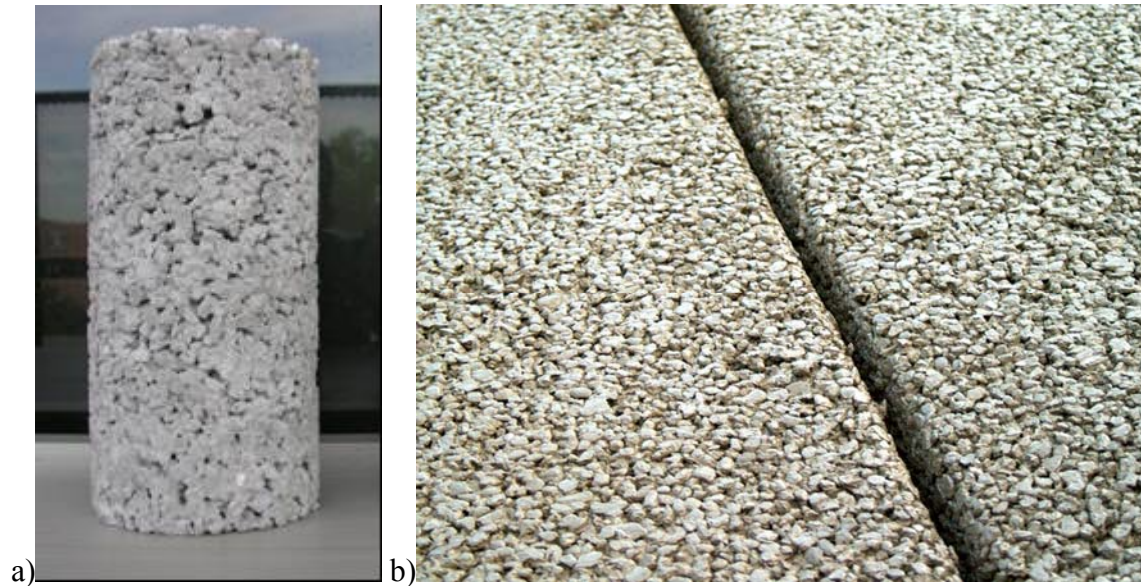
Figure 22 (a) Cylinder sample of the pervious concrete mix used for parking lot at ASU (b) Close up of a pervious concrete surface with an wet expansion joint.

Table 4 Approximate mix design for the pervious Portland cement concrete used in the parking lot

	Units	Value	% by weight
Aggregate diameter	m (in)	0.009 (0.375)	-
Aggregate	kgm^{-3} (lbs/yd^3)	1556 (2623)	77%
Water	kgm^{-3} (lbs/yd^3)	105 (178)	5%
Cement	kgm^{-3} (lbs/yd^3)	311 (525)	15%
Flyash	kgm^{-3} (lbs/yd^3)	59.3 (100)	3%

Source: Ricker, Atkinson, McBee, Morman & Associates Inc. (RAMM), Tempe, Arizona 2007.

The temperature beneath the surface of the pavement and the adjoining landscaping were measured to gain a better understanding of the thermal behavior of these materials. To date, there is limited literature documenting the thermal transport properties or field thermal interactions of pervious cement concrete. At a central location in the parking lot, a temperature tower consisting of 17 temperature sensors located at various depths were installed within the mix during construction. There were at least two sensors placed at the following depths; 1cm (0.5in), 2cm (1in), 10cm(4in), 15cm(6in), 20cm(8in), and 28cm(11in) below the surface. The redundancy was to insure readings even in the event of sensor failure (see Figure 23). Temperature sensors were also installed at a location in the landscaping. There were three depths monitored in the landscaping at 2.5cm (1in), 28cm (11in) and 49cm (19in). The deepest two sensors depths corresponded with soil moisture probes whose results are not within the scope of this report.

surface

PERVIOUS CONCRETE

1cm (0.5in)
2.5cm (1in)
5cm (2in)
10cm (4in)
15cm (6in)

15cm (6in)

GRAVEL BASE

10cm (4in)

20cm (8in)

FILTER FABRIC

28cm (11in)

SUBGRADE

○ temperature sensor*
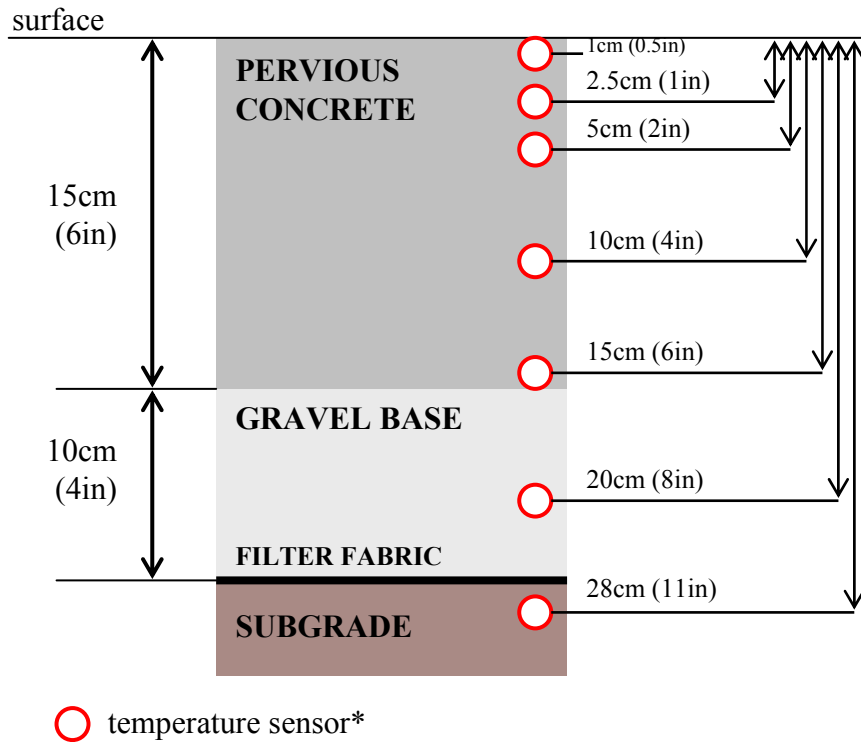
Figure 23 Cross section of pavement structure and depths of temperature and moisture sensors.

Temperature results for pervious concrete

The sensors were installed during the first week of January 2007 and data was collected until September 2007. Temperature information was set to record every 20 minutes which required the data to be downloaded every 28 days. Due to the high volume of data points recorded during the monitoring stage and the variability that can occur hourly during the course of a day an averaging methodology was employed. This method created a generalized profile and eliminated noise from meteorological and traffic influences of specific time periods. The hourly temperature data from each sensor depth was averaged over a time period of twenty or more days at each hour for 2007. For example, the air temperature value representing the 0800 temperature at a depth of 1cm (0.5in) for the period from August 9 to September 5 is the mean of all 0800 temperature values recorded during that time period of 2007 at the pervious concrete parking lot. This can be represented mathematically as:

$$\overline{T}_{p,h,L} = \frac{\sum_{d=1}^{n_p} \overline{T}_{d,h,L}}{n_p}$$

where $\overline{T}_{p,h,L}$ is the mean sensor temperature at hour h, at depth L, over the time period p, from the first day d, to n_p days later. $\overline{T}_{d,h,L}$ is the mean temperature of the multiple sensors located at a depth L below the surface at hour h, and day d.. The results for August are shown in Figure 24. The average temperature profiles indicate that the near surface temperature (depth = 1cm (0.5in)) undergoes the greatest daily changes in temperature in direct response to the solar insulation. As expected the farther away from the surface the cooler the temperatures are during the day. The opposite is true once the sun sets: the surface temperature decreases rapidly. The temperatures within the pavement have lower daily fluctuation and remain fairly constant, but depend on the depth within the pavement layer. The period of from August 9 to September 5 (Figure 24) showed the highest average temperatures with and average peak temperature of 62°C (144°F) around 14 40 in the afternoon just below the surface. The maximum near surface temperature experienced in August was 66.7°C (152°F), which occurred at 15 00 on August 12, 2007.
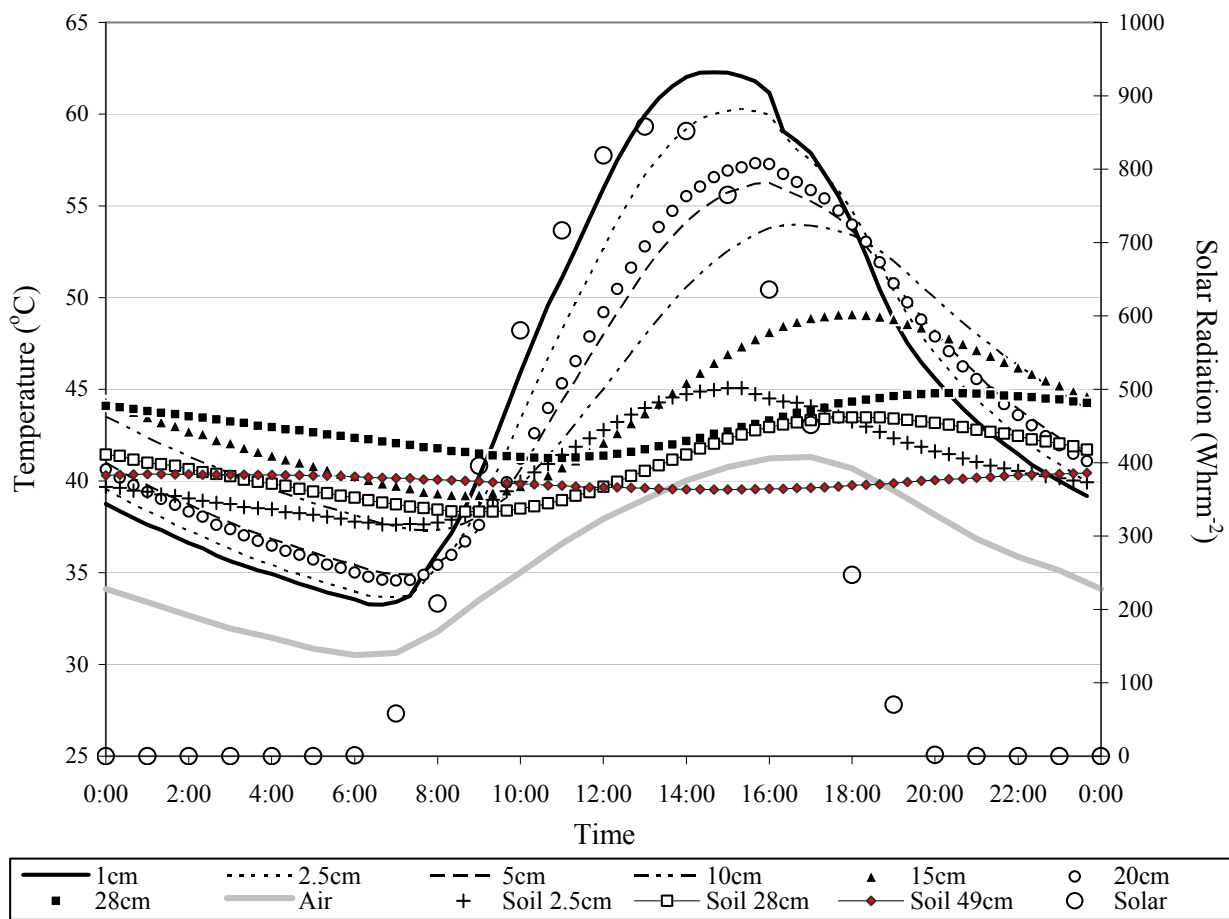
Figure 24 Averaged diurnal temperatures at T$_P$, T$_L$, air temperature, and solar radiation for the period of August 9 to September 5 2007 for the Pervious Concrete pavement.

Figure 24 also includes the temperature of the subgrade soil temperatures recorded underneath the pavement and filter fabric and outside of the lot in the landscaped area. The plot shows the temperatures beneath the landscaping do not experience nearly the magnitude of those in the pavement. In fact the temperature sensor located just 2.5 cm (1in) below the base layer reaches a peak average temperature of 45°C (113°F), while the same depth below the pavement peaked at 60°C (140°F). An interesting note is the behavior of the temperatures at 28cm (11in) below both surfaces. The temperature profiles of these two points have a similar maximum temperature however, the time at which they reach these temperatures is shifted. The temperature at this location under the pervious concrete stays relatively constant.

Plots of depth versus temperature are shown in Figure 25. Each line represents the average temperature profile below the pavement at a specific time. The times were selected in 4 hour increments from 04 00 through midnight. The Y axis shows the range of depths for each material layer. The shape of the temperature curves is as expected for the pavement over the course of the day; concave to the left during the morning hours and concave to the right during the day as the surface layers heat up. The highest temperature gradient is observed for 16 00.
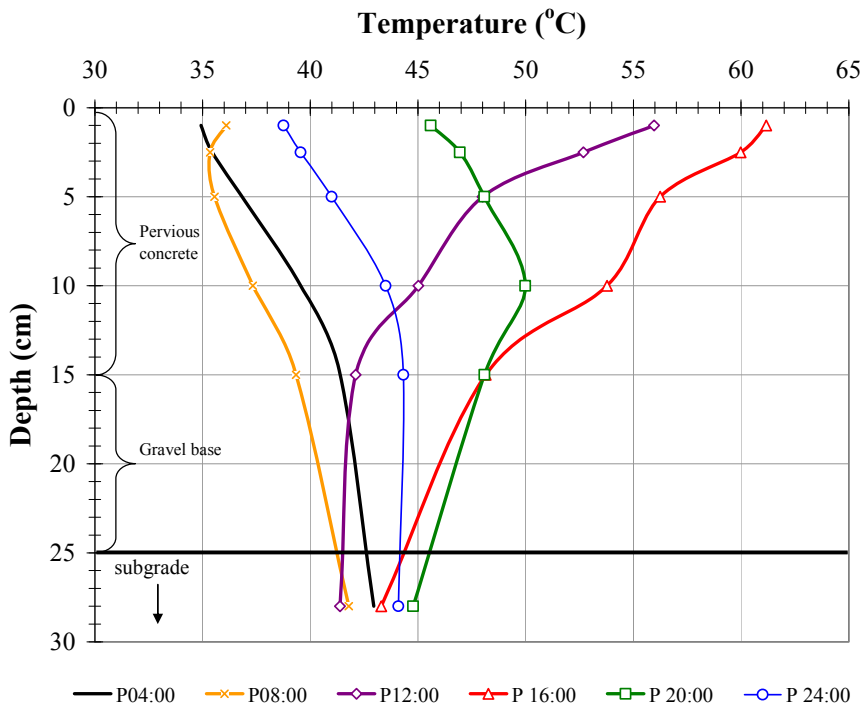
Figure 25 Average temperatures with depth ever 4 hours (4:00, 8:00, 12:00, 16:00, 20:00, 24:00) below the surface of the Parking lot (P) and the landscaped Soil (S) for the period of August 9 – Sept 5th, 2007.

Deep ground hole-boring experiments

When developing heat transfer models it is important to set boundary conditions. In a one dimensional pavement structure, the upper boundary is the pavement surface while the lower boundary can be assumed to be the deep subgrade. Because thermal energy is transferred from one boundary to the other, it is important to understand what is occurring, or what is the condition at each location. The surface boundary condition is governed by the energy balance equations between radiation, convection, and conduction to the outside environment and will

constantly be changing throughout the day. The lower boundary condition, the deep subgrade soil, exchanges energy with the system through heat conduction. This lower boundary condition is expected to act as a seemingly endless heat sink. It is important to know what the temperature of the deep subgrade soil is and whether it can be assumed to be constant or varying.

In order to ascertain these conditions, an experiment was carried out in August 19th, 2005, using rotary drilling and placing an array of temperature sensors into the ground beneath a pavement structure to a depth of 3 m (10 ft). Figure 26 presents the drilling sites on the campus of Arizona State University - Tempe, equipment used and the final layout, while Figure 27 shows the area map which the sites are located.
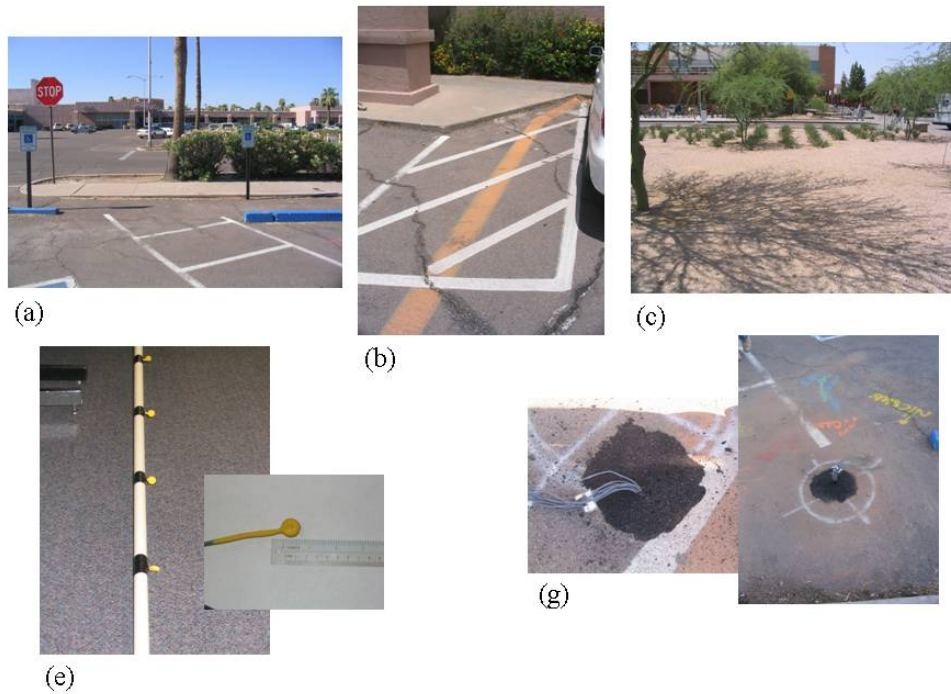
Figure 26 Deep ground temperature sensing experiment at (a) ASU parking lot 16 North, (b) South, and (c) Memorial Union desert landscape area, by embedding (e) an array of iButton[TM] temperature sensors, set at an interval of 1 foot, mounted on a 10-ft PVC pipe (g) vertically into the ground
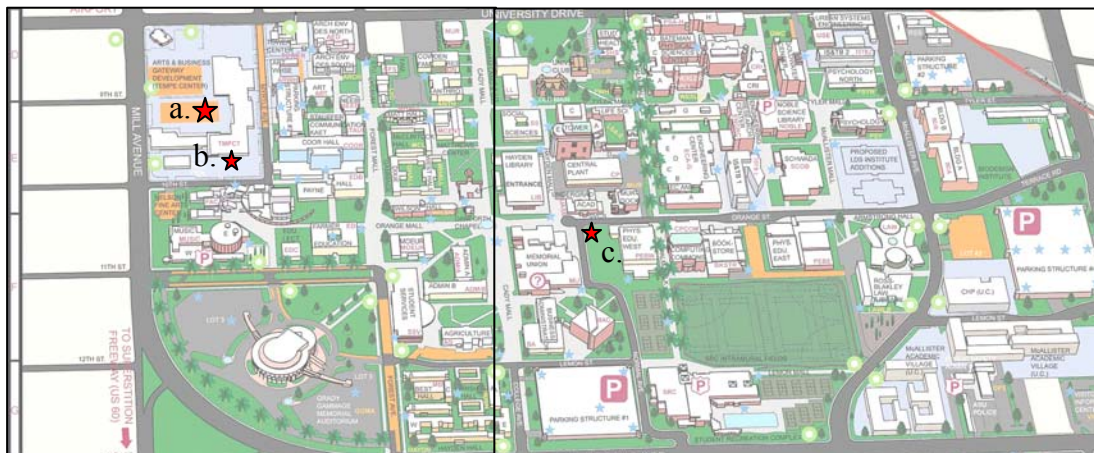
Figure 27 Area map of the site locations in Arizona State University – Tempe. a. ASU parking lot 16 North, b. ASU parking lot 16 South, and c. Memorial Union desert landscape area

30

For this ground hole-boring experiment, the temperature sensors were programmed to continuously capture the temperature data at an interval of 20 minutes, which allowed the sensors to store up to 28 days of data before downloading. The data has since been downloaded at approximately one month intervals. Figure 28 shows the graphical representation of the results collected at Tempe Center North parking lot (located at the southeast corner of Mill Avenue and University Drive at Arizona State University) for the months of August through September 2005. As can be seen from the graph, the ground temperatures became constant with respect to time (i.e. independent of the surface fluctuations) at about 60 cm (2 ft) from the surface, thereafter decreasing linearly with depth, as shown in Table 5.

The second law of thermodynamics states that heat is transferred in the direction of decreasing temperature. It was anticipated that the ground temperature will have to eventually stabilize at a certain depth; however, the result obtained did not indicate reaching a steady state. The monitored depth was not long enough to observe this stabilized temperature. It was assumed that the ground temperature of 33.5°C at 3 m (10 ft) depth was reasonable as a deep ground boundary condition.
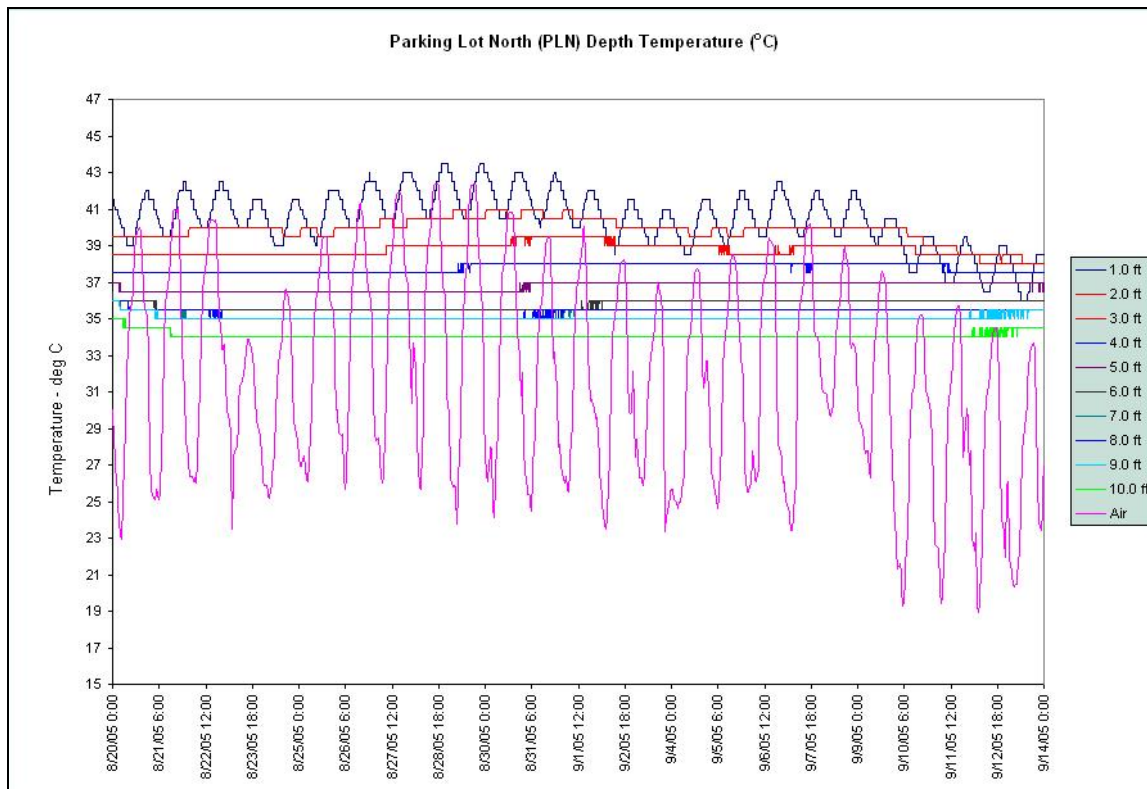
Figure 28 Deep ground temp data collected from August 20, 2005 to September 14, 2005 at ASU parking lot.

Table 5 Ground temperatures with respect to depth

Depth m (ft)	Temperatures ^{o}C (^{o}F)
0.000 (0)	Varying
0.305 (1)	Varying
0.610 (2)	40 (104)
0.914 (3)	39 (102)
1.219 (4)	38 (100)
1.524 (5)	37 (98)
1.829 (6)	36 (96.5)
2.134 (7)	35.5 (96)
2.438 (8)	35 (95)
2.743 (9)	34 (93)
3.048 (10)	33.5 (92)

Thermophysical properties of paving materials

Developing reliable tools for predicting transient heat transfer within pavements is dependant on accurate material property data. While the physical and mechanical properties have been extensively researched and their relationship to material selection and mix design is readily available (Mamlouk & Zaniewski, 2005), such detailed study of the relationships between paving thermal properties and mix designs has been relatively limited. Thermal properties, including thermal conductivity, specific heat capacity and thermal diffusivity, have become increasingly necessary for pavement modeling programs for a variety of purposes. Several models have been developed to understand the cooling rate of pavement during construction of concrete and asphalt pavements (Corlew & Dickerson 1968; Jordan & Thomas 1976; Wolfe et al. 1980; Highter & Wall 1984). In these studies, researchers have relied on the thermal properties to estimate the time available for compaction and curing as a function of the environmental parameters (wind speed, incident solar radiation, humidity, and air temperature) above the surface and soil conditions below the pavement. Others have focused on moisture settling, ice formation and internal stresses due to the freeze-thaw conditions in pavements located in colder regions (Dempsy & Thompson 1970; Samonsen et al. 1997; Phukan 1985). Historically, these models were developed for determining the impact of environmental effects on the engineering performance of pavements. Recently, however, urban climate studies have revealed the significant impact of pavements on the environmental conditions within cities (Pomerantz et al. 2000; Golden et al. 2005; Golden & Kaloush 2006; Bhardwaj 2006). This resulted in an increased interest in determining the contribution of pavements in relationship to the Urban Heat Island effect (UHI). Given the many applications presented above, it is clear that thermal properties are essential to pavement material selection and design, construction techniques, maintenance and rehabilitation cycles, and urban climate studies.

In the following section, the thermal properties for a range of paving materials are presented based on previous research and literature. This will be followed by a description of the methodologies and equipment used for the determining physical and thermal properties of paving materials as well as new results and experimentation obtained from the NCE laboratories.

Perhaps the most noted accomplishment during this study is the development of a novel test procedure for measuring thermal conductivity using cylindrical cores. A description of this technique is included in the laboratory section.

Thermophysical properties defined

Analyzing the thermal behavior of urban materials requires understanding the thermophysical properties of matter that govern thermal phenomenon. There are two distinct categories of these properties, those related to transport of energy through a system and those related to the thermodynamic, or equilibrium state of a system (Incropera and DeWitt, 1996). Transport of energy through a system, also referred to as heat transfer, occurs by three modes, radiation, conduction and convection. Transport properties relating to radiative heat transfer such as albedo and emissivity that were discussed earlier in Chapter 2 are presented again in great detail here. The rate coefficients that govern conduction and convection heat transfer are also discussed in this section. The thermodynamic properties differ from transport properties in that they are concerned with the equilibrium state of a system. These properties include density, ρ, and specific heat, c_p, that form the basis for such terms as volumetric heat capacity and thermal diffusivity. These properties and terms are discussed in further detail in the sections below.

Albedo

Thermodynamics tells us that a portion of radiation, incident to a pavement surface, will be absorbed by the surface and increase its thermal energy. The rate at which this energy is absorbed per unit surface area is dependant on the absorptivity, α_{abs}, of the surface material (Incropera and DeWitt, 1996). In other words;

$$G_{abs} = \alpha_{abs}G$$

Where,

G_{abs} = total radiation absorbed by the surface per unit area
G = total radiation per unit area incident to the surface
α_{abs} = absorptivity of the surface

The radiative property α_{abs}, ranges from 0 to 1; 0 implies that no energy is absorbed by the surface. Most opaque (transmittance = 0) surfaces have an $\alpha_{abs} < 1$ which means some of the incoming radiation to the surface is reflected. The rate at which energy is reflected by the surface is known as the albedo, β, of the surface. Mathematically this can be described as follows;

$$\beta = 1 - \alpha_{abs}$$

More simply, the albedo is the ratio of electromagnetic radiation reflected to the radiation incident to a surface. It takes into account the full spectrum of solar radiation and not just those in the visible range. Very often, high albedo is related to lighter shades of colors. This is true to a point however, a more complete analysis is required to determine the true albedo of a given surface. The American Society for Testing and Materials (ASTM) describes methods for determining solar reflectance in the following standards; ASTM E 903, ASTM E 1175, and ASTM E 1918. Albedo is regarded as the most important factor in the mitigation of urban heat island effect in urban centers (Rosenfeld et al.,1995).

Emissivity

A portion of the thermal energy contained within a pavement is constantly being emitted as radiation back into the atmosphere. The rate at which the energy is emitted per unit area is referred to as the surface emissive power, E (Wm^{-2}) (Incropera and DeWitt 1996). The maximum emissive power of any surface is governed by the Stefan-Boltzmann law;

$$E_b = \sigma T_s^4 \quad (6)$$

Where,

E_b = the total emissive power of a blackbody or ideal radiator
σ = Stefan-Boltzmann Constant = 5.67 x 10^{-8} W/m^2*K^4
T_s = absolute temperature (K)

A real surface does not completely radiate all of its energy like that of a blackbody. Therefore, the power emitted from a real body is determined by the following equation (Incropera and DeWitt, 1996);

$$E = \varepsilon \sigma T_s^4$$

Where,

ε = the emissivity of the surface
E = the emissive power of a real body with emissivity ε

Emissivity values are very useful for estimating how efficient a surface can emit energy relative to a blackbody. The emissivity of a surface greatly depends on the surface material and its finish. For instance, a polished copper surface will have a very low emissivity close to 0.06 while rough surfaces such as PCC or ACC in most cases is greater than 0.92 (FLIR, 2003). Thermal emissivity can be measured using ASTM E 408, ASTM C 835, and ASTM C 1371.

Thermal Conductivity

As mentioned earlier, heat transfer in an urban area occurs as conduction, convection or radiation. Conductive heat transfer is a result of energy transfer from the more energetic particles of a substance to the less energetic particles due to the random interactions of atom at the molecular level (Incropera and DeWitt, 1996). Heat transfer processes can be described using rate equations. In the case of conduction, the Fourier's Law is applied. For a one dimensional plane this conduction equation is expressed as (Incropera and DeWitt, 1996);

$$q_x{}'' = \frac{-kdT}{dx}$$

Where,

$q_x{}''$ = heat flux (W/m2)

$\dfrac{dT}{dx}$ = temperature gradient through a surface in the x direction

k = the thermal conductivity $(Wm^{-1}K^{-1})$

Thermal conductivity is the rate constant that governs the heat flux through a body. It is a transport property characteristic of the material. Many different factors play a role in the thermal conductivity of a given material. In most cases, involving pavement materials, thermal conductivity values are not easily available in the literature. These thermal transport characteristics have never been of much concern during paving applications. In addition, the thermal conductivity of a pavement is generally dependent on the type of mix, the aggregates

used, percentage of each component in the mix, and its level of compaction. At the time of this study, there was a very limited amount of information published on the correlation between these mix characteristics and the resulting thermal conductivity of in-place pavement. For this reason it is important that extensive testing is conducted when estimating the thermal properties for pavement materials.

Density

Density, ρ, is widely used in thermal analysis. It is the measure of mass per volume of a substance. Mathematically it is expressed as;

$$\rho = \frac{m}{V}$$

     Where,
          m = the mass of the material
          V = volume of the material
Density is typically given in units of kgm^{-3} or $lb_m ft^{-3}$.

Specific Heat

Specific heat, c_p, is also a very important property used in thermodynamics. It is defined as the amount of heat energy required to raise the temperature of one gram of a substance by 1^oC. Common units of specific heat are $Jkg^{-1}K^{-1}$ and $Btulb_m^{-1 o}F^{-1}$.

Volumetric Heat Capacity

When the density and specific heat of a substance is multiplied together, ρc_p, they form the volumetric heat capacity ($Jm^{-3}K^{-1}$) of the substance (Incropera and DeWitt, 1996b). The volumetric heat capacity quantifies the ability of a material to store thermal energy. Most substances that have large densities also have small specific heats which counter act each other. So, in instances where good energy storage is required, substances having equally large densities and specific heats are valuable (Incropera and DeWitt, 1996b). Volumetric heat capacity is a very important term when trying to understand and estimate the hysteresis lag potential of urban materials. An ideal material for this situation, where thermal storage is not desired, might have both a low density and low specific heat.

Thermal Diffusivity

The ratio of thermal conductivity to the volumetric heat capacity is an important property used in heat transfer analysis. This property, termed thermal diffusivity, α, is the ability of a material to conduct heat relative to its ability to store heat energy (Incropera and DeWitt, 1996b). Mathematically it is expressed as;

$$\alpha = \frac{k}{\rho c_p}$$

Where,
      α = thermal diffusivity
      k = thermal conductivity
      ρ = density
      c_p = specific heat

The common unit for thermal diffusivity is m^2 s^{-1}. The thermal diffusivity enables one to estimate how a material will behave under certain conditions. For instance, a material having a very large α will respond quickly to thermal changes than a material of small α. And therefore, the smaller the material's α, the longer it will take to reach an equilibrium state.

These thermodynamic properties, in combination with the transport coefficients mentioned earlier, play a very significant role in the thermal behavior of pavements in regards to the urban heat island effect.

Porosity and Permeability

The porosity of a material is commonly defined as the ratio of the volume of pores in a substance to its total volume (Somayaji, 2001). This term is widely used when talking about groundwater transport through soils however the same concept can be applied to permeable pavements that are being used for storm water management in parking lots and sidewalks (Cahill, 1994). Porosity is an important design consideration when permeability is desired.

Permeability is commonly defined as the ability of a surface material to allow the fluids such as rainwater to move through it (Somayaji, 2001). The majority of HMA and PCC pavement designs limit the transport of water through them. The more porous a pavement, the greater probability that the voids are interconnected, and the more permeable it is. Permeability is also important factor when considering surface energy fluxes. Permeable areas such as exposed soil and grass landscaping are often cooler during the day because of their ability to transform incident solar radiation into latent heat (Taha, 1997b). Non permeable pavements lack this ability, therefore increasing the thermal energy that becomes stored in the material.

Published values for thermal properties of pavements and their constituent materials.

The thermophysical properties of common pavement materials, such as PCC and HMA, are summarized in Table 6. The table provides common values for these pavements, soil properties for both wet and dry conditions, as well as the material constituents: binders, aggregates, water, and air.

Laboratory investigation techniques

The thermal and physical properties of concrete pavement materials were measured for several different samples. Material samples were obtained from a variety of sources including concrete suppliers, construction projects, and laboratory prepared at Arizona State University. The flow chart in Figure 29 describes a typical path followed for testing. This flow chart extends beyond just thermal and radiative property testing and describes the mechanical testing, which is often part of the sequence as well.

Table 6 Published thermal properties of pavements and their constituents materials. DFG, Dense Fine Grade; DCG-Dense Coarse Grade; AR OGFC-Asphalt Rubber Open Grade Friction Course.

		Density ρ [kg m^{-3}]	Specific Heat c [J kg^{-1o}C^{-1}]	Heat Capacity ρc [kJm^{-3o}C^{-1}]	Thermal Conductivity k [W m^{-1o}C^{-1}]	Thermal Diffusivity $\alpha = k/\rho c$ [m^{2}s^{-1}] x 10^{-6}
Pavement Mixes						
Portland Cement Concrete (PCC)	(stone mix)	2300	880	2024	1.40	0.69
	(light weight aggregates)	1280	840	1075	0.54	0.50
Hot Mix Asphalt (HMA)	DFG	2238[+]	921[+]	2061	1.21[+]	0.59
	DCG	2100[#]	866[#]	1819	2.00[#]	1.10
	AR OGFC	2160[*]	805[*]	1739	0.40[^]	0.23
Constituent Materials						
Binders	asphalt cement	2115	920	1946	0.06	0.03
	portland cement	1920	-	-	0.29	-
Aggregates	sand	1515	800	1212	0.2-1.0	0.165 - 0.825
	granite	2630	775	2038	2.79	1.37
	marble	2680	830	2224	2.80	1.26
	rubber, soft	1100	2010	2211	0.13	0.06
Air and Water	air	1.161	1007	1.170	0.03	22.13
	water	996	4178	4161	0.62	0.15
Subgrade Materials						
Soil	dry	1500	1900	2850	1.00	0.35
	wet	1900	2200	4180	2.00	0.48

[+]Corlew,1968; [#]Chadbourn,1998; [^]Caltrans, 2003; [ξ]Bentz, 2001; [*]unpublished; all other values from Çengel, 2003

Flow Chart for Material Samples

New Material

Collect Material Info

Thermal & Radiative Properties
(Flat Plate Method)

Are flat plate specimens appropriate for this mix design?

Yes

Manufacture Flat Plate Samples
Minimum Quantity = 4
Dimensions = 1" x 12" x 12"

ID, Label & Photograph Samples

Measure & Weigh

Reflectivity & Emissivity
(Spectrophotometer, FT-IR)

Porosity Test

Permeability Test

Thermal Conductivity (*k*)
(2 Installs x 2 Thermal Cycles) per Sample ID

No

Manufacture Cylindrical Samples
Minimum Quantity = 12
Dimensions = 4"d x 8"

ID, Label & Photograph Samples

Measure + Weigh

Porosity Test

Permeability Test

Thermal Testing
(Cylindrical)

4   Divide Samples   6

Cut Height to 6 inches
Drill 7/16" Center hole

Specific Heat Capacity (c)
2 Runs per Sample ID

Thermal Conductivity (*k*)
(2 Installs x 2 Thermal Cycles) per Sample ID

2

For Display

Mechanical Testing
(Cylindrical)

2   Modulus Testing, E & E*

2   Confined and Unconfined Compression Tests

Thermal-Physical Testing
(Cylindrical)

2   Coefficient of Thermal Expansion (CTE)

Mechanical Testing
Thermal Properties

The NCE on SMART
Material Properties Database

Figure 29 Flow chart of Physical, Mechanical, and Thermal testing of materials at the National Center of Excellence at Arizona State University.

Most testing methodologies employed by the center follow testing standards as defined by the American Society of Testing and Materials (ASTM). However, a new test method for measuring thermal conductivity was developed during the course of this study and is described later in this section. A brief description for relevant test properties including a brief description of the test setup and procedure for determining each property is presented in the next sections.

Specimen Geometries

Material samples described in this study include cylindrical cores (diameter and heights vary) and flat plates (12"x12"x1"). Both geometries can be used for testing the physical and thermal properties however cylinders are preferred for mechanical testing and flat plates are preferred for radiative testing. The flow chart in Figure 29 shows testing sequences for both types of concrete specimen geometries. The majority of testing conducted at the center use cylindrical samples as these are the most commonly available specimens in the pavement industry. Figure 30 presents an ideal testing process chart for cylindrical samples. The testing is grouped by Physical, Mechanical, and Thermal Testing.

Physical Properties Testing

Density, air voids, and permeability

Specimen's dimensions, density, and % air voids are determined. These properties are often good indicators for the permeability, and sometimes the thermal behavior of the mix. The sequence is performed as follows;

1) MEASURE SAMPLE GEOMETRY
The dimensions of each sample are measured using digital Vernier calipers after the ends were cut so that the top and bottom are parallel.

2) HEAT SAMPLE TO REMOVE MOISTURE
The weight of each sample is recorded before heating to determine their 'as is' mass. The samples are then heated in an oven at 80°C for 24 hours to remove any moisture that may be trapped within.
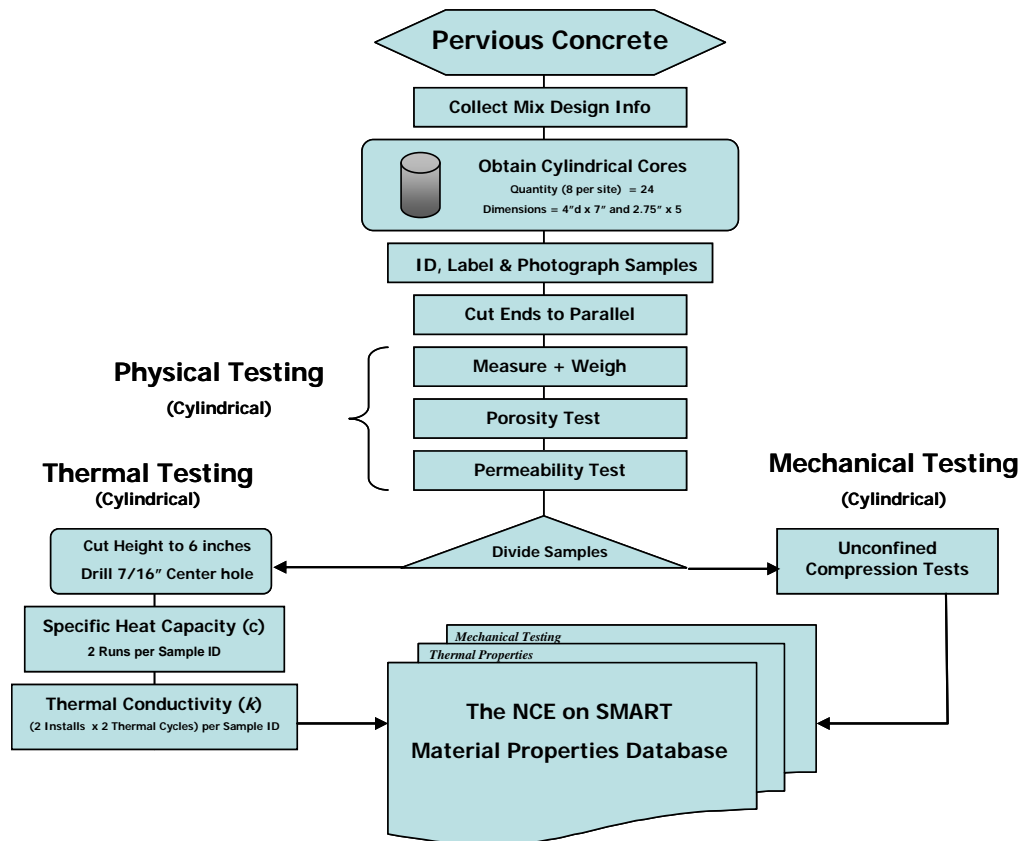
Figure 30 Testing flow chart for cylindrical samples received by the National Center of Excellence at Arizona State University.

3) OVEN-DRY MASS MEASUREMENT
Immediately following removal from the oven the samples are weighed. The resulting dry weight, designated in this procedure as A, is then compared to their original weights to verify whether moisture had been lost. In most cases there is less than 5 grams change in sample mass.

4) IMMERSED MASS MEASUREMENT

The samples are then submerged into a water bath of approximately 19°C (66.2°F). While keeping the samples submerged they were rotated slowly several times in all directions over a two minute period to be sure that all air bubbles had been removed and the sample were totally saturated (Figure 31). This step is especially important for porous materials such as pervious concrete which have many pockets where air can remain trapped. The submerged samples are then weighed using a basket that was suspended under a digital scale as shown in Figure 32. This value is referred to as the immersed apparent mass and is designated as D.

Figure 31 It is important to remove trapped air from within sample until completely saturated.

a)   b)
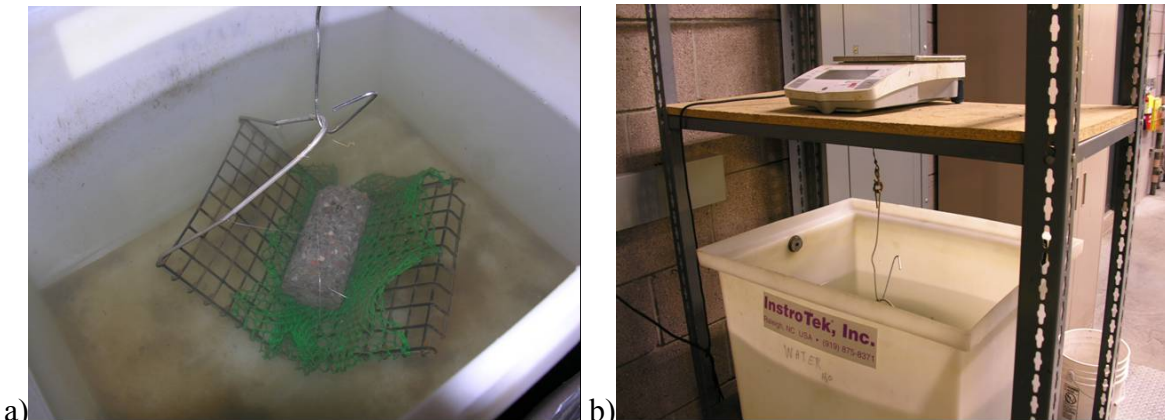
Figure 32 a) Saturated sample is weighed using a basket in the water bath. b) Scale and water bath used to measure the immersed mass of sample.

5) SATURATED MASS MEASUREMENT AFTER IMMERSION

After the immersed mass measurement is recorded, it is important that the samples remain submerged to maintain their complete saturation. In this step the objective is to measure the saturated sample out of water to determine the mass of water that is contained within the material. In porous materials with high air void contents polystyrene is wrapped tightly around the circumference of each cylinder wall while still under water. Next, while still submerged, an elastic material, in this case a balloon is used to cap the top and bottom of each cylinder. This

combination adequately traps the water within the sample. Figure 33 below shows a completely sealed specimen.

Figure 33 A sample is sealed underwater using polystyrene and elastic rubber caps.

Once the sample surfaces is sealed, it is quickly removed from the water bath, then wiped down with a dry cloth to remove excess water on the outer surface, then dropped in a water tight plastic bag as shown in Figure 34a. The bag containing the saturated sample is then placed on the scale (Figure 34b). The mass of the bag and wrapping is subtracted from this measurement resulting in the saturated mass designated as B for this procedure. This step is performed a minimum of two times to insure a consistency.

a)   b)
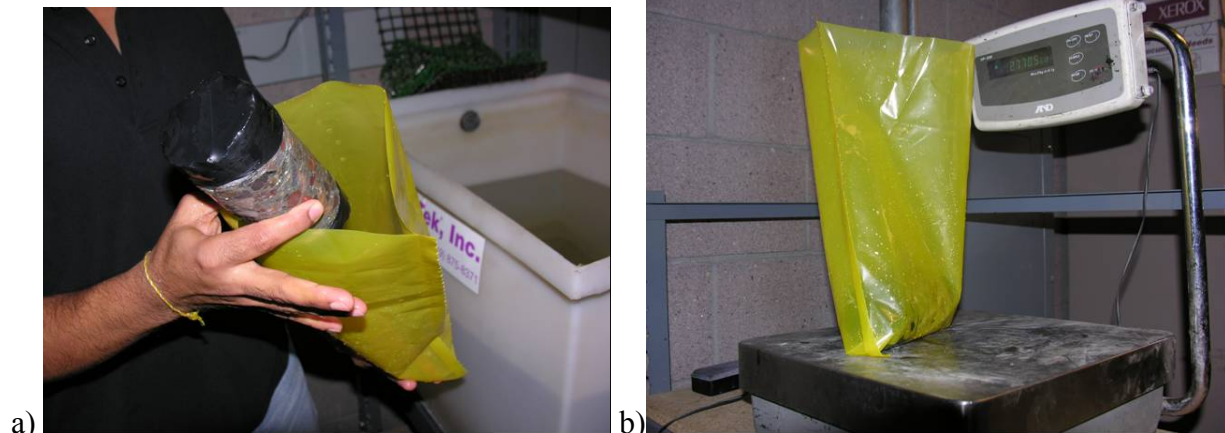
Figure 34 a) The sealed saturated sample is towel dried and place in a water proof bag; b) The saturated sample being measuring on the scale.

6) CALCULATING AIR VOIDS (POROSITY)

Porosity is synonymous with the percentage of voids within the sample by volume. The previous three steps that determined values A, D and B are all essential to calculation of porosity. In accordance with ASTM Standard C 642-97: *Standard Test Method for Density, Absorption, and Voids in Hardened Concrete* the porosity of each sample is determined using the following equation;

$$\text{Volume of permeable pore space (voids)}, \% = \frac{B - A}{B - D} \times 100$$

Where,
A = dry weight (step 3)
B = saturated Mass (step 5)
D = immersed apparent mass (step 4)

7) LABORATORY PERMEABILITY

The second part of the physical testing has to do with permeability, or the rate at which water flow through the material. Common units for permeability are cm/s (in/hr). This is commonly referred to as hydraulic conductivity in geotechnical engineering and is determined using a similar procedure. Both indoor and outdoor (field) testing can be performed to determine permeability. The indoor test uses a modified constant head permeameter. In this set up the sample cylinder is confined in the radial axis by a positive air pressure applied against an impermeable membrane. Next a constant fluid pressure is applied to the top using a pump and the rate at which the water flows through the specimen cross section is the permeability.

8) FIELD PERMEABILITY

The 'in place' permeability of a concrete pavement can be measured using a falling head field permeameter. This device, pictured to the right was devised and tested at the National Center for Asphalt Technology (NCAT) for measuring permeability of open graded asphalt pavements. The device is constructed of a series of acrylic graduated cylinders decreasing in diameter at each additional level. The bottom surface is sealed around the edges using plumber's putty to fill the voids near the surface preventing water from exiting in the radial direction. Once the permeameter is secured on the concrete surface and the edges are adequately sealed several weights are applied the edges of the base plate. Next, water is poured through the top using a funnel. The water is stopped when the water inside the permeameter reaches the top cylinder. Using a stop watch the rate at which the water level drops within the permeameter is measured. For surfaces with low permeability the cylinders with smaller diameters are used while the large cylinders are used for faster rates of permeability. This type of flow is not truly one dimensional so the rate is adjusted based on the thickness of the pavement. The coefficient of permeability is calculated using the following equation;

Figure 35 Field permeameter.

$$k = \frac{a \cdot L}{A \cdot t} \ln\left(\frac{h_1}{h_2}\right)$$

Where,
k = coefficient of permeability
a = inside cross-sectional area of standpipe, cm^2 (varies with each tier)

L = length of the sample, cm (depth of pavement)
A = cross-sectional area of permeameter through which water can penetrate the pavement, cm^2.
t = elapsed time between h_1 and h_2.
h_1 = Initial head, cm.
h_2 = Final head, cm.

Mechanical Property Testing

This portion of the testing is performed in the Structures Lab at Arizona State University. The test is performed in accordance with ASTM C 39 *Standard Test Method for Compressive Strength of Cylindrical Concrete Specimens*.

Thermal Properties Testing

Determination of Specific Heat of Paving Materials

One main objective as part task for this study was to obtain the *specific heat* of commonly used paving materials and to recommend a simple laboratory test procedure in order to calculate the same. Specific heat, c_p of a material can be defined as *the amount of heat required to raise the temperature of a material by one unit* and it can be measured in the units of J/kg ^{o}C or J/kg ^{o}F.

ASTM C 351

The specific heat of materials can be experimentally determined using ASTM C 351-92b *Standard Test Method for Mean Specific Heat of Thermal Insulatio*n (Figure 36). A material with known mass and known high temperature is immersed in a known mass of calorimetric fluid (in this case, water) with known temperature and the equilibrium temperature is determined. The heat gained by the water is equated to the heat lost by the material and thus the specific heat of the material is calculated.
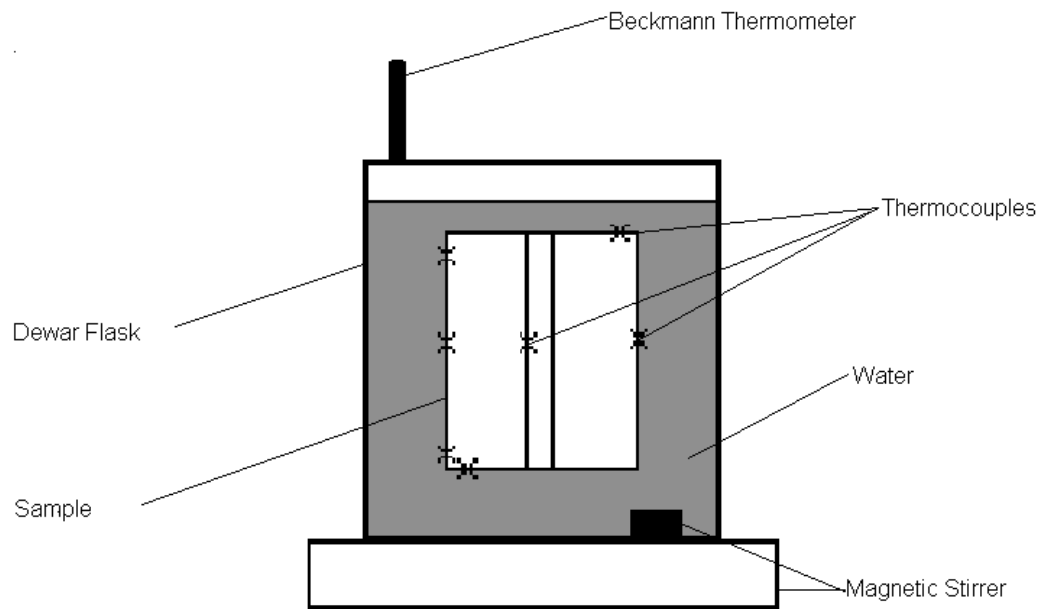
Figure 36 Schematic of experimental setup for determining specific heat

Deviations to the equipment used in this study:
1. Dewar Flask: The capacity of the flask used in the current experiment is larger than that used in the ASTM C 351 as a larger sample size is used.
2. Heater: In the ASTM C 351 procedure, a heater is used to heat the sample. The current procedure uses a convection oven in order to heat the sample.
3. Capsule: A brass hollow cylinder is used in the ASTM C 351 as a capsule and the specimen is enclosed in this capsule. The current procedure does not use a capsule and the specimen is directly immersed in the water.

Equations used:
The equation used in the ASTM C 351 accounts for water equivalent because of the capsule used. The procedure uses a simpler equation taken from the Law of Conservation of Energy in thermodynamics.

Specific Heat Standard:
ASTM C 351 uses *electrolytic copper* (390 J/kg ^{o}C) as the specific heat standard. In the current experiment aluminum (903 J/kg ^{o}C) was used as the specific heat standard as it was close to the specific heat of the materials being tested.

44

Equipment

1. <u>Dewar Flask:</u> The Dewar flask acts as a calorimeter. The capacity of the flask must be not less than 3.8 *l* and not more than 4 *l*. The internal diameter of the flask has to be greater than 5 ½ inches to ensure allowance for the sample and the Beckmann differential thermometer. The internal depth of the flask has to be greater 9 inches. The Dewar flask reduces the heat losses from the mixture very significantly.
2. <u>Beckmann Differential Thermometer:</u> A sensitive thermometer with a sensitivity of 0.01 ^{o}C and a range of at least 5 ^{o}C should be used to measure the temperature change. The thermometer needs to be calibrated before use and the procedure for which is in section 6.
3. <u>Magnetic Stirrer:</u> A magnetic stirrer with a stirring pill is to be used in order to keep the temperature of water uniform and it helps reducing the formation of a temperature gradient within the flask.
4. <u>Thermocouples:</u> T-type thermocouples are used and mounted on the sample, flask wall and water. The T-type absolute thermocouples have a sensitivity of 0.5 ^{o}C.
5. <u>Weighing scales:</u> A weighing scale with a sensitivity of 0.001g should be used to measure the weight of the sample and water.
6. <u>Oven:</u> A convection oven is preferred to a gravity oven. Convection oven provides more uniform heating of the specimen.
7. <u>Data Acquisition System:</u>

The cylindrical sample has to be drilled through the center to create a hole of diameter 5/32 inch. After the insertion of the thermocouple into this hole, cement paste is to be used to fill up the hole. T-type Thermocouples need to be mounted onto the sample at various locations shown in Figure 36. In order to mount the thermocouples, Arctic Alumina, a thermal adhesive, can be used. To read the water temperature a thermocouple needs to be immersed in the water; also a thermocouple must be mounted on the flask wall.

General Testing Procedure

1. Measure the mass of the sample (m$_s$) and the water (m$_w$) required for the experiment to the nearest 0.001 kg. (Use approximately m$_s$ = m$_w$). (Figure 37).

Figure 37 Each sample is weighed dry before testing begins and between repeat tests to verify that all moisture has been removed from the specimen.
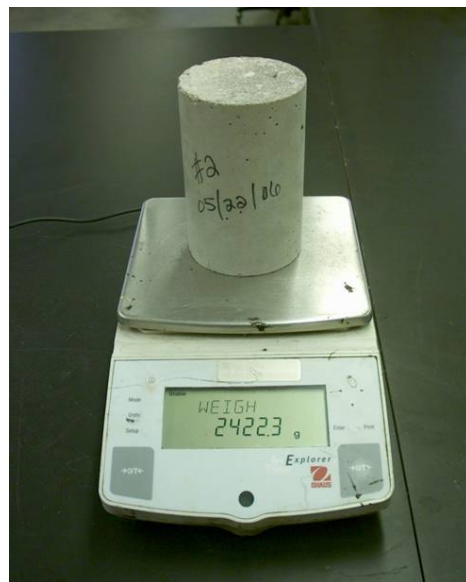
2. Place the sample in the oven and heat it to a temperature of 50°C (122°F) (T_s) (Figure 38). Care must be taken to make sure that the entire sample has been heated uniformly

Figure 38 Convective oven used for heating suspended material specimens.

3. After placing the flask with water on the magnetic stirring plate, measure the initial temperature of water (T_w) and the temperature of the flask wall (T_f).
4. Immerse the sample in to the flask. Caution must be taken to minimize the heat loss while immersing the sample into the flask. The temperature of the sample (T_s) should be the one at the point of immersion. (Figure 39).

Figure 39 a) Immersing heated specimen into insulated flask. b) View of fully immersed specimen as it reach equilibrium with water temperature.

5. Determine the temperature of the entire mixture after an equilibrium state is attained (T_m). The change in temperature of the water is recorded on Beckmann thermometer.

Calculation of specific heat (c_p)

$$c_{p,s} = \frac{m_w c_{p,w} \Delta T_w + m_f c_{p,f} \Delta T_f}{m_s \Delta T_s}$$

Where,

$c_{p,s}$ = Specific Heat of the sample, kJ/kg $^{\circ}$C
m_s = Mass of the sample, kg
ΔT_s = Temperature difference of the sample, $^{\circ}$C
  = $T_s - T_m$
$c_{p,w}$ = Specific Heat of the water, kJ/kg $^{\circ}$C
m_w = Mass of the water, kg
ΔT_w = Temperature difference of the water, $^{\circ}$C
  = $T_m - T_w$
$c_{p,f}$ = Specific Heat of the glass coating of the flask, kJ/kg $^{\circ}$C
m_f = Mass of the glass coating of the flask, kg
ΔT_f = Temperature difference of the flask, $^{\circ}$C
  = $T_m - T_f$

Uncertainty Analysis

An experimental uncertainty analysis was conducted to estimate the uncertainty of the values determined using this apparatus and methodology. The analysis used the base equation and the values in Table 7.

$$c_{p,s} = \frac{Q_{total}}{m_s \Delta T_s}$$

Where,

$c_{p,s}$ = Specific heat of the sample specimen
Q_{total} = the combined thermal energy gain of the water (w) and flask (f)
m_s = dry mass of the sample
ΔT_s = the change in temperature of the sample during the experiment

Table 7 Standard values used during the evaluation of uncertainty.

Parameter	Variable	Equipment	Approx. Value	Approx. Error
Temperature	T_s	Type T	50 ^{o}C	0.5 ^{o}C
	T_m	Beckmann Thermometer	26 ^{o}C	0.001 ^{o}C
	T_f	Type T	20 ^{o}C	0.5 ^{o}C
	T_w	Type T	20 ^{o}C	0.5 ^{o}C
Mass	m_s	Weighing Scale	2.5 kg	0.001 kg
	m_w	Weighing Scale	2.5 kg	0.001 kg
	m_f	Weighing Scale	1 kg	0.001 kg
Constant	c_w	-	4.186 kJ/kg ^{o}C	-
	c_f	-	0.8 kJ/kg ^{o}C	-

The uncertainty of the specific heat, Uc_s, determined using this apparatus is presented mathematically as;

$$U_{c_s} = \sqrt{(\frac{\partial C_s}{\partial Q_{Total}} \times U_{Q_{Total}})^2 + (\frac{\partial C_s}{\partial m_s} \times U_{ms})^2 + (\frac{\partial C_s}{\partial T_s} \times U_{\Delta Ts})^2}$$

Where,

$$Q_{Total} = Q_w + Q_f$$

$$U_{Q_{Total}} = \sqrt{(U_{Q_w})^2 + (U_{Q_f})^2}$$

$$U_{Q_w} = \sqrt{(\frac{\partial Q_w}{\partial m_w} \times U_{m_w})^2 + (\frac{\partial Q_w}{\partial T_w} \times U\Delta T_w)^2}$$

$$U_{Q_f} = \sqrt{(\frac{\partial Q_f}{\partial m_f} \times U_{m_f})^2 + (\frac{\partial Q_f}{\partial T_f} \times U\Delta T_f)^2}$$

Using the standard values given in Table 7 the uncertainty was determined using these equations. The uncertainty of the apparatus was thus +/- 0.024kJ/kg^{o}C or approximately 2.4% of the anticipated values for concrete materials.

Results for Specific Heat

A variety of pavement materials; conventional and modified were tested using the method described above. For each material type at least two cylinders of the same mix were run multiple times. This allowed for a 95% confidence interval to be determined for each material. The results of this investigation are shown in Table 8.

Table 8 Experimental results for specific heat of various concrete materials.

Material	Symbol	Mean Specific Heat (J/kg°C) c_p	Sample Size n	Standard Deviation (J/kg°C) S	95% Confidence (J/kg°C) $C_{95\%}$	
Portland Cement Concrete	PCC	1016	8	32	22	2.2%
Crumb Rubber Modified Portland Cement Concrete	CRPCC (80)	1055	4	74	73	6.9%
(lbs rubber per yd³)	CRPCC (160)	992	4	42	41	4.1%
	CRPCC (240)	956	4	56	55	5.7%
Plastic Fiber Modified Portland Cement Concrete	PF PCC (0)	964	8	33	23	2.3%
(%Content)	PF PCC (3)	997	8	33	23	2.3%
	PF PCC (5)	977	4	22	22	2.2%
	PF PCC (8)	971	4	24	23	2.4%
Hot Mix Asphalt Concrete	HMA	987	4	16	16	1.6%
Gap Graded Asphalt Concrete	GGAC	977	4	63	62	6.3%
Asphalt Rubber Open Grade Friction Course	AR OGFC	875	4	23	22	2.6%

There are several interesting trends in the results. The samples of Portland cement concrete resulted in a mean specific heat of 1016 ±32 J/kg°C (95% Confidence) which was higher than the published value for concrete (840 - 880 J/kg°C) given in Table 6. It is expected that the specific heat of denser concrete mix would have a larger specific heat however more testing is required to understand the true variability in concrete mixes. Next, a the Portland cement concrete samples with varying contents of crumb rubber particles were evalauted. Each mix contained a different amount of crumb rubber (pounds) per cubic yard of concrete. The specific heat seemed to decrease as more crumb rubber was added to the mix. The specific heat of the fiber reinforced concrete specimens did not seem to be affected by the amount of fibers added to the mix (pounds per cubic yards). The three asphalt concrete specimens test results and variations were consistent with the values reported in Table 6.

Thermal conductivity

Thermal conductivity, *k*, is defined from Fourier's law of heat conduction,

$$\frac{Q}{A} = -k\frac{dT}{dx}$$

where *Q/A* is the steady-state conduction heat flux (W m^{-2}), and *dT/dx* the steady-state temperature gradient (Cengel, 2005). The unit most commonly used for *k* is W m^{-1}°C^{-1}.

In the above formula *Q/A* is the heat flux which is causing the thermal gradient of *ΔT/t*. The measurement of thermal conductivity, therefore, always involves the measurement of the heat flux and temperature difference. Where the measurement of the heat flux is done directly (for example, by measuring the electrical power going into the heater), the measurement is called absolute. Where the flux measurement is done indirectly (by comparison), the method is called comparative.

In all cases, the entire heat flux must be one dimensional, that is it has to flow through the sample (and the references, in the comparative case). Thus, the heat losses or heat gains must be minimized in the radial direction. To some degree, this can be accomplished with packing insulation around the sample, or, at higher temperatures, where such simple solutions become inefficient, with installation of a "guard". If the guard is controlled to have the identical temperature gradient as the sample, then the radial heat flow will be minimized.

The configuration of a given measurement system and of the specimen itself is influenced most prominently by the magnitude of the thermal conductivity. When the thermal conductivity is high, the specimens are usually "long" (for example, in the form of cylinders). When the conductivity is low, the specimens are usually "flat" (for example, in the form of plates or disks). Simple thermal considerations indicate why this is so. When the specimen conductivity is high, the heat flux is usually fairly high so that, relatively speaking, heat losses from the large lateral surface area of the specimen are small; a long specimen in the direction of flow helps establish a reasonably high temperature gradient which can then be accurately measured. When the specimen conductivity is low and the heat flux correspondingly low, only a relatively small thickness is required to generate a large, accurately measurable gradient. With this low specimen heat flux, lateral losses are of concern, thus a plate-type specimen itself tends to minimize these unwanted flows since the lateral surface area is small. As a matter of fact, in some cases the lateral surfaces of the specimen are surrounded by pieces of the same specimen material to provide self-guarding. Another independent parameter of fundamental importance is the magnitude of specimen conductivity relative to the surroundings. It is generally desired that the specimen effective conductance be as high as possible relative to that of the surrounding insulation. This generally becomes more of a problem as the temperature of the measurement system rises. With some measurement techniques used at very high temperatures, the lateral losses are allowed to be high, but they are accounted for quantitatively in the conductivity measurement.

Guarded Hot Plate Method (ASTM C 177)

The method adopted for measuring the thermal conductivity of paving materials is ASTM C 177-04 Standard Test Method for Steady-State Heat Flux Measurements and Thermal Transmission Properties by Means of the Guarded-Hot-Plate Apparatus (referred to here as the Guarded Hot Plate Method). The procedure established in ASTM C 177-04 employs a guarded heated section to create an adiabatic region that limits transverse heat loss.

ASTM C 177-04 widely used method for measuring the thermal conductivity of insulations. A flat, electrically heated metering section surrounded on all lateral sides by a guard heater section controlled through differential thermocouples, supplies the planar heat source introduced over the hot face of the specimens. The most common measurement configuration is the conventional, symmetrically arranged guarded hot plate where the heater assembly is sandwiched between two specimens. In the single sided configuration, the heat flow is passing through one specimen and the back of the main heater acts as a guard plane creating an adiabatic environment.

This is an absolute method of measurement and its applicability requires: (a) the establishment of steady-state conditions, and (b) the measurement of the unidirectional heat flux in the metered region, the temperatures of the hot and cold surfaces, the thickness of the specimens and other parameters which may affect the unidirectional heat flux through the metered area of the specimen. Three different categories of measurement systems can be distinguished: apparatus working around room temperatures, apparatus working below room temperatures (down to about -180°C), and apparatus working at high temperature (600°C or above).

Experimental Design
The Fourier's law of heat conduction can be rewritten in terms of thermal conductivity (*k*) as,

$$k = \frac{Qt}{A\,\Delta T}$$

Where,

       k = thermal conductivity through the material.
       Q = power required for heating the material (Figure 40).
       t = thickness of the specimen material being considered.
       A = exposed area of the specimen to the heater.
       ΔT = temperature difference across the thickness of the specimen.
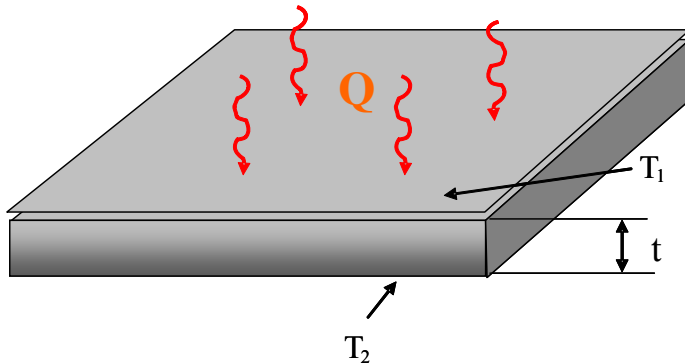
Figure 40 Simple diagram of one dimension heat transfer through a flat plate specimen.

There are two ways of measurements involved in determining the final result, they are:
Direct Measurements: These are the measurements that are obtained by the direct readings from the experiment. For example, the variables like temperature, thickness of the specimen are obtained from direct measurements.
Indirect Measurements: These are the variables that involve measurement of the parameters related to them. For example, the variables like power required for the heater is determined through the measurement of current *I* and voltage *V*. They are related by the following equation,
$Q = IV$

The second example, the second variable is the area *A* of the exposed surface to the heater, which in turn is determined by the measurement of the length *L* of the exposed surface to the heater. The equation is given as follows,
$A = L^2$
In the current experiment, the heat flow is restricted in one direction only. A diagram of the components for the experiment is shown in Figure 41 below.
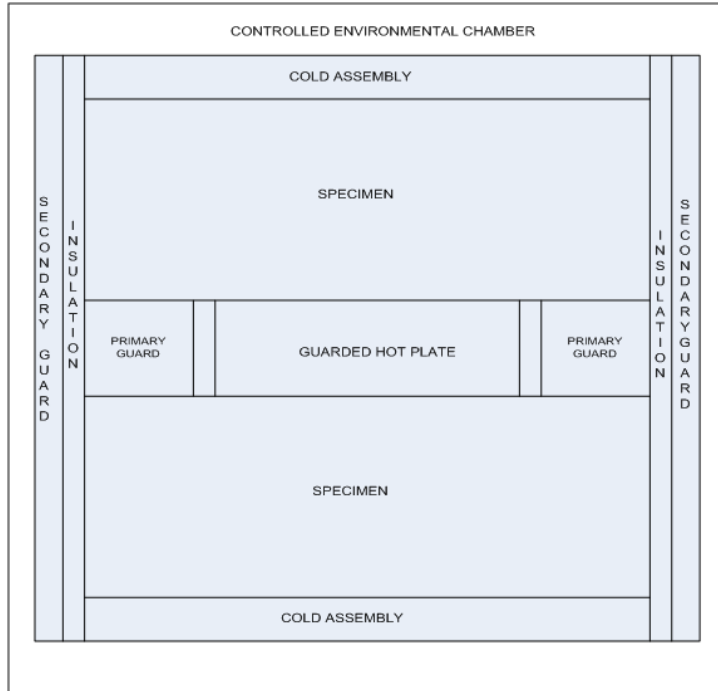
Figure 41 Setup for ASTM C 177-04 the Guarded Hot Plate Method

Uncertainty Analysis

    The uncertainty of the experimental test method was conducted for the guarded hot plate method. The thermal conductivity k is the dependent variable and the independent parameters are the power Q given to the heater, Area A of the heater exposed to the specimen, thickness t of the specimen and the temperature difference ΔT across the thickness of the specimen.

The combined uncertainty, $U(k)$, of these independent variables can be can be calculated using the propagation of uncertainty equation,

$$U^2(k) = \left[\frac{\partial f}{\partial i}*U(i)\right]^2 + \left[\frac{\partial f}{\partial v}*U(v)\right]^2 + \left[\frac{\partial f}{\partial(t)}*U(t)\right]^2 + \left[\frac{\partial f}{\partial A}*U(A)\right]^2 + \left[\frac{\partial f}{\partial(\Delta T)}*U(\Delta T)\right]^2$$

    Therefore, after substituting the respective values the equation we end up with a combined uncertainty of $0.1168 \mathrm{Wm^{-1}K^{-1}}$

$$U(k) = \sqrt{(6.43e-3) + (5.9e-4) + (3.97e-7) + (1.96e-4) + (6.43e-3)}$$

$$U(k) = 0.1168 Wm^{-1}K^{-1}$$

    To decrease the uncertainty, we measured the voltage directly using a more accurate voltmeter resulting in smaller uncertainties for the current and voltage values; $U(I) = 0.01$ amps and $U(V) = 0.01$ volts. The uncertainty using these values results in a combined uncertainty of $0.081 \mathrm{Wm^{-1}K^{-1}}$,

$$U(k) = \sqrt{(6.43e-5) + (5.9e-6) + (3.97e-7) + (4.57e-4) + (6.43e-3)}$$

$$U(k) = 0.081 Wm^{-1}K^{-1}$$

Table 9 gives the values of the measurements along with the uncertainty of the equipments and the thermal conductivity.

Table 9 Two cases for the uncertainty observed in the final result

Current, I	U(I)	Voltage, V	U(V)	Thickness, t	U (t)	Area, A	U(A)	Temp. gradient, ΔT	U(ΔT)	Thermal conductivity, k	U(k)	% U(k)
[amps]	[amps]	[volts]	[volts]	[m]	[m]	[m2]	[m2]	[°C]	[°C]	[Wm^{-1o}C^{-1}]	[Wm^{-1o}C^{-1}]	%
2	0.10	6.6	0.1	0.0254	1E-05	0.0522	4.57E-04	4	0.2	1.28	0.117	9.1%
2	0.01	6.6	0.01	0.0254	1E-05	0.0522	4.57E-04	4	0.2	1.28	0.081	6.3%

There are some significant factors that contribute to the final result of the thermal conductivity, they are:

- CURRENT AND VOLTAGE: Power supply given to the heater which, in turn depends on the current and the voltage generated. In order for more accurate results the resolution of the instrument should be very high.
- SAMPLE AREA: The area that is calculated from the measurement of the length is also very significant in contributing to the uncertainty of the result. Therefore, it is necessary to measure the dimensions of the exposed area as accurate as possible.
- TEMPERATURE GRADIENT Measuring the temperature drop across the sample thickness is the most important variable and can introduce the largest about of uncertainty. T-type Thermocouples were used because they have a Seebeck coefficient of $43\mu VK^{-1}$.

Experimental Setup

The guarded hot plate apparatus is used in measuring the thermal conductivity of the materials with flat specimens. Figure 42 shows the system diagram and general illustration of the complete experiment.
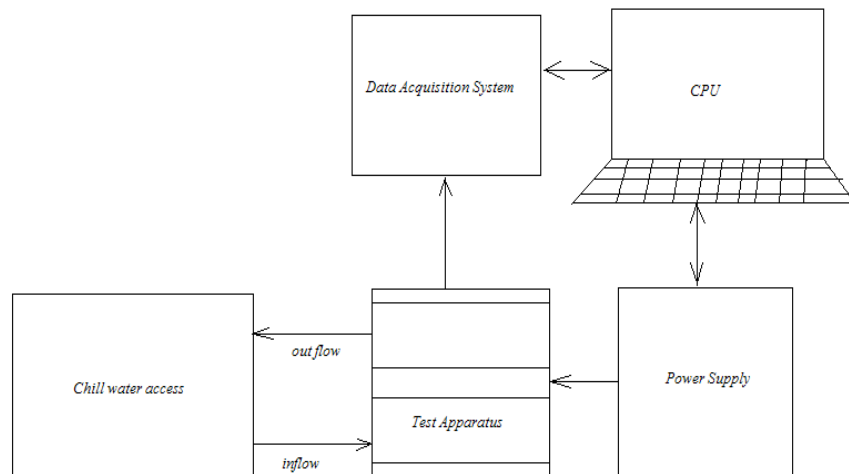
Figure 42 System diagram for the guarded hot plate experiment.

The experimental system is comprised of the following components,

- *Test Apparatus:* This is the main setup of the experiment. The setup consists of the heaters, specimens and the heat sink. In this setup the thermal conductivity is determined by passing heat through the specimen with the help of heaters.
- *Power Supply*: This unit is responsible for heating the specimen by the heater to the required power. The power supply is dual power supply for the main guarded heater and the other for the primary guarded heaters. Power supply is controlled by the computer, based on data from the temperature recordings.
- *Chilled water access*: This unit is responsible for dissipating the additional heat generated from the setup. In this unit the chilled water is allowed to run through the heat sink; this water then takes the heat which help's in maintaining a constant temperature difference across the test setup. Water that is entering through the inlet of the heat sink is then let out through the outlet.
- *Data Acquisition System* (DAQ): The data that is collected from the various parts from the setup like the temperature recordings, power input etc; these are stored in the data acquisition system. The DAQ is connected to the computer for retrieve the data that was recorded.
- *Computer*: The computer is used in data retrieving from the test setup and also in controlling the power that is supplied to the heater. The program that is used in this experiment is LabView™. This program helps in data collection at the various required points with in the setup.

The test apparatus is comprised of three subassemblies

- Hot Surface Assembly
- Cold Surface Assembly
- Data Acquisition System (DAQ)

The setup of the experiment with the above components is illustrated in Figure 43 below,
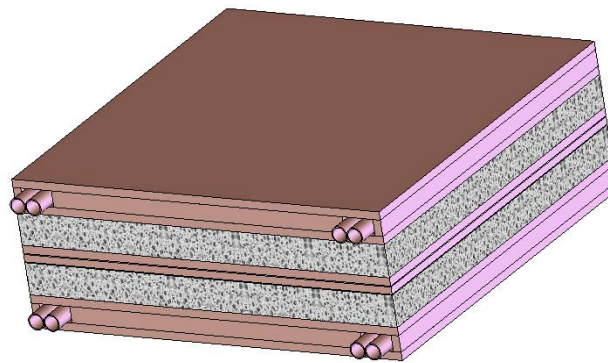
Figure 43 CAD drawing of test apparatus including the heated, cold assemblies and two identical material samples.

In the above drawing, the main heater is sandwiched in between two samples. The guarded heater is surrounded by the primary guarded heaters with an air gap between the two; this air gap is known as isothermal region. The guarded heater is thermally isolated from the primary guards.

54

Further, the heat that is liberated from the heaters and conducted through the sample is dissipated by placing a heat sink (cold surface assembly) which considerably reduces the heat that is being liberated. The description of the components is given as follows (Figure 44),
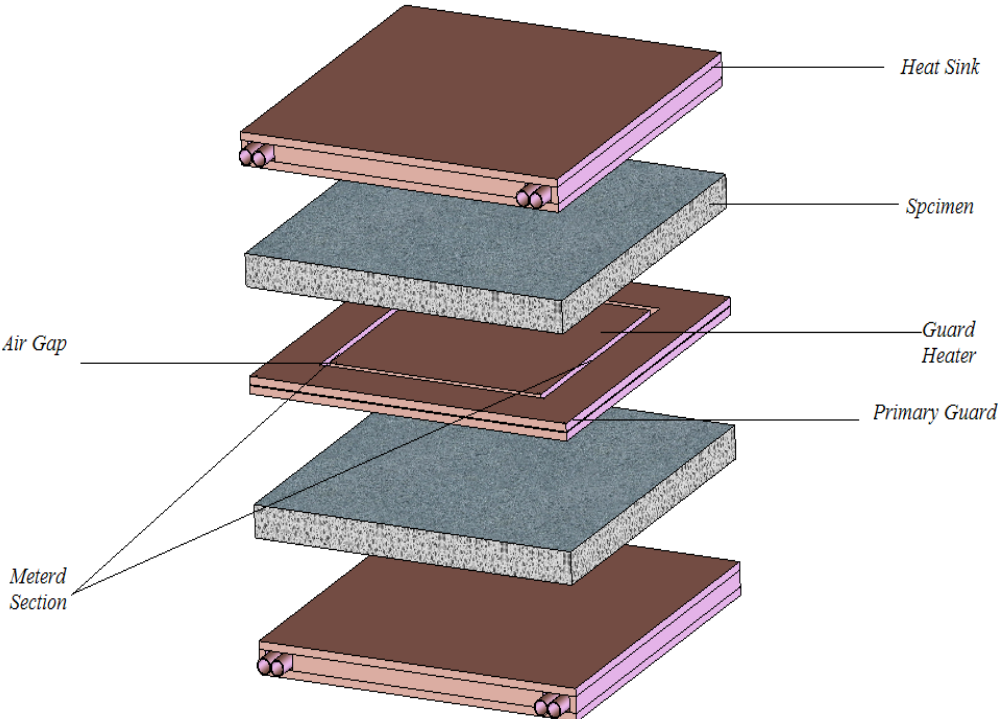
Figure 44 Exploded view of subassemblies within the test apparatus.

Hot Surface Assembly

There are two heaters, the main heater and the guard heater that surrounds it. The following Figure 45 illustrates the description of the heater section.

Primary
Guareded
Heaters

Guarded
Heaters
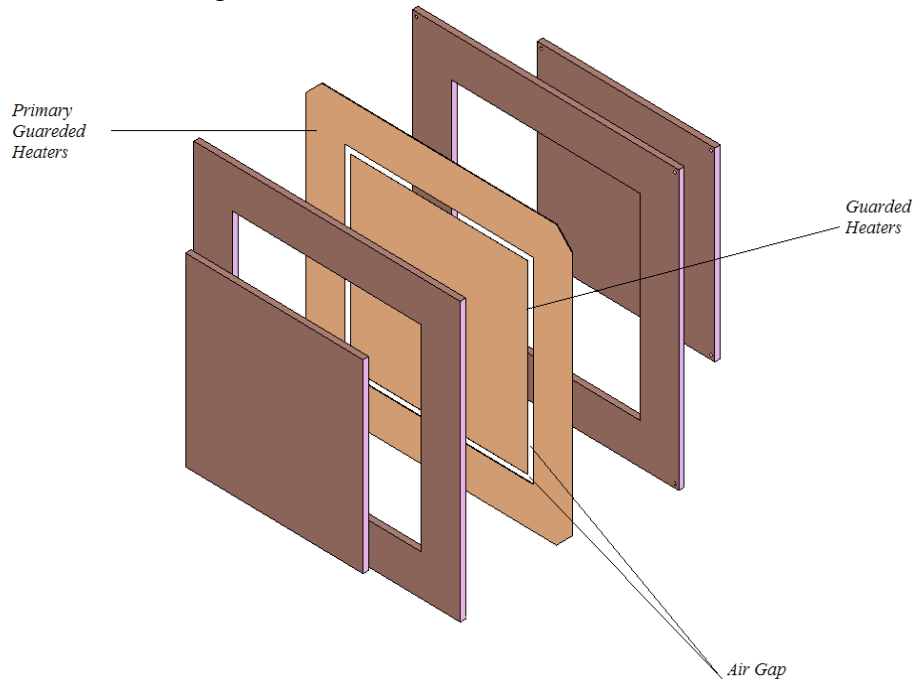
Air Gap

Figure 45 Exploded view of the two sets of heaters and copper plates.

In the above diagram the guarded hot plate is surrounded by the primary guard heat. The air gap between the two heaters is the isothermal region. The guarded hot plate provides the power (heat flow per unit time) for the measurement and defines the actual test volume, that is, that portion of the specimen that is actually being measured. The function of the primary guard is to provide the proper thermal conditions within the test volume to reduce the lateral heat flow within the apparatus. The guarded and the primary heaters, thin etched resistance heaters (Figure 46), are sandwiched in between the copper plates.
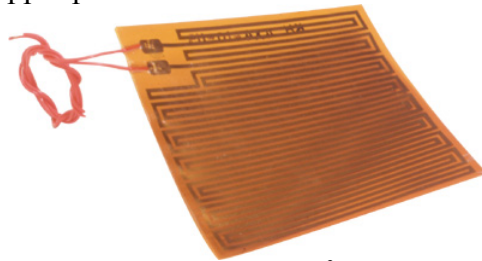
Figure 46 Kapton thin etched resistance (5W/in^2) heater used for guarded heater.

The copper ensures a good distribution heat through out the specimen area that is being measured. The heat transfer diagram shown in Figure 47 below describes the flow of energy within the heated assembly.
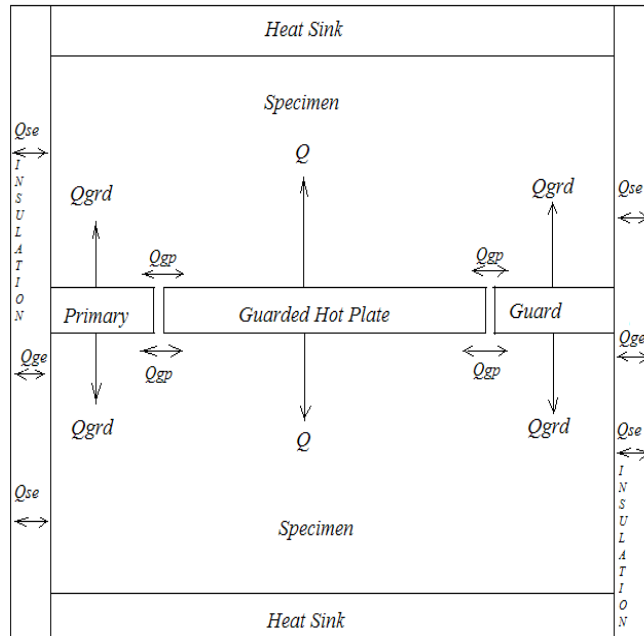
Figure 47 Heat flow diagram in the test apparatus

In the above figure,

Q = heat flow in the metered section

Q_{grd} = guard heat flow through the specimen

Q_{gp} = lateral heat flow rate across the air gap

Q_{se} = edge heat flow between specimen and the controlled environment

Q_{ge} = lateral edge heat flow between primary guard and the controlled environment.

When the experiment is being run; the temperature difference between the metered section surface plate and the primary guard surface plate shall not exceed 0.2K. The surfaces of the metered and primary guard surface plates that are in contact with the test specimen shall be treated to maintain a total hemispherical emittance greater that 0.8 over the entire range of the operating conditions.

Cold Assembly (heat sink)

A heat sink is an environment or object that absorbs heat from another object. Chilled water is flowed through pipes in a copper plate assembly as shown in Figure 48. The governing equation in the design of the heat sink is as follows,

$$Q = mC_p\Delta T$$

Where,

Q = power required for the heater (13.2 W)

m = mass flow rate through the heat sink

C_p = specific heat capacity of water (4200 J/kg^{0}C)

ΔT = temperature difference across the heat sink from inlet to outlet (3^{0}C)

The heat sinks are generally categorized as air-cooled and liquid-cooled heat sinks. The air flow means of air-cooled heat sinks includes natural convection and forced convection and the convective approach of liquid-cooled heat sinks includes forced convection water and heat pipe construction.
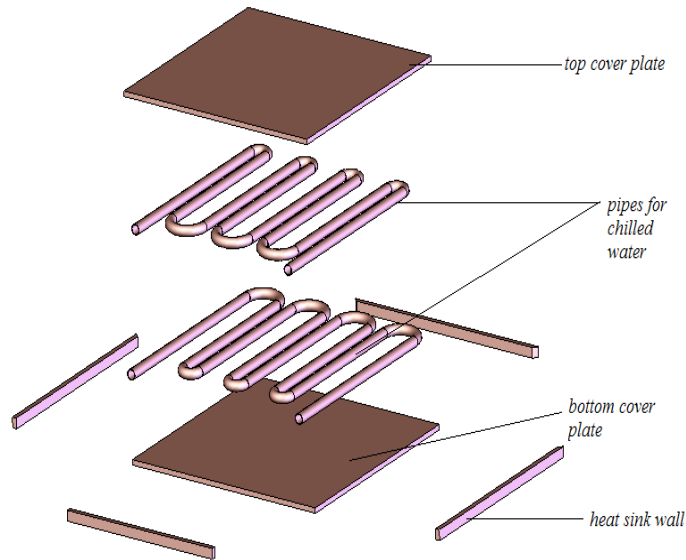
Figure 48 Heat sink assembly design

The figure above shows the piping arrangement for the chilled water to run through the heat sink. The two pipes are arranged in such a manner that the two pipes are nested together on one of the plates. Both heats sinks use an identical design.

Data Acquisition System
The function of this system is to acquire data from the test setup when the experiment is in function. The main data acquisition system consists of temperature sensors, volt/amp meters, a data logger/controller.
Temperature measurement - When the experiment is run the temperature readings are very much necessary for the test setup to be in control and to maintain a steady state condition through out the experiment. Further, the temperature recordings are measured using the standard type T thermocouples (Figure 49). These thermocouples have an accuracy of $\pm 0.2^0C$.
Volt/amp meter - The electrical power supplied to the heaters is measured in terms of current and voltage using voltmeter. The power supplied is to the guarded heater and the primary guards. The power required for heater is 26.4Watts for heating the both the specimens.
Datalogger/controller - The data from temperature recordings and the power units are recorded by a National Instruments SCXI 1000. A test program developed in LabVIEW™ manipulates, records, and displays the data while the experiment is running. The power supplies are also controlled using the LabVIEW™ to maintain the isothermal region between the main heater and guard heater.

Experimental results

The results of this work will be presented as a separate technical paper after all testing of concrete samples have been completed. The test results for the materials obtained from CTL will be included however they do not fall within the specific deliverables of this project.

● **Thermocouple locations**
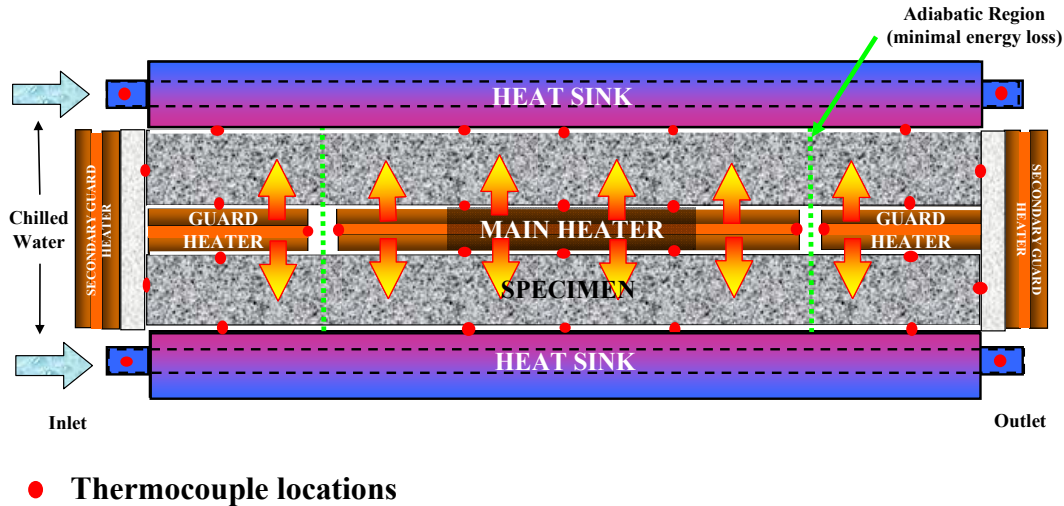
Figure 49 Diagram of complete test assembly indicating important energy and mass flows through the system.

Cylindrical Method

As mentioned previously, the standard procedure for measuring thermal conductivity is ASTM C 177-04. This method requires the temperature at steady state to determine *k* and mandates slab specimen geometries. It is not recommended for highly inhomogeneous materials as the size of aggregates in a pavement layer can sometimes exceed 25 mm (1 in.). Specifying plate thicknesses that are considerably larger than the maximum aggregate diameter in the mix will cause non-uniform heat flux through the material. To maintain one-dimensional conduction heat transfer through a slab of 25 mm (1 in.) thickness would require sides of at least 30 cm (12 in.) or more. These large dimensions present several difficulties in the fabrication of laboratory asphalt or concrete samples. In addition, obtaining this size of pavement specimen from in-service pavement would disturb a large section of the pavement and entail additional costs to traditional materials sampling techniques.

Mechanical testing standards for determining moduli of paving materials require *cylindrical* samples to be laboratory fabricated or extracted by coring in-service pavements (Witczak et al, 2002). A typical specimen size is 100 mm (4 in.) in diameter and 150 to 200mm (6 to 8 in.) in height. Quality control of materials at concrete project sites often requires material samples be made to verify the appropriate modulus or compressive strength characteristics (Mamlouk & Zaniewski, 2005). Asphalt concrete quality is determined by measuring the compaction density using a nuclear gauge or by obtaining cored samples from the actual pavement. Volumetric properties are verified by collecting specimens at the project site and then replicating the compaction process in the laboratory (Witczak et al, 2002). It is estimated that thousands of samples per year are taken during paving construction projects and at mix plants as part of their

quality control operations. Therefore, the amount of cylindrical testing samples available is significant. Utilizing common sample geometries for determining thermal properties would simplify the addition of thermal properties testing as part of an overall materials testing regime. The objective of this part of the study was to develop a test method for accurately measuring the thermal conductivity of pavement materials using a cylindrical specimen geometry commonly used for mechanistic testing of paving materials. This new experimental method will allow thermal and mechanical properties to be determined from identical material geometry with minimal additional preparation. This section presents the theoretical basis for the experimental design, a thorough experimental uncertainty analysis, and results for a known material sample and for two types of commonly used pavement materials.

Methodology
An important factor when measuring thermal conductivity in materials is establishing a one-dimensional heat flow. One-dimensional conduction heat transfer is achieved relatively easily through a homogeneous and highly conductive material and can be measured with minimal edge losses and minimal non-uniform heat transfer through the monitored surface area. When measuring materials that are of low conductance (insulators) such as pavement it is more difficult to establish one-dimensional heat transfer. The procedure established in ASTM C 177-04 employs a guarded heated section to create an adiabatic region that limits transverse heat loss. Even with a guarded heated section a nonhomogeneous material may not yield a uniform heat flux. For instance, if a slice of pavement is thinner than the largest aggregate diameter the heat energy will transfer more quickly through the aggregate section than through the section that is almost entirely binder. This uneven spread of heat will result in the surface temperature measurement being highly dependent on the location of the sensor. To compensate, a larger thickness would be required so that any surface or cross section of a pavement slab will have a uniform amount of binder, air, and aggregate. The resulting combination of these constituents, each with their own thermal properties, will more accurately represent the behavior of the entire composite. For the purpose of this study, an appropriate thickness for a specimen is one that is at least twice the diameter of the material's largest aggregate size. To achieve this thickness and also reduce edge losses in slab geometry a large area is required. ASTM C 177-04 specifies a minimum width-to-thickness ratio of 3 to 1. Obtaining this large material sample in plate or slab geometry from an in-service pavement may be difficult and costly, making it impractical for many paving materials.
A cylindrical geometry can be used to solve several of these problems. By embedding a heat source from end to end through the axis of a cylinder of material the desired ratio of thickness to heated surface area can be obtained. By thermally isolating the top and bottom of the cylinder, losses can be reduced such that uniform one-directional heat flow in the radial direction can be achieved. The following section describes the theoretical basis for this type of arrangement.

Theoretical Analysis
This type of heat transfer design can be analyzed for steady-state conditions using fundamental heat transfer equations. Figure 50 presents the heat transfer diagram used for this analysis.
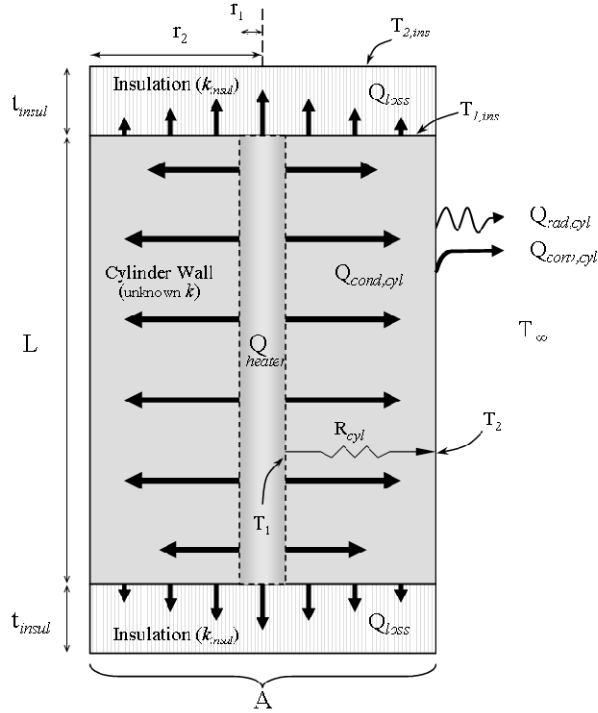
Figure 50 Heat transfer diagram for theoretical analysis.

The steady-state heat conduction solution for a tube with heat source in the central axis and of infinite length;

$$\dot{Q}_{cond,cyl} = \frac{T_1 - T_2}{R_{cyl}} \tag{1}$$

The heat transfer rate through the cylinder wall, $\dot{Q}_{cond,cyl}$, can be calculated at steady state if the surface temperatures of the inner wall, T_1, and of the outer surface, T_2, and the equivalent thermal resistance of the cylinder wall, R_{cyl}, are known. According to (Cengel, 2002), R_{cyl} is a function of the radii r_2 and r_1, the total length of the cylinder, L, and the thermal conductivity, k, of the wall material:

$$R_{cyl} = \frac{\ln(r_2 / r_1)}{2\pi L k} \tag{2}$$

Substituting equation 3 into equation 2 yields

$$\dot{Q}_{cond,cyl} = 2\pi L k \frac{T_1 - T_2}{\ln(r_2 / r_1)} \tag{3}$$

While the above relationship is appropriate for cylinders of infinite length, the real world requires that energy losses be accounted for. In the diagram shown in Figure 50, the majority of undesired heat loss will occur in the top and bottom of the cylinder. The conservation of energy equation for the system becomes

$$\dot{Q}_{cond,cyl} = \dot{Q}_{heater} - \dot{Q}_{loss} \tag{4}$$

61

where $\dot{Q}_{heater}$ is the total power supplied to the heat source and $\dot{Q}_{loss}$ is the rate of energy lost through the top and bottom of the cylinder. If the heat source is assumed to be a resistance heater the total power in the heater is the product of the voltage, V, and current, I, in the circuit.

$$\dot{Q}_{heater} = V \times I \tag{5}$$

The heat loss through the axial direction is estimated using the temperature difference through the insulation layer of thermal conductivity, k_{insul}, thickness, t_{insul}, and the circular area of contact, A:

$$\dot{Q}_{loss} = k_{insul} A \frac{T_{1,ins} - T_{2,ins}}{t_{insul}} \tag{6}$$

Solving equation 3 for k leads to

$$k = \frac{\dot{Q}_{cond,cyl} \ln(r_2 / r_1)}{2\pi L (T_1 - T_2)} \tag{7}$$

Substituting equations 4, 5, and 6 for $\dot{Q}_{cond,cyl}$ yields

$$k = \frac{\left[(VI) - k_{ins} \pi . r_2^{\,2} \frac{\left(T_{1,ins} - T_{2,ins} \right)}{t_{ins}} \right] \ln(r_2 / r_1)}{2\pi L (T_1 - T_2)} \tag{8}$$

This equation forms the basis for the experimental test design for cylindrical sample geometries. The following section will discuss how this theoretical analysis was developed into an experimental testing apparatus and then validated using an uncertainty analysis and experimental results.

Experimental Setup

The experimental test apparatus developed for this investigation comprises the test specimen, central heat source, insulation, temperature sensors, data acquisition system and environmental chamber (Figure 51). This section describes each of these components in detail and discusses the most important considerations when assembling the apparatus.
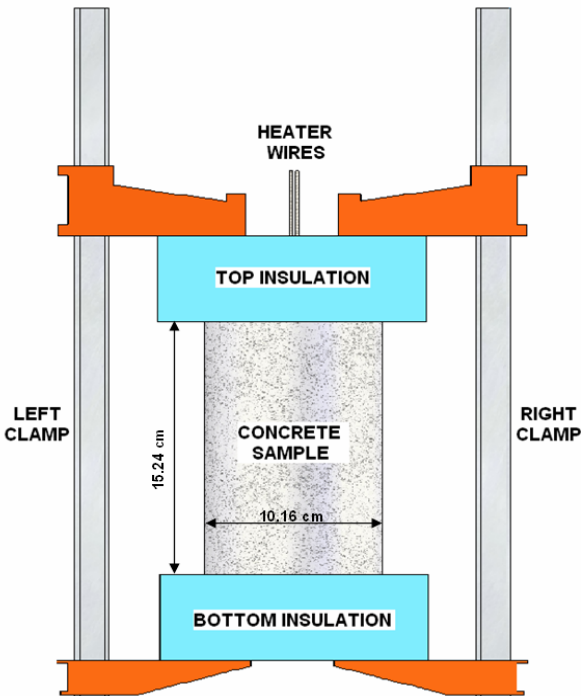
Figure 51 CAD rendering of testing apparatus.

Specimen preparation -The specimen geometry for this study specified a cylinder with diameter of 100mm (4in). A 11mm (0.437 in) diameter hole was drilled through the center. The height of the cylinders during this investigation was held constant at approximately 152mm (6 in), however, this can be increased depending on the length of the heating element. It is important that the hole be drilled completely vertical through the cylinder's axis and the inner walls are not excessively jagged or loose. Ensuring symmetry in the hole is critical to the uniform radial heat distribution from the heater. This can be achieved on a drill press or lathe for materials that can be drilled using standard cutting bits. When preparing Portland cement concrete and asphalt concrete samples it was necessary to use an 11mm (0.437 inch) diamond tip coring bit.

Heat source - The constant heat source applied to the core of the cylinder consisted of a 55 Ohm cartridge heater (FIREROD™, Part No. G6A83 - Watlow Electric Manufacturing Company, St. Louis, Missouri, USA) with dimensions of 152mm (6 in) length and 9.5mm (0.375 in) diameter (Figure 52). The cartridge heater is a cylindrical resistance heater with two lead wires. When a voltage is supplied across the heater wires heat is generated at the core and then transferred to the surface through a stainless steel outer sheathing. During this study the heater was controlled using a Protek™ P6000 programmable DC power supply capable of 0-30V and 0-3 amps. The cartridge heater was pressed into the cylinder during the apparatus assembly. The diameter of the heater was specifically designed to be 3mm (0.125 in) smaller than the hole's diameter to leave room for three different thermocouple wires. This gap made it possible to slide the heater in very smoothly, however, the air that remained between the inner wall and the heater sheath prevented heat from transferring uniformly to the specimen. To overcome this barrier the hole and heater were coated with a high thermal conductivity paste manufactured and distributed by Omega Engineering, Inc., product # OT-201-16 ($k = 10$ W m^{-1}°C^{-1}). The paste, consisting of silicon and metallic particles, filled the air gaps and greatly reduced the interface resistance between the two

surfaces. The paste never hardens and makes it possible to remove the heater after testing is completed.
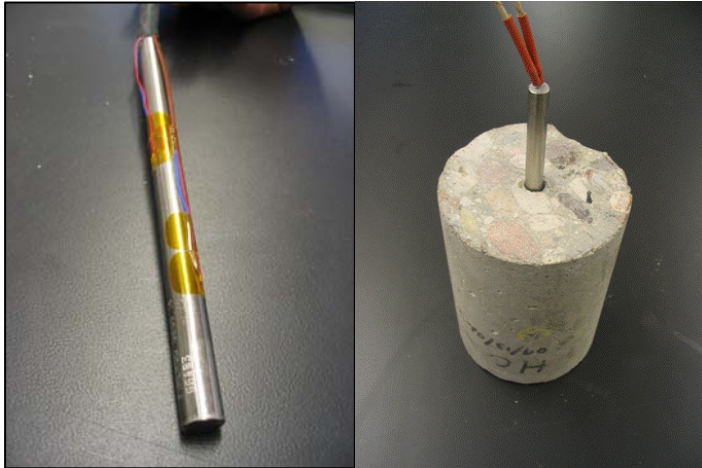
Figure 52 Cartridge heater with thermocouples attached. Example of inserting the heater into a concrete specimen.

To prevent excessive heat loss from the top and bottom surfaces of the sample during testing two layers of 25 mm (1 in) thick insulation (k_{insul} = 0.02 W m^{-1}°C^{-1}) were used. The insulation was secured with two large clamps, to prevent movement and to insure uniform contact with the top and bottom material surfaces.

Temperature sensors - The metered section of the testing apparatus utilized 30 gauge T-type thermocouples rated with an accuracy of 0.5°C (0.9°F). The surface temperature at eight different locations on each sample was monitored during the testing sequence. This included locations at the top, bottom, top outer side, bottom outer side, bottom inner surface, top inner surface, and heater sheath as shown in Figure 53. While most locations were monitored using absolute thermocouple configurations, there were two differential thermocouples used to measure the temperature difference between the inner and outer surfaces of the cylinder. Differential thermocouples improve the uncertainty of these values over the absolute method. Four additional absolute thermocouples not shown in Figure 53 measured the temperature at 25mm (1in) into the top and bottom insulation layers and the ambient air temperature surrounding the testing apparatus. The thermocouple tips were embedded in small surface indentions in the outer surface of the specimen and secured using a highly conductive (10 W m^{-1}°C^{-1}) silver adhesive. This method of attachment improved the accuracy and repeatability of measuring the true material surface temperature.
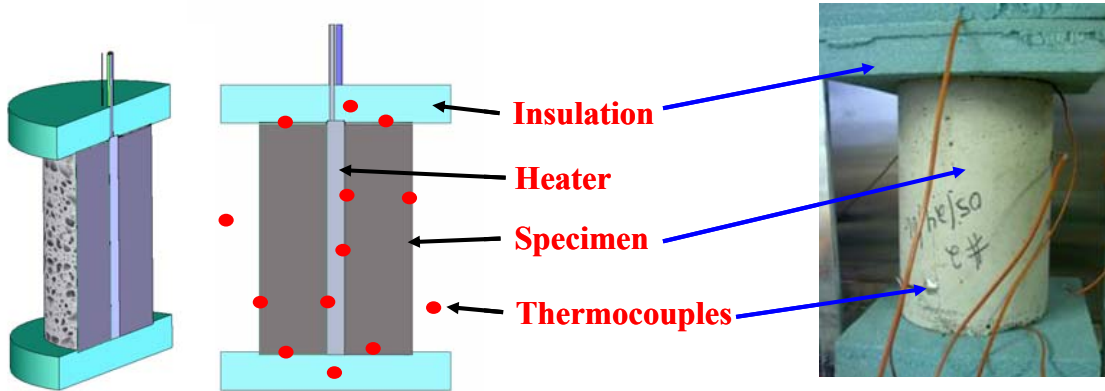
Figure 53 Cross section of specimen indicating the location of thermal couples.

The inner wall temperature was the most challenging to measure. The limited maneuverability within the hole, the stress applied by the heater as it is pushed into the hole and the heat transfer paste prevented the thermocouples from being easily attached to the inner wall using an adhesive. Attaching the thermocouples to the heater itself was not an option as it would measure the temperature of the metal sheath which was greater than the temperature of the inner wall of the specimen material due to the contact resistance between them. A device was created to overcome this adhesion problem. Figure 54 shows a thin strip of steel with flexible tabs to which the thermocouples were attached. The tabs created a spring action pushing the thermocouple directly into the inner wall as the cartridge heater is slid into the hole. The variation in the results that had existed before the tabs were implemented was greatly reduced. This improved the overall repeatability of the results between reassembly and disassembly of the apparatus. The locations of the inner wall thermocouples were staggered, one at 1/4L from the surface and one at 3/4L from the top surface. These two different locations were used to determine if the temperature distribution was relatively uniform through the sample in the axial direction.

Data acquisition - The data acquisition system consisted of a 32-channel cold junction compensation module which plugged into the SCXI data acquisition system by National Instruments® (Figure 54). The temperature information was recorded to a data file and displayed at a rate of 1 Hz. The thermocouples were calibrated using a purified ice bath and a temperature-controlled hot bath. The results of the calibration were very similar to the calibration sheet provided by the thermocouple wire manufacturer.

Environmental Chamber - The entire test setup was assembled and run within a 1.5 cubic meter environmental chamber manufactured by Industrial Process Controls, LTD. The chamber provided the heat sink for the experimental system by controlling the air temperature around the apparatus. The air surrounding the apparatus was maintained at 20°C and a small fan within the chamber provided enough air movement to prevent temperature stratification within the chamber. Figure 55 shows an infrared image of a concrete test specimen during a testing sequence
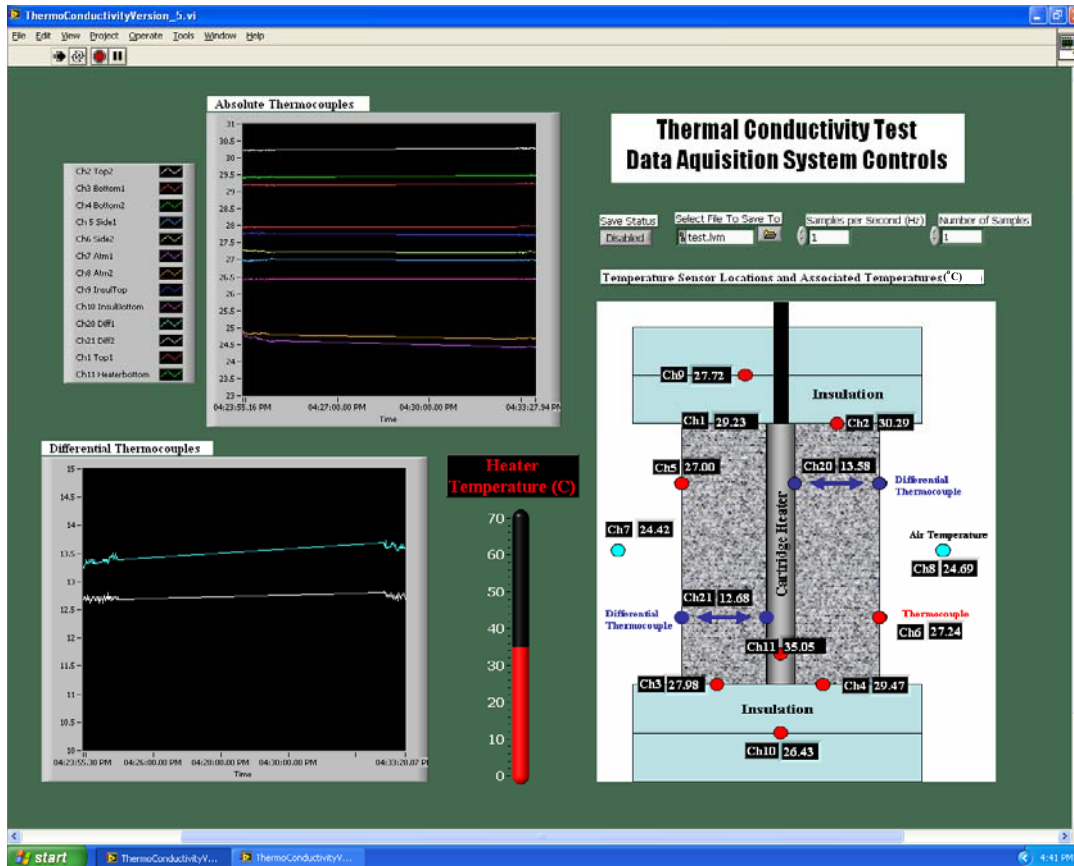
Figure 54 Screen capture of display that allows users to monitor and capture data in real time.
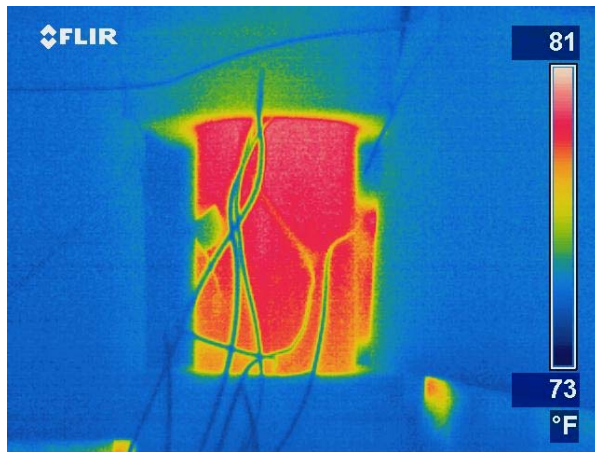
Figure 55 Infrared image of a concrete test specimen during a testing sequence. The colors indicated elevated temperatures on the surface.

Uncertainty Analysis

The systematic uncertainty for this experimental apparatus is ±0.021 W m^{-1}°C^{-1} which equates to a percentage error of nearly 4.7% for a k value of 0.44 W m^{-1}°C^{-1}. This implies that any value determined using this apparatus can range $\pm$ 4.7% around the calculated value. The column to the far right of Table 10 indicates that the most significant sources of uncertainty are the

66

differential temperature measurement, $T_{diff,avg}$, (57.2%) and the inner radius of the cylinder, r_1 (23.3%). The temperature gradient through the specimen wall is the most important parameter for determining thermal conductivity so it was expected that this measurement also constitutes over half of the experimental uncertainty. In order to reduce the uncertainty in this measured value, two sensors were used, hence $T_{diff,avg}$ represents the mean of these two sensors and the measured error of 0.35 is the propagated uncertainty of $T_{diff,\ avg}$. Adding additional differential thermocouples could improve this uncertainty as would the use of more accurate temperature sensors such as an RTD. Given the small size of the area between the heater and inner wall the research team decided to continue to use the 30-gauge T type thermocouples.

Results and Discussion
The results in this section include those measured for a reference specimen, ultra high molecular weight polyethylene (UHMWPE), a Portland cement concrete and asphalt cement concrete specimens. The purpose of these tests is to determine whether the new cylindrical test method can produce accurate and repeatable results for heterogeneous materials with relatively low thermal conductivity.

Accuracy of test methods - Ultra high molecular weight polyethylene, UHMWPE, was used as the 'known' reference sample because it has a low thermal conductivity range of 0.42 – 0.46 W $m^{-1}{}^{\circ}C^{-1}$ (Boedecker Plastics, Inc., 2007; San Diego Plastics, Inc., 2007) Eight separate runs were conducted for the UHMWPE sample. In between each run the test apparatus was completely disassembled and then reassembled. A single run typically required about 1.5 hours to reach steady state. For the purposes of this study, steady state was defined as when the temperature changes less than 1% over a 5-minute period.

The results for the UHMWPE sample runs indicated an acceptable repeatability between runs with a standard deviation of 0.012 W $m^{-1}{}^{\circ}C^{-1}$. The population mean of 0.441 W $m^{-1}{}^{\circ}C^{-1}$ with a total uncertainty $\pm$ 0.0217.W $m^{-1}{}^{\circ}C^{-1}$ ($\pm$ 4.9%) at 95% confidence falls within the values given by two UHMWPE suppliers. The mean, standard deviation, random uncertainty, systematic uncertainty, and total uncertainty were calculated as described in the methodology section and the results are provided in Table 11 for all three types of materials. It should be noted that the systematic uncertainty (0.021 W $m^{-1}{}^{\circ}C^{-1}$) for the UHMWPE is nearly three times the random uncertainty (0.008 W $m^{-1}{}^{\circ}C^{-1}$), indicating that the test method is accurate and repeatable within the uncertainty of the physical design.

A field-extracted core of PCC was obtained from U.S. Interstate 10 in Phoenix, Arizona. This sample was chosen because it represents a typical PCC pavements used for highways in Arizona. The specimen (bulk density of 2,857 kg m^{-3}) was run eight separate times. The results for the PCC specimen shown in Figure 56 had a larger range and nearly five times the standard deviation of the UHMWPE and HMA specimens. The mean of the experimental runs was 1.719 W $m^{-1}{}^{\circ}C^{-1}$ with a total uncertainty of $\pm$ 0.048 W $m^{-1}{}^{\circ}C^{-1}$ (2.8%) at 95% confidence. In this case the random uncertainty was larger than the systematic uncertainty. The increased variation between runs may be a result of the heterogeneity and larger aggregate size (37.5mm diameter aggregate) used in the PCC mix. This result falls within the available literature values for PCC of this density range, 1.37 -2.77 W $m^{-1}{}^{\circ}C^{-1}$ (Khan, M.I. 2002).

Table 10 Values for determining systematic uncertainty of the experimental design.

Variables	Symbol	Nominal Value	Units	Bias Error	Sensitivity Index	Contribution of Uncertainty	u^2	% of total uncertainty
Heater Voltage	V	18.92	Volts	0.01	4.86E-02	4.86E-04	2.36E-07	1.5%
Heater Current	I	0.350	Amps	0.001	2.63E+00	2.63E-03	6.91E-06	7.9%
Insul. Th. Cond	k_{ins}	0.020	W/m C	0.001	3.17E-01	3.17E-04	1.00E-07	1.0%
Inner Radius	r_1	0.0055	m	0.0001	-7.67E+01	7.67E-03	5.88E-05	23.2%
Outer Radius	r_2	0.0480	m	0.0001	-3.83E-01	3.83E-05	1.47E-09	0.1%
Length of Sample	L	0.1460	m	0.0001	6.26E+00	6.26E-04	3.92E-07	1.9%
Insul. Thickness	t_{ins}	0.0254	m	0.0001	-2.49E-01	2.49E-05	6.22E-10	0.1%
Insul/Ttop/Tbot	$T_{1,ins}$	29	C	1.5	7.92E-04	1.19E-03	1.41E-06	3.6%
Insulation	$T_{2,ins}$	21	C	1.5	7.92E-04	1.19E-03	1.41E-06	3.6%
Average Cylinder Wall Surface Differential	$T_{diff,avg}$	17.0	C	0.35	-5.41E-02	1.89E-02	3.59E-04	57.2%

Total   4.278E-04 $Wm^{-1}C^{-1}$

Systematic uncertainty of apparatus, B_k =   0.021 $Wm^{-1}C^{-1}$

% of true value   4.7%

Confidence interval
$k' = 1.719 \pm 0.048\ W\,m^{-1}{}^\circ C^{-1}$ (95%)

Range of published values for PCC
$k = 1.37 - 2.77\ W\,m^{-1}{}^\circ C^{-1}$
Source: Khan, 2002
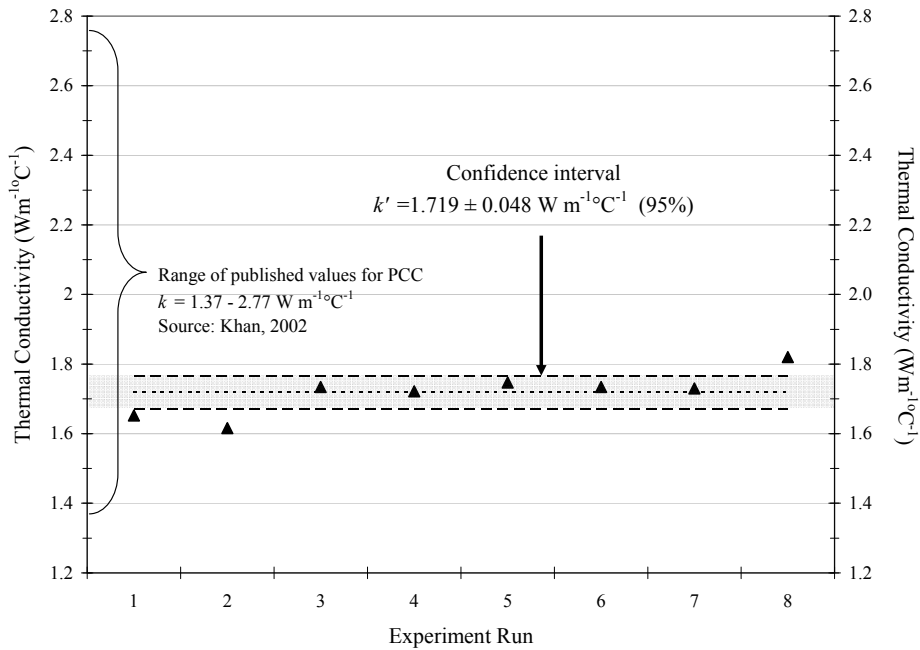
Figure 56 Results for Portland cement concrete.

Table 11 Results of eight experimental runs for Ultra High Molecular Weight Polyethylene (HMWPE), Hot Mix Asphalt (HMA), and Portland Cement Concrete (PCC).

Experimental Run		UHMWPE	HMA	PCC	Units
1		0.438	0.92	1.652	$Wm^{-1}C^{-1}$
2		0.425	0.913	1.616	$Wm^{-1}C^{-1}$
3		0.429	0.892	1.734	$Wm^{-1}C^{-1}$
4		0.455	0.882	1.722	$Wm^{-1}C^{-1}$
5		0.452	0.883	1.747	$Wm^{-1}C^{-1}$
6		0.454	0.891	1.734	$Wm^{-1}C^{-1}$
7		0.441	0.897	1.73	$Wm^{-1}C^{-1}$
8		0.435	0.886	1.82	$Wm^{-1}C^{-1}$
mean	k	0.441	0.896	1.719	$Wm^{-1}C^{-1}$
literature values	-	0.42-0.46*	0.8-1.6**	1.37-2.77***	$Wm^{-1}C^{-1}$
standard deviation	S_k	0.012	0.014	1.37-2.77	$Wm^{-1}C^{-1}$
sample size	n	8	8	8	-
confidence level	P%	0.95	0.95	0.95	-
random uncertainty	P_k	0.008	0.01	0.043	$Wm^{-1}C^{-1}$
systematic uncertainty	B_k	0.021	0.021	0.021	$Wm^{-1}C^{-1}$
total uncertainty (95%)	u_k	0.022	0.023	0.048	$Wm^{-1}C^{-1}$
% uncertainty	-	5.10%	2.60%	2.80%	-

*Boedeker Plastics, Inc. & San Diego Plastics, Inc.

**Highter and Wall, 1984

***Khan, 2002

Summary

A new test method was developed for determining the thermal conductivity of pavement materials. The method utilizes a cylindrical geometry common among field and laboratory samples prepared for mechanical testing of Portland cement concrete and asphalt mixtures. A theoretical analysis using fundamental heat transfer theory was applied to determine the appropriate design parameters for an experimental apparatus. An experimental apparatus was developed, constructed and evaluated using the propagation of uncertainty method. The apparatus was used to measure thermal conductivity of three different types of specimens: an Ultra High Molecular Weight Polyethylene (UHMWPE), hot mix asphalt and Portland cement concrete. The experimental runs of these pavement materials resulted in k values that fall within known values and previous estimates in the literature. Despite some variations in the repeatability of the test results, the confidence intervals found for all three specimens were determined to be within acceptable limits of accuracy for determining thermal conductivity of cylindrical samples.

Chapter 3: Modeling Heat Absorption and Transfer in Concrete Pavements

In this part of the study, the objective was to develop a one-dimensional mathematical model to calculate the pavement near-surface temperatures using the hourly measured solar radiation, air temperature, dew-point temperature and wind velocity data. This model was based on the fundamental energy balance, and takes into account convection and radiation at the surface, as well as conduction to and from the ground.

The model was subsequently validated against measured temperature data collected from the pavement test sections coordinated jointly with the Arizona Department of Transportation pavement test facility located in Phoenix, Arizona, using embedded thermocouples and climatic field equipment. The model was then used to identify the influence of the pavement thermophysical and geometry properties on the surface temperatures. This would allow ascertaining the optimal properties that would lower these temperatures, and consequently mitigate the UHI effects. It would also give insight on how future pavements could be constructed for mitigating such effects, while still maintaining satisfactory performance and lifetime.

One recent similar modeling tool is the Enhanced Integrated Climatic Model (EICM) in the Mechanistic Empirical Pavement Design Guide (NCHRP 2004). Similar to the model developed in this study, the EICM is a one-dimensional coupled heat and moisture flow program that simulates changes in the behavior and characteristics of pavement (asphalt concrete and Portland Cement Concrete) and subgrade materials in conjunction with climatic conditions over several years of operation. Thermal conductivity, heat capacity, and surface shortwave absorptivity are needed for paving materials in order for the EICM to estimate the temperature and moisture in the pavement system. However, there are some differences between the two models. First, the model developed in this study is a stand-alone tool to evaluate different scenarios of pavement heat absorption and transfer; whereas the EICM model is integrated and used within a comprehensive pavement design analysis program. Second, the EICM program uses the daily wind speed, which is determined by linear interpolation between adjacent months for its computations of the convection heat transfer coefficient, whereas the model of this study employs hourly wind speed data. Third, given the stability condition for the forward finite difference method, which shall be discussed later, this study's model is able to provide a more refined temperature profile at closer nodal spacing within the pavement as compared to the EICM model. It is also capable of independent study into the different thermophysical properties of the different paving layers, such as the base, sub-grade and natural soil. Finally, the model in this study is also capable of accounting for the thermal resistances between each pavement layers.

Common Pavement Materials & Configurations

Prior to model simulations, it is important to understand the construction design and materials used in roads and pavements, as this will stipulate the necessary parameters for the model inputs, and hence result in a more accurate representation of the pavements. Figure 57 depicts a typical representation of the pavement configuration and the energy balance between the layers and its environment.
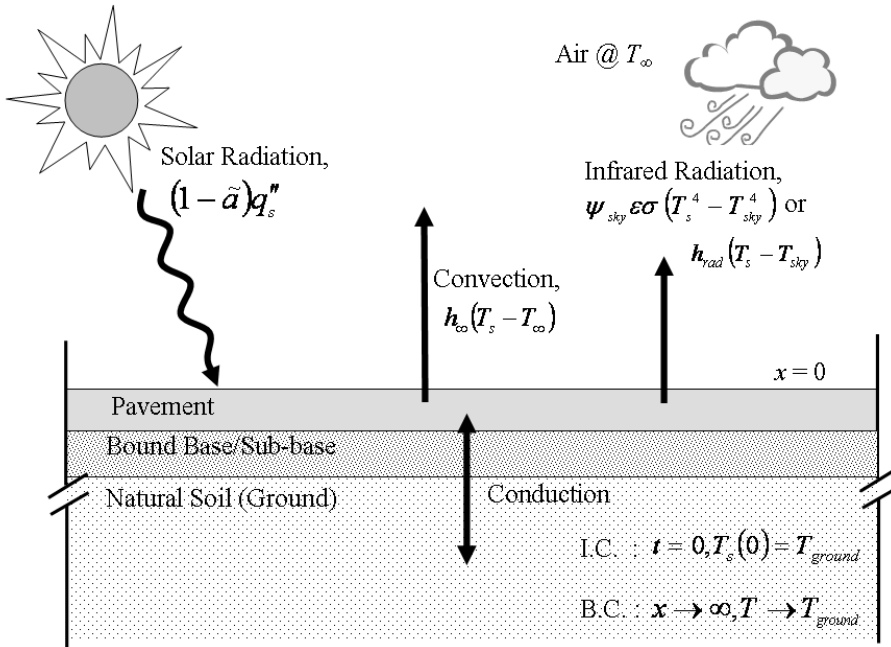
Figure 57 Heat transfer modes between pavement and its surrounding

where $\tilde{a}$ is albedo, q''_s is incoming solar radiation, h_∞ is convective heat coefficient of air, and h_{rad} is abbreviated parameter for the radiative coefficient defined as $\psi_{sky}\varepsilon\sigma(T_s^2+T_{sky}^2)(T_s + T_{sky})$, with ψ_{sky} being the sky view factor, ε the infrared emissivity of the pavement surface, σ the Stefan-Boltzmann constant (= 5.68×10^{-8} W m^{-2} °C^{-4}), and T_s and T_{sky} are the surface and sky temperatures respectively. T_∞ is the ambient air temperature

As presented in Figure 57, roads and pavements are usually comprised of 3 to 4 different layers, which are generally classified into surface, base and/or sub-base, and sub-grade (or ground). Of these, the sub-grade layer is the only non-manmade material. It is usually the native soil that is compacted to ensure a stabilized foundation before overlaying with the Hot Mix Asphalt (HMA) and/or Portland Cement Concrete (PCC) layers, which are consequently the two most commonly used materials in road and pavement construction (Golden *et al*., 2005).

Although the selection and construction of the pavement type is dependent on many different factors, such as traffic loads, cost, environmental conditions, maintenance, etc., the most critical consideration would be the load which the pavements are expected to carry.

Hot mix asphalt (HMA) pavement

Hot mix asphalt (HMA) is one of the most widely used paving materials in the United States. In 1996 alone, over 500 million tons of hot mix asphalt was produced (Zubeck, 2001). Table 12 describes the two generic HMA pavement designs as stipulated in the *HMA Pavement Mix Type Selection Guide* (NAPA, 2001) for different traffic loads.

Table 12 Typical HMA pavement designs for low to heavy traffic levels(NAPA, 2001)

Traffic Levels	Low to Medium (Typical Thickness Range)	Medium to High (Typical Thickness Range)
Surface	Dense Fine Grade	Dense Coarse Grade

	(62.5 – 175.0 mm)	(75.0 – 125.0 mm)
Base/Sub-base	Dense Fine Grade (50.0 - 150.0 mm)	Dense Coarse Grade (50.0 - 150.0 mm)
Sub-grade	Natural Soil	Natural Soil

Portland cement concrete (PCC) pavement

Unlike HMA pavements, concrete pavements generally do not need the structural support capacity of the base or sub-base layers to sustain traffic loads. The PCC layer has a higher modulus and strength when compared to HMA, and hence they are constructed to withstand higher loads as compared to HMA pavements. Typical base/sub-base thickness range is 75 to 350 mm.

Composite pavement

In recent years, there has been an increasing trend in pavement construction using both HMA and PCC as a composite pavement system to withstand specific traffic flow or satisfy certain functional performance criteria. Examples are thin and ultra thin-white topping (UTW) pavement. In UTW design, the pavement is composed of a thin layer of PCC (normally 50 to 100 mm or 2 to 4 inches) over 4 to 6 inches (or more) of an existing HMA pavement (Mobasher, 2004). Such technique has been reported on favorably to help mitigate the urban heat island effect (Golden and Kaloush, 2006) due to the higher albedo factor and lower thermal mass of the PCC layer.

Principles of Model

The principle behind the thermal model is based on a transient energy balance of the pavement, which includes heat transfer by convection, conduction, solar and near-infrared radiation. The heat transfer modes considering rain and surface water evaporation are not taken into consideration, not because of their complexity in modeling, but because such occurrences will in fact help lower the pavement surface temperatures, resulting in mitigating the UHI effects.

Radiation Heat Transfer

There are two radiation heat transfer modes occurring at the pavement surface: incoming solar radiation q''_s, and outgoing infrared radiation, q''_{rad}. The outgoing radiation q''_{rad} is described by:

$$q''_{rad} = \psi_{sky}\varepsilon\sigma\left(T_s^4 - T_{sky}^4\right) = h_{rad}\left(T_s - T_{sky}\right)$$ [1]

where ψ_{sky} is the sky view factor, ε the infrared emissivity of the surface, σ the Stefan-Boltzmann constant (= 5.68 x 10^{-8} W m^{-2} $^{\circ}$C^{-4}), and T_s and T_{sky} are the surface and sky temperatures respectively. h_{rad} is the abbreviated parameter for the radiative coefficient defined as $\psi_{sky}\varepsilon\sigma(T_s^2 + T_{sky}^2)(T_s + T_{sky})$.

The sky view factor is an indication of the relationship between the visible area of the sky and the area covered by urban structures (Souza *et al*. 2003). As the sky temperatures are generally lower than the surrounding urban structures, the sky serves as a heat sink and thereby results in

outgoing infrared radiation from the pavement to the sky. In this model, the sky view factor has been approximated to be 1.0 as it is assumed to have an unobstructed open field for the pavement. The sky temperature, T_{sky} in K, can be expressed as follows (ASHRAE 2004).

$$T_{sky} = T_\infty \left(0.004\ T_{dew} + 0.8\right)^{0.25} \qquad\qquad [2]$$

where T_∞ and T_{dew} are the atmospheric dry-bulb temperature in K and dew-point temperature in °C, respectively.

Convection Heat Transfer

The pavement is largely cooled by the convective heat transfer occurring at its surface. The rate of this heat transfer q''_{conv} can be expressed by Newton's law of cooling:

$$q''_{conv} = h_\infty \left(T_s - T_\infty\right) \qquad\qquad [3]$$

where h_∞ is the convective heat coefficient of air.

The parameter h_∞ is primarily dependent on the air above the pavement. It can be derived from an appropriate expression for the Nusselt number, assuming laminar flow[1] over a flat plate (Çengel 2003).

$$h_\infty = 0.664 \left[k_\infty\ \mathrm{Pr}_\infty^{0.3}\ \nu_\infty^{-0.5} U_\infty^{0.5} \right] \qquad\qquad [4]$$

where k_∞, Pr_∞ and ν_∞ are the thermal conductivity, Prandtl number and kinematic viscosity of the air, respectively. They are dependent on the film temperature, which is the average of the pavement surface temperature, T_s and the air temperature, T_∞. Wind velocity is expressed as U_∞.

Conduction Heat Transfer

Conduction is the heat transfer mode occurring between the pavement layers and the ground. Its rate of transfer q''_{cond} can be represented by Fourier's law of heat conduction:

$$q''_{cond} = -k \frac{dT}{dx} \qquad\qquad [5]$$

where k is the thermal conductivity of the medium that heat is conducted through, and dT/dx is the temperature gradient occurring within the medium into the ground. In this model, the heat transfer into the ground is considered as conduction into a semi-infinite solid; which is to say, given enough depth, there are no temperature fluctuations with respect to time. This is because with increasing depth, the increasing thermal mass of the soil renders the temperature at such depths independent of the heating and cooling cycles on the pavement surface. However, there is still heat flux flowing into the ground, as temperature decreases with depth for finite depths. Hence this forms the initial and boundary conditions for the model.

---

[1] Reynolds number computation over test site over the 3-day study period shows Re < 5 x 10⁵

Governing Equations

The fundamental equation which governs the transient heat conduction within the pavement can be expressed as:

$$\frac{\partial T}{\partial t} = \alpha \frac{\partial^2 T}{\partial x^2} \tag{6}$$

where α is the thermal diffusivity (which is the ratio of the pavement thermal conductivity, k to its volumetric heat capacity, ρc) of the pavement, and $\partial T / \partial t$ is the rate of change of temperature. The governing equation, Eq. [6], however is subject to a number of boundary and interfacial conditions, as well as an initial condition, particularly at the pavement surface and the pavement multi-layers interface. For instance, at the pavement surface ($x = 0$), the governing equation with its respective boundary conditions is:

$$\rho c \frac{\Delta x}{2} \frac{\partial T_s}{\partial t} = \left(1 - \tilde{a}\right) q_s'' + h_\infty \left(T_\infty - T_s\right) + h_{rad} \left(T_{sky} - T_s\right) + k \frac{\partial T_s}{\partial x} \tag{7}$$

where $\frac{\Delta x}{2}$ is the thickness of the pavement surface layer, T_s is the surface temperature and $\tilde{a}$ is the albedo of the pavement surface layer.

For the multi-layer interfaces between the pavement and its sub-base, as well as between the sub-base and the ground, the boundary condition is such that the continuity of heat flux must be maintained:

$$k_{layer1} \frac{dT_{layer1}}{dx} = k_{layer2} \frac{dT_{layer2}}{dx} \tag{8}$$

and the thermal contact resistance, R_c, must be accounted for at these interfaces:

$$R_c = \frac{T_{layer1,int} - T_{layer2,int}}{q_{int}''} \tag{9}$$

where $T_{layer1,int}$ and $T_{layer2,int}$ are the interfacial temperatures at layer 1 and 2 respectively, and q''_{int} is the heat flux flowing through the interface.

Because of the lack of information on R_c, it was considered to be equal to zero. This may lead to inaccuracies in the predictions of temperatures with depth, but apparently had little effect on the near-surface temperatures, which were the primary focus of this research.

Expressing the Eq. [6], [7], [8] and [9] numerically using the explicit finite difference method (Refer to Appendix A for detail workings) gives the nodal temperatures as such:

i.   Interior node, T_m (for m=1,2....n):

$$\rho c \Delta x \left(\frac{T_m^{p+1} - T_m^p}{\Delta t} \right) = k \frac{T_{m-1}^p - T_m^p}{\Delta x} + k \frac{T_{m+1}^p - T_m^p}{\Delta x} \tag{10}$$

ii.   Surface node, T_s:

$$\frac{\rho c \Delta x}{2 \Delta t} T_s^{p+1} = (1 - \alpha) q_s'' + h_\infty (T_\infty^p - T_s^p) + h_{rad} (T_{sky}^p - T_s^p) + k \frac{T_1^p - T_s^p}{\Delta x} \tag{11}$$

iii.   Interface node, T_{int}:

$$k_{layer\,1} \frac{T_n - T_{layer\,1,int}}{\Delta x} = k_{layer\,2} \frac{T_{layer\,2,int} - T_{b1}}{\Delta x} \tag{12}$$

iv.   Thermal contact resistance, R_c:

$$R_c = \frac{\Delta x k_{layer\,1} (T_n - T_{layer\,1,int}) + \Delta x k_{layer\,2} (T_{b1} - T_{layer\,1,int})}{k_{layer\,1} (k_{layer\,2} T_{layer\,1,int} - k_{layer\,2} T_n)}$$

$$= \frac{\Delta x k_{layer\,2} (T_{b1} - T_{layer\,2,int}) + \Delta x k_{layer\,1} (T_n - T_{layer\,2,int})}{k_{layer\,2} (k_{layer\,1} T_{layer\,2,int} - k_{layer\,1} T_{b1})} \tag{13}$$

where Δx and Δt are the nodal and time-step spacing respectively. The superscripts represent the time-step *(p)* or *(p+1)* while the subscripts in numerals represent the nodal positions from the surface. $T_{layer1,int}$ and $T_{layer2,int}$ are the interface temperatures on the respective layers, and T_n and T_{b1} are the last temperature node in the upper layer and first temperature node in the lower layer, respectively.

As in all explicit finite difference schemes, each finite difference equation has to satisfy the Courant-Friedrichs-Lewy (CFL) condition, which is necessary for hyperbolic partial differential equation to be stable for each mesh point (Heath 2002). In this model, the following equation, which specifies the time-step (Δt) to nodal (Δx) spacing relationship, has been identified as the most stringent criterion for the model stability condition:

$$\Delta t \leq \left(\frac{\rho c \Delta x^2}{2 (h_{rad} \Delta x + h_\infty \Delta x + k)} \right) \tag{14}$$

Computations

Parameters
Apart from the hourly solar radiation data, wind velocity, air temperature and dew-point temperature, the model requires several other parameter inputs, such as the pavement material properties. While most of these parameters had been experimentally obtained and referenced, others were not studied and hence require adaptation to fit the field results.

In this study, it was assumed that the thermal resistances between the different pavement layers to be almost negligible. This is a reasonable assumption considering the compaction and

tack coat provided between the pavement layers during construction. Nonetheless, future experimental studies might provide more insight regarding the thermal resistances between these pavement layers. Table 13 summarizes the input parameter used for calibration purposes as part of this study's model.

Table 13 Thermal properties of pavement layers

Layers	Material	Thermal Properties	Reference
Layer 1 (Pavement)	Hot Mix Asphalt (HMA)	Density, ρ = 2238 kg/m^3 SHC, c = 921 J kg^{-1} $^\circ$C^{-1} Conductivity, k = 1.21 W m$^{-1\circ}$C^{-1} Albedo, $\tilde{a}$ = 0.17 Emissivity, ε = 0.85	(Corlew and Dickson 1968) Unpublished data (Çengel 2003)
		Thermal resistance, Rc = 0.0 (Layer 1 and 2)	Assumed
Layer 2 (Base)	Bound Base (old HMA)	Density, ρ = 2238 kg/m3 SHC, c = 921 J kg^{-1} $^\circ$C^{-1} Conductivity, k = 1.21 W m$^{-1\circ}$C^{-1}	(Corlew and Dickson 1968)
		Thermal resistance, Rc = 0.0 (Layer 2 and 3)	Assumed
Layer 3 (Subgrade)	Dry Soil	Density, ρ = 1500 kg/m3 SHC, c = 1900 J kg^{-1} $^\circ$C^{-1} Conductivity, k = 1.00 W m$^{-1\circ}$C^{-1}	(Çengel 2003)

Programming

The computation was carried out by programming the relationships derived between the parameters and input data into an MS Excel© spreadsheet. With these inputs, the program performs iterative computations, over a 3-day study period, with the initial condition of 33.5 $^\circ$C across the pavement to a depth of 3.0 m (10 ft) for each temperature node. The number of iteration cycles required was determined by the comparison of the model computations against the actual temperature measured at the average daily maximum and minimum temperatures. Table 14 shows the comparison of the actual measured data and the computed average temperatures at 10, 20 and 30 iteration cycles.

Table 14 Comparison of actual average temperatures and computed temperatures at 10, 20 and 30 iteration cycles

	Avg Max Temp	% diff	Avg Min Temp	% diff
Actual Temp:	67.17°C		31.67°C	
10 cycles	66.72°C	-0.67%	32.31°C	2.02%

76

| 20 cycles | 67.43°C | 0.39% | 32.96°C | 4.07% |
| 30 cycles | 67.88°C | 1.06% | 33.56°C | 5.97% |

Although the average maximum temperature is modeled most accurately at 20 iteration cycles (0.39%), its corresponding minimum temperature is not close to the actual (4.07%). On the other hand, at 10 iteration cycles, the modeled minimum temperature is the closest at about 2.0%, with its maximum at about 0.7%. Therefore, to model both maximum and minimum temperatures to be as close as possible to the actual, 10 iteration cycles was selected to be used as the criterion for the model computation. The step-by-step procedures to operating the thermal model are described fully in the Appendix.

Thermal Model Accuracy

Figure 58 shows the comparison results between the field measured temperature data and the simulated surface temperatures predicted with the model, over a 3-day study period. From the plot, it can be seen that there is a slight time lag between the model and the actual data during the cooling cycle of the pavement. This is possibly due to the additional cooling by evapotranspiration, which is not accounted for in the model. However, for the heating cycle portion, the model is reasonably accurate in its simulation.

Despite these observations, the critical importance of the plot lies in the accuracy of the maximum and minimum temperatures simulated. This is because it provides an understanding of human comfort, due to the direct influence of the air temperature above the pavement, which can result in higher energy and water consumption (Golden and Kaloush 2005). It is also an indirect indication of health and environmental impact, as elevated surface temperatures contributes to smog production, particularly during the day. Thus it can be seen that these factors are significant to the study of the urban heat island effect.
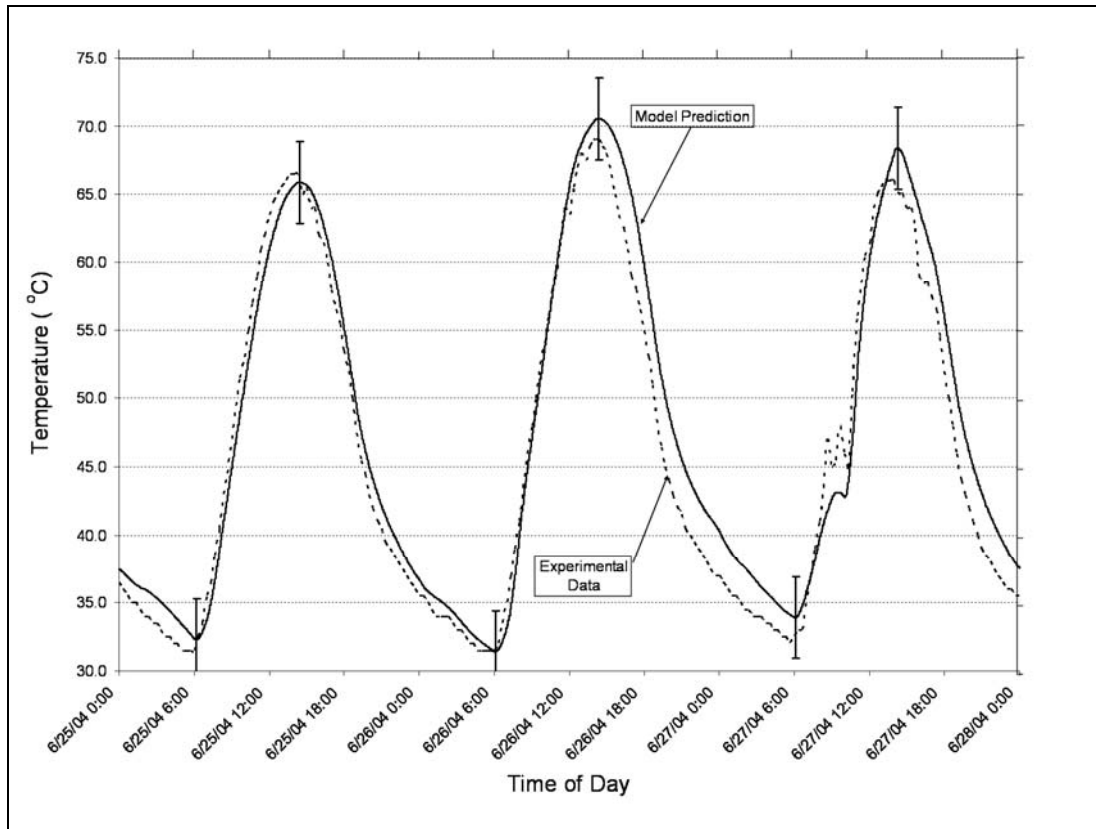
Figure 58 Pavement temperatures at 12.7 mm (0.5 inch) depth for 3 days period

Computation showed that the average difference between the measured and predicted temperatures was about 2.7% (or +/-1.9°C) and 1.6% (+/- 2.4°C) for minimum and maximum temperatures respectively, which are within their respective one standard deviation, σ_s (+/-2.2°C for maximum and +/-1.3°C for minimum temperatures). Hence the model is fairly accurate in providing a close estimate of the near-surface pavement maximum and minimum temperatures.

Effects of Pavement Thermophysical Properties

Given the ability to vary the material thermal properties independently of one another, the temperature model allowed the evaluation of the effects of each pavement property on the surface temperatures separately. The thermophysical properties focused on in this report were the pavement *thermal conductivity, volumetric heat capacity, thermal diffusivity, albedo* and *emissivity*.

Thermal conductivity, k

Thermal conductivity determines the rate of heat transfer across the pavement and into the ground or vice versa; the higher the value, the faster the heat transfer rate (Çengel, 2003). In this study, the pavement thermal conductivity, *k,* is varied from 0.60 W m^{-1} °C^{-1} to 2.60 W m^{-1} °C^{-1}, while maintaining the other parameters constant so that they are isolated, thereby allowing the observation of the surface temperatures under the pure effect of conductivity changes. Figure 59 presents the variations of the 3-day average pavement maximum and minimum surface

78

temperatures with respect to this range. Included in the plot are also some typical pavement k values (US Army 1988).
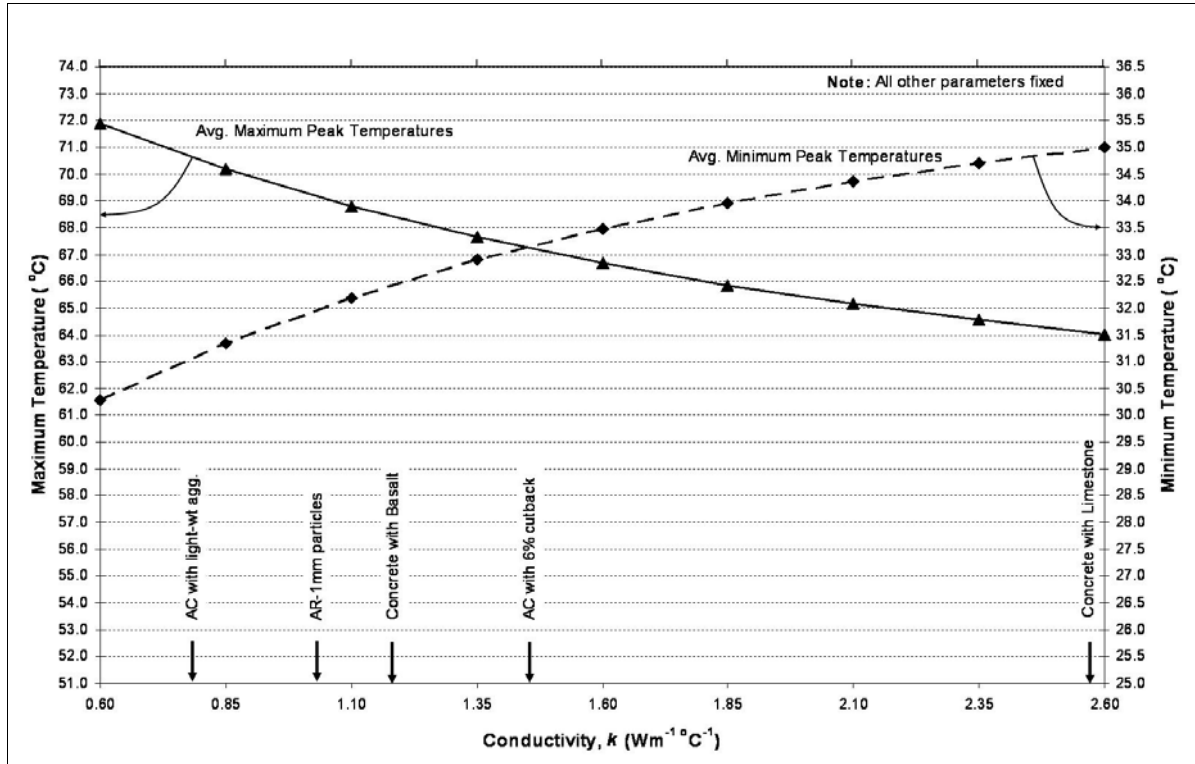

Figure 59 Thermal conductivity effect on pavement maximum and minimum surface temperatures

The average maximum temperature, which occurs during the day, is observed to decrease with increasing pavement k. This can be explained by the fact that the high conductivity allows the heat gain from the solar radiation at the surface to be transferred away rapidly and consequently absorbed into the ground, which acts as a heat sink. Conversely, the minimum surface temperature, which occurs during the night, increases with k for the same reason. Since more of the ground, at greater depths, is able to absorb the heat during the day, the effective thermal mass of the ground is increased. Consequently, it becomes more difficult to release the heat at night, giving rise to the increased minimum temperatures.

Volumetric heat capacity, ρc

Volumetric heat capacity, as represented by ρc, is a parameter that describes the material heat storage capability. It measures the amount of energy required to raise the temperature per unit volume of the material by 1 °C. The higher the ρc, the more is the energy required to raise the material temperature (U.S. Army, 1988). Figure 60 illustrates the effect of the pavement volumetric heat capacity on the maximum and minimum surface temperatures, from 1.40×10^6 to 2.80×10^6 J m^{-3} °C^{-1}, while maintaining the other parameters constant. It is observed that the maximum temperature decreases while the minimum temperature increases with increasing ρc.
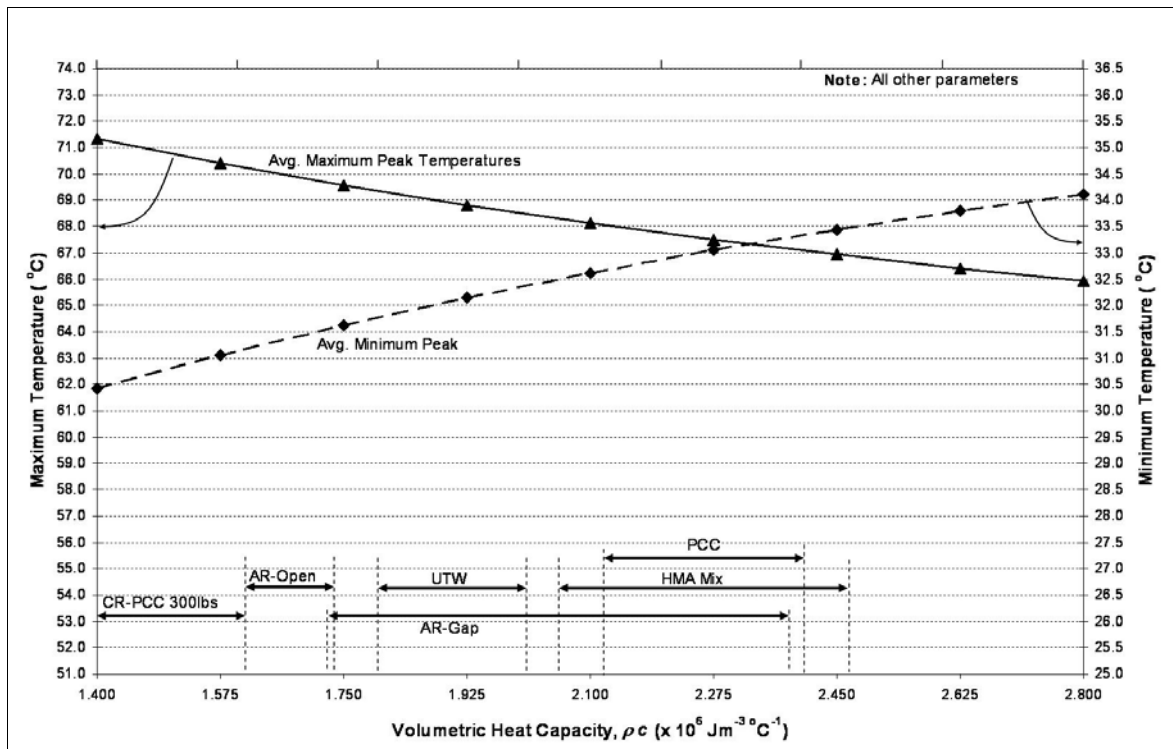
Figure 60 Volumetric heat capacity effect on pavement maximum and minimum surface temperatures

Similar to the effect of increased k discussed above, increased energy storage caused by the increased ρc increases the thermal mass, which slows down the rate of increase of temperature during the day, leading to decreased maximum temperatures. But at the same time, the higher thermal mass causes the consequential higher night time (minimum) temperatures, due once again to the increased difficulty in removing that heat at night.

Thermal diffusivity, α

The thermal diffusivity, α, which is a ratio of the thermal conductivity, k, to its volumetric heat capacity, ρc, determines the rate of heat propagation through the medium. The higher the diffusivity, the faster the heat propagates or "diffuses" into the material (Çengel, 2003). The effect on the pavement maximum and minimum surface temperatures for diffusivities ranging between from 2.0×10^{-7} to 12.0×10^{-7} m²/s is depicted in Figure 61.
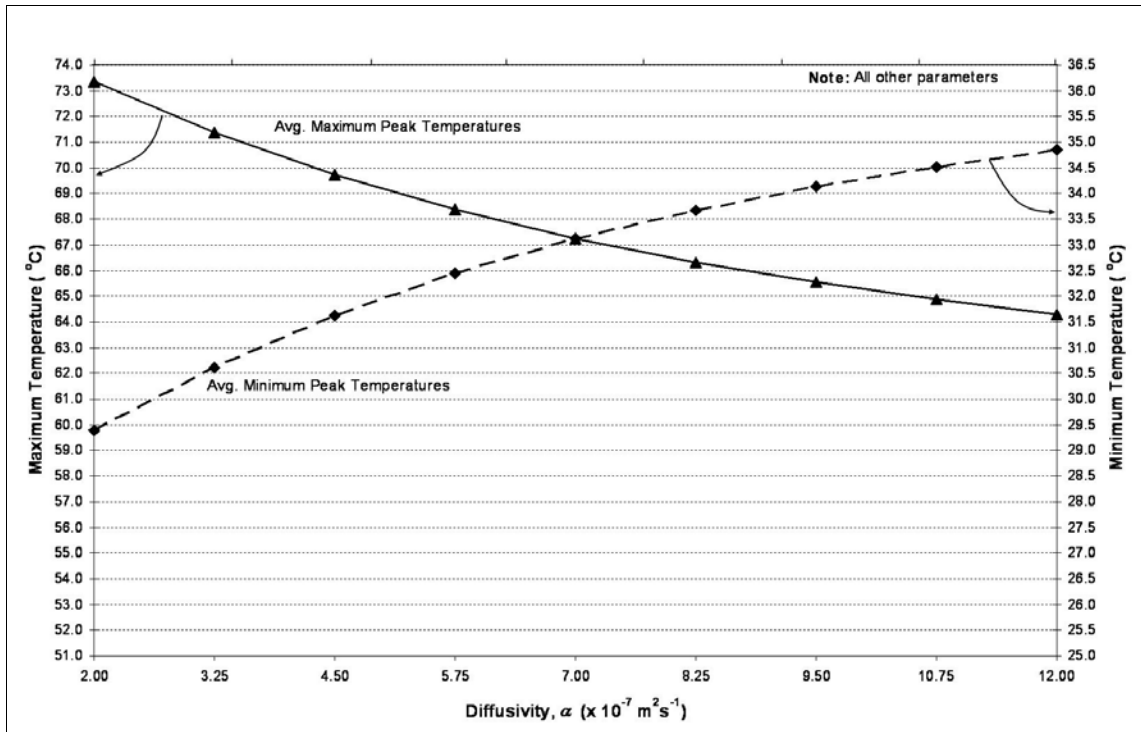
Figure 61 Thermal diffusivity effect on pavement maximum and minimum surface temperatures

Similar to the trend shown in the effects of *thermal conductivity* and *volumetric heat capacity*, the average maximum surface temperature reduces while the minimum temperature increases with increasing diffusivity. The observed trends closely track those resulting from changes in *k* (Figure 59) because the thermal diffusivity was varied by changing *k*, while leaving ρc constant.

Albedo, ã

Albedo, *ã*, or reflectivity of the pavement, plays an important part on the pavement temperatures. It is a non-dimensional parameter which measures the reflected radiation energy from the pavement from incident solar radiation. The higher the albedo value, the higher is the reflected energy back to its surroundings, which means the less energy is absorbed into the pavement (Taha, 1988). Hence it is hardly a surprise to anticipate a reduction in both pavement maximum and minimum temperatures alike with increasing albedo. However, it is observed that the maximum temperature is affected more than the minimum temperature. This is because albedo factor, which depends solely on the presence of the sun, affects the daytime maximum temperature directly. The reduction in night time minimum temperature is a result of the decreased energy absorbed during the day. Figure 62 shows the plot of the maximum and minimum temperatures for pavement albedo values between 0.1 and 0.5.
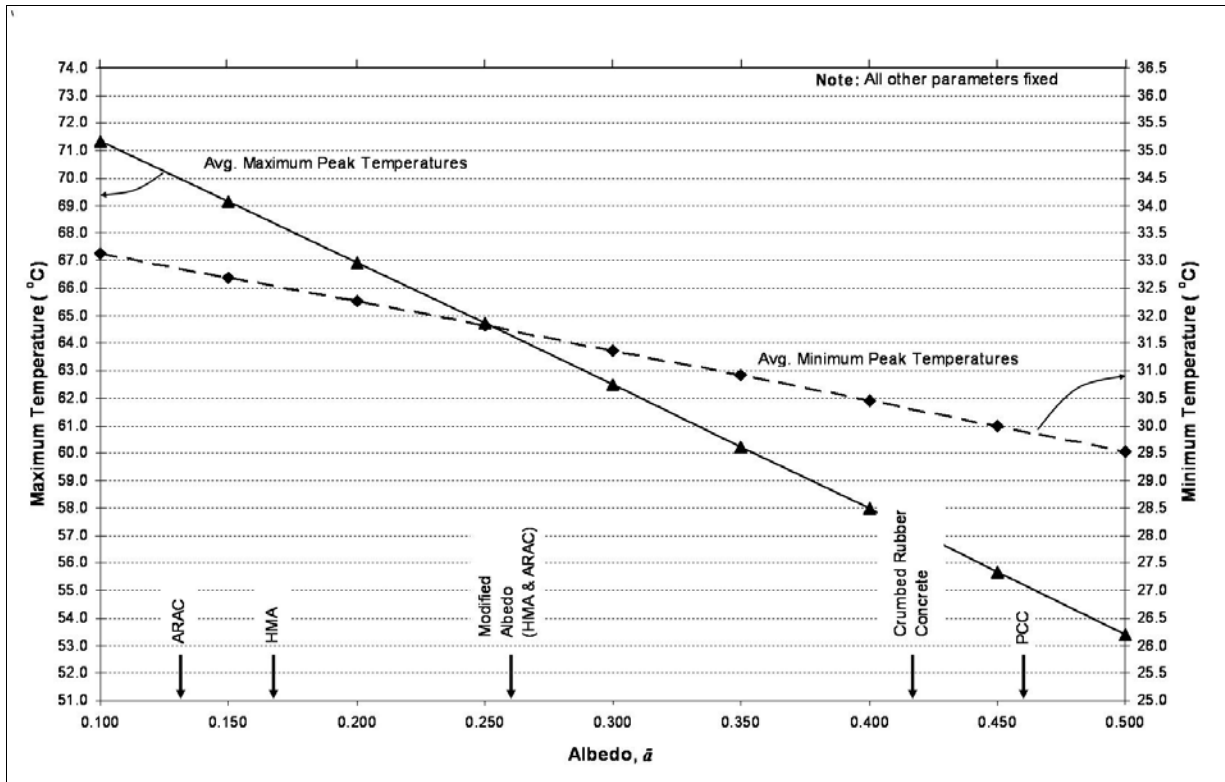
Figure 62 Albedo effect on pavement maximum and minimum surface temperatures

Emissivity, ε

Finally, the emissivity, ε, of a surface represents the ratio of the radiation emitted by the surface at a given temperature to the radiation emitted by a blackbody at the same temperature (Çengel 2003). In accordance with the Stephan-Boltzmann law, the higher the emissivity, the greater is the radiation emitted. Similar to albedo, ε is a dimensionless parameter. Figure 63 shows the decreasing trends of both the maximum and minimum surface temperatures with increasing emissivity from 0.7 to 1.0, with the minimum temperature being affected more. This is because the emitted irradiation is the only heat transfer by radiation occurring during the night. During the day, the additional incoming solar radiation nullifies part of the emitted irradiation, causing the effect of emissivity on the maximum temperature to be less than that compared to the night time minimum temperature.

82

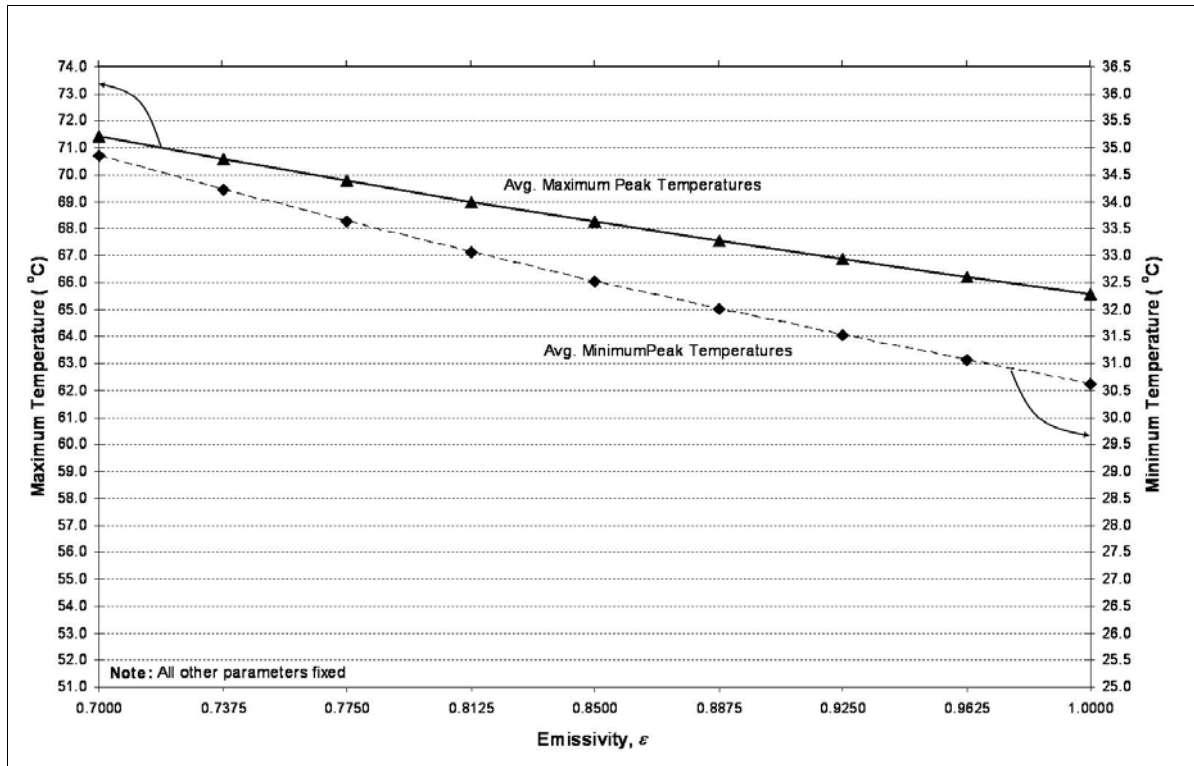**Figure 63 Emissivity effect on pavement maximum and minimum surface temperatures**

Comparison of pavement thermophysical properties effects

The effects of the various individual pavement thermophysical properties were shown in Figure 59 through Figure 62, however, there is a need to understand the relative importance of each of these factors. Prior to such a comparison, it is prudent that the property parameters, with their different units and ranges, are made comparable to one another. In this study, each of these parameters was normalized as follows:

$$\frac{\partial \theta_{max,\ min}}{\partial(property\ )^*} = \frac{\dfrac{\partial T_{max,\ min}}{\partial(property\ )}}{\dfrac{T_{ref\ (max,\ min)}}{\Delta(property\ )}} \qquad [15]$$

where $\dfrac{\partial T_{max,\ min}}{\partial(property\ )}$ is the change in the maximum (or minimum) temperatures with respect to a

given thermophysical property, i.e., the slope of the temperature gradient. This is taken with respect to the reference temperature, $T_{ref(max,min)}$, of the model with the original property values and the range of the property values over which the respective slope of the temperature gradient holds true. Figure 64 summarizes the comparison of the thermophysical properties effect on the pavement maximum and minimum surface temperatures, with increasing property values. It can be seen that the factor with the highest negative temperature gradient representing the highest decrease in the pavement maximum temperature is albedo, followed by thermal diffusivity, thermal conductivity, emissivity and volumetric heat capacity; while the reduction in the

83

pavement minimum temperature is most affected by emissivity and albedo. Thermal diffusivity with its largest positive temperature gradient on the surface minimum temperature has the largest adverse effect, followed by thermal conductivity and volumetric heat capacity, in that order.

Though increasing thermal diffusivity, thermal conductivity and volumetric heat capacity have positive decreasing effects on the modeled pavement maximum temperature; their effects on the minimum temperature are unhelpful. Instead of a reduction, they increase the pavement minimum temperature. In addition, it is also observed that the extent of their adverse effect on the minimum temperature outweighs their benefit on the maximum temperature. Hence it may not be justifiable to consider the increase (nor decrease) of these properties alone to mitigate the Urban Heat Island effect alone.
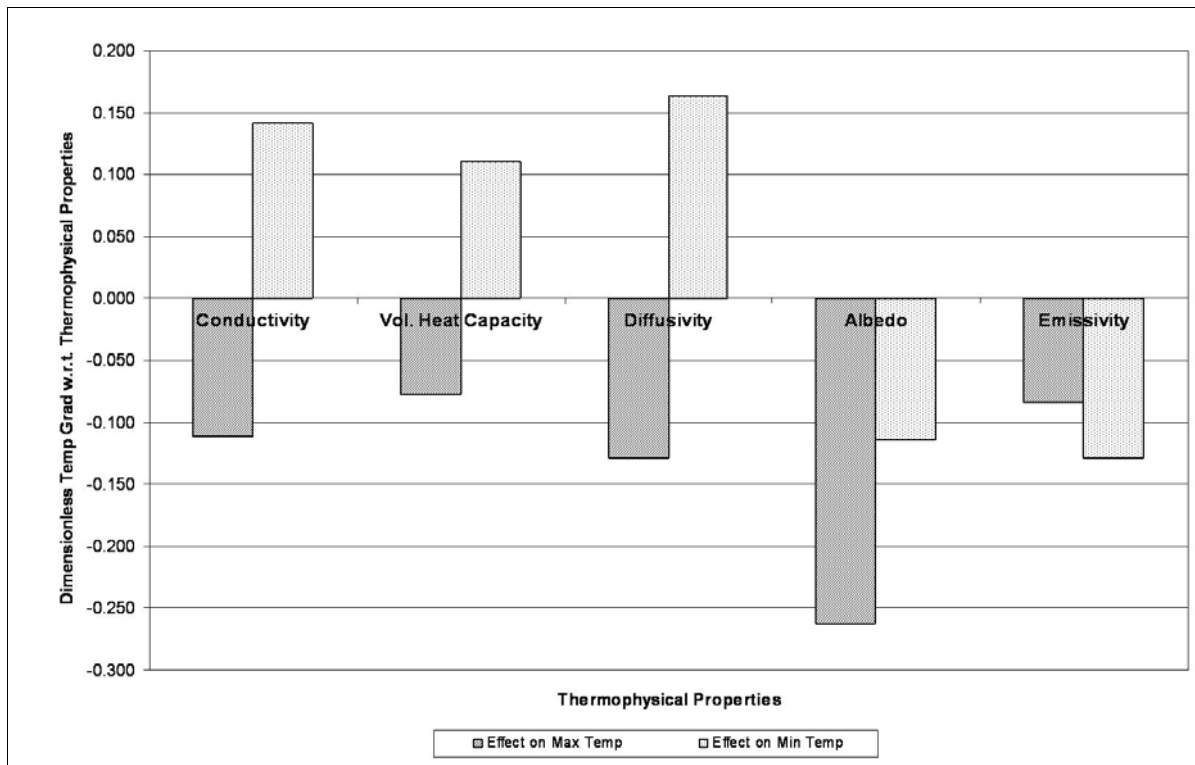
Figure 64 Comparison of the dimensionless thermophysical properties on pavement maximum and minimum temperatures

In contrast, both albedo and emissivity have positive responses in the reduction of the pavement temperatures, both maximum and minimum even though their effects on each temperature are different. Albedo affects the pavement maximum temperature more than it does the minimum temperature. On the other hand, emissivity is of a greater factor to the minimum temperature than the maximum. As discussed earlier, this is highly attributed to the presence of the sun during the day, which affects the albedo factor more directly, as well as nullifying part of the emitted radiation.

Effects of Pavement Geometry - Thickness

With the generic pavement construction design and materials identified earlier and using the additional pavement material properties summarized in the first section of this chapter for the respective materials, simulations of the surface temperature were carried out for the five cases shown in the table below.

Table 15 Thermal properties table of different pavement materials and grades

Material		Thermal Properties					Reference
		Density ρ [kg m^{-3}]	SHC c [J kg^{-1}^{o}C^{-1}]	Conductivity k [W m^{-1}^{o}C^{-1}]	Albedo $\tilde{a}$ -	Emissivity ε -	
HMA	DFG	2238[+]	921[+]	1.21[+]	0.17[*]	0.85[^]	[+]Corlew, 1968
	DCG	2100[#]	866[#]	2.00[#]	0.17*	0.85^	[^]Çengel, 2003
	AR OGFC	2160[*]	805[*]	0.40[@]	0.13*	0.85^	[#]Chadbourn, 1998
PCC	Standard	2350[ξ]	1000[ξ]	1.50[ξ]	0.46*	0.88[^]	[@]Caltrans, 2003
	Light Wt.	1280[^]	805[^]	0.54[^]	0.46*	0.88[^]	[ξ]Bentz, 2001
Dry Soil (Sub-grade)		1500[^]	1900[^]	1.00[^]	N.A.	N.A.	[*]unpublished

Figure 65 to Figure 69 illustrate the average maximum and minimum surface temperature responses across the different paving materials, with different layer thicknesses. From these figures, it can be seen that there exists a common trend in the surface temperature variations with respect to the thickness. It is observed that the average maximum temperature, in general, displays a minima with respect to increasing layer thickness, while the minimum temperature exhibits a monotonically increasing trend with increasing thickness.

Figure 65 Pavement thickness effect on maximum and minimum surface temperatures for Case 1

Figure 66 Pavement thickness effect on maximum and minimum surface temperatures for Case 2
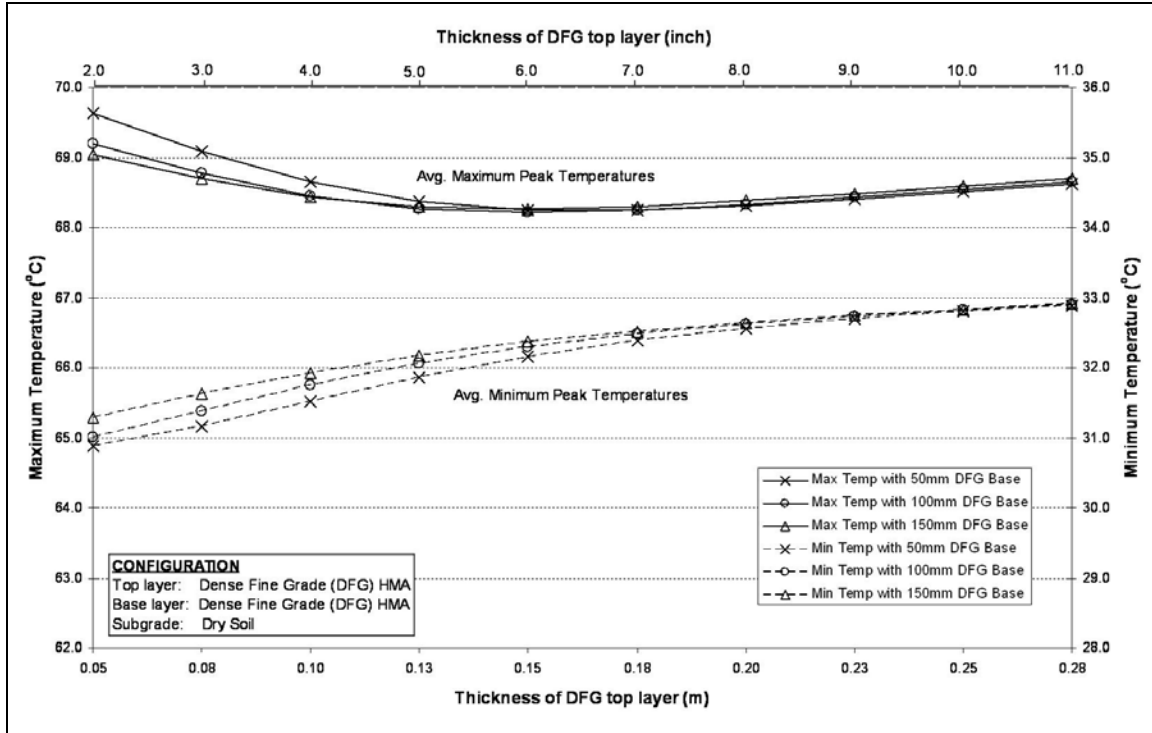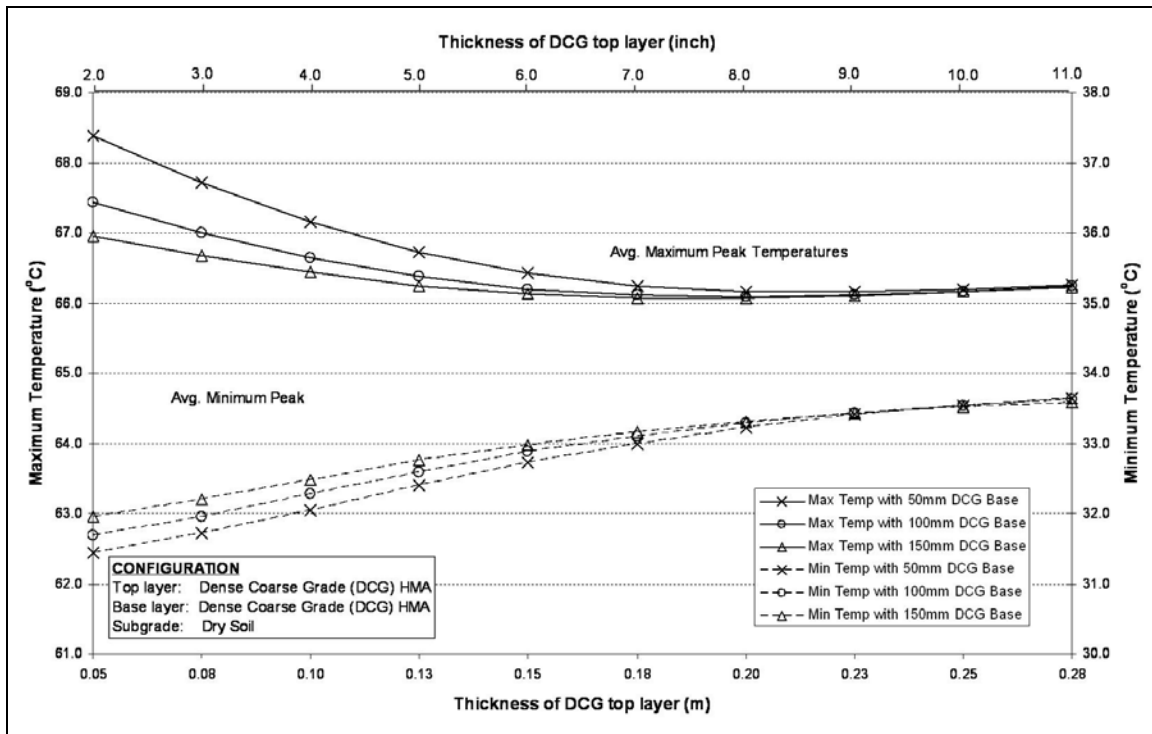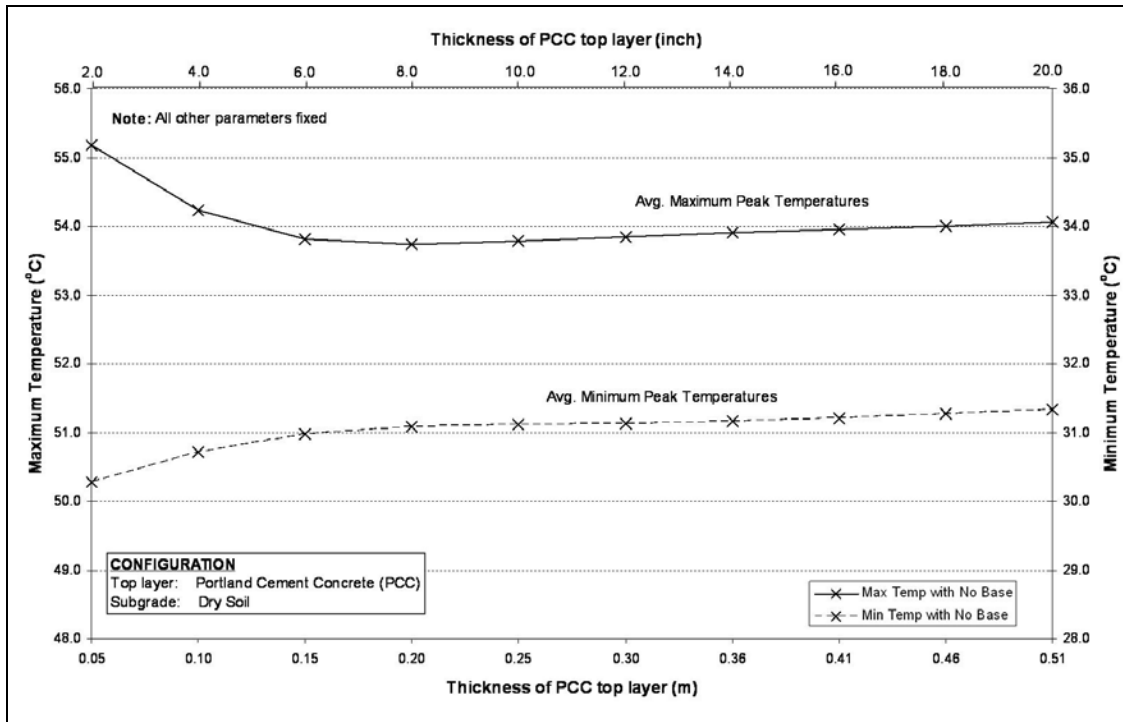
Figure 67 Pavement thickness effect on maximum and minimum surface temperatures for Case 3
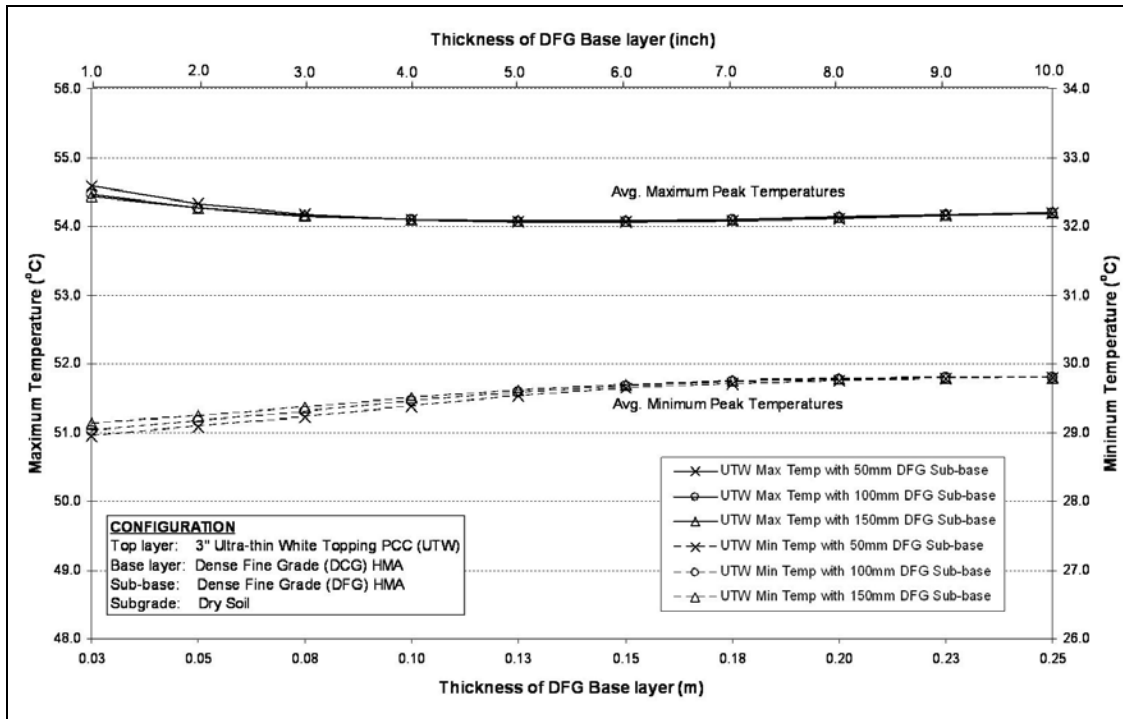

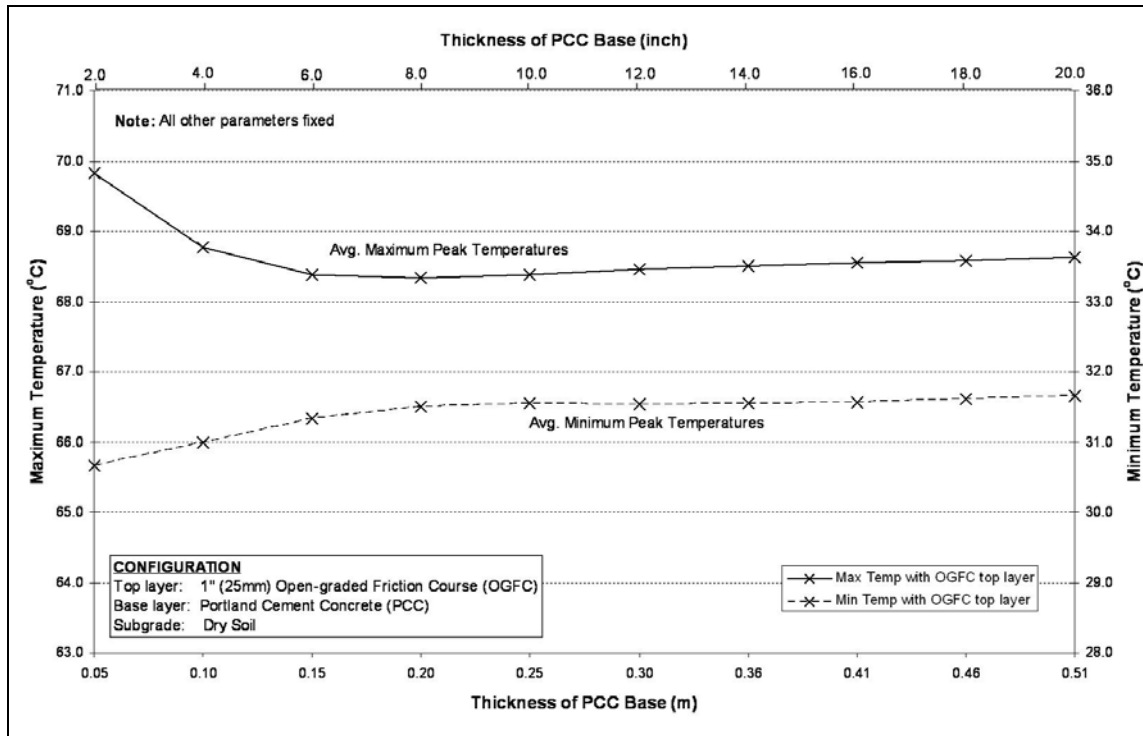**Figure 68 Pavement thickness effect on maximum and minimum surface temperatures for Case 4**

87

Figure 69 Pavement thickness effect on maximum and minimum surface temperatures for Case 5

Maximum surface temperature

The initial reduction observed in the maximum surface temperatures can be explained by the fact that the increase in the layer thickness results in an increase in the pavement thermal mass which is affected by the incident sunlight. This causes the pavement to have a higher heat storage capability, i.e. it is able to absorb more heat per unit ^{o}C rise in temperature. Therefore the maximum temperature initially reduces with increasing thickness.

The minima in the surface temperatures observed for each case (in the maximum, or daytime, temperature) occurs roughly where the pavement thickness is equal to the thermal penetration depth, $\delta \approx \sqrt{\alpha t}$, where the characteristic time t corresponds to the daylight hours, or approximately 12 hours. For instance, the penetration depth δ computed for the dense fine grade HMA pavement in Case 1 is 0.159m, which agrees with the modeled minima of the daytime temperature.

It is expected that a change in thermal behavior would be observed as the pavement thickness l becomes equivalent to δ. It was initially anticipated that as l becomes greater than δ, the maximum surface temperature would reach an asymptote and no longer vary with increasing l. However, the maximum surface temperature increases with increasing l after $l \approx \delta$. This behavior is corroborated by an analytical solution for the temperature of a slab subjected to a periodic temperature boundary condition.

Apparently the pavement no longer conduct heat as effectively into the ground for pavement thickness beyond $l \approx \delta$, since the temperature at the bottom of the slab for $l > \delta$ is less than that for $l \approx \delta$. This means that the temperature difference available to conduct heat from the bottom of the slab into the ground below is lesser for $l > \delta$ than for $l \approx \delta$, and decreases further with

88

increasing *l*. With such lesser heat conducted into the ground, the maximum surface temperature of the slab hence increases as *l* increases for *l* beyond δ.

Minimum surface temperature

Unlike the maximum surface temperature, the minimum surface temperature is continuously rising. This is due to the increase in thermal mass with pavement thickness, which increases the heat storage capacity. Hence there is an increase in the amount of heat stored that is required to be dissipated during the night and thus the temperature will only get higher with an increase in pavement thicknesses.

Effects of Pavement Materials

Figure 70 and Figure 71 summarize the lowest maximum temperature achieved for each pavement type at their respective critical thickness and the corresponding minimum surface temperature, respectively.
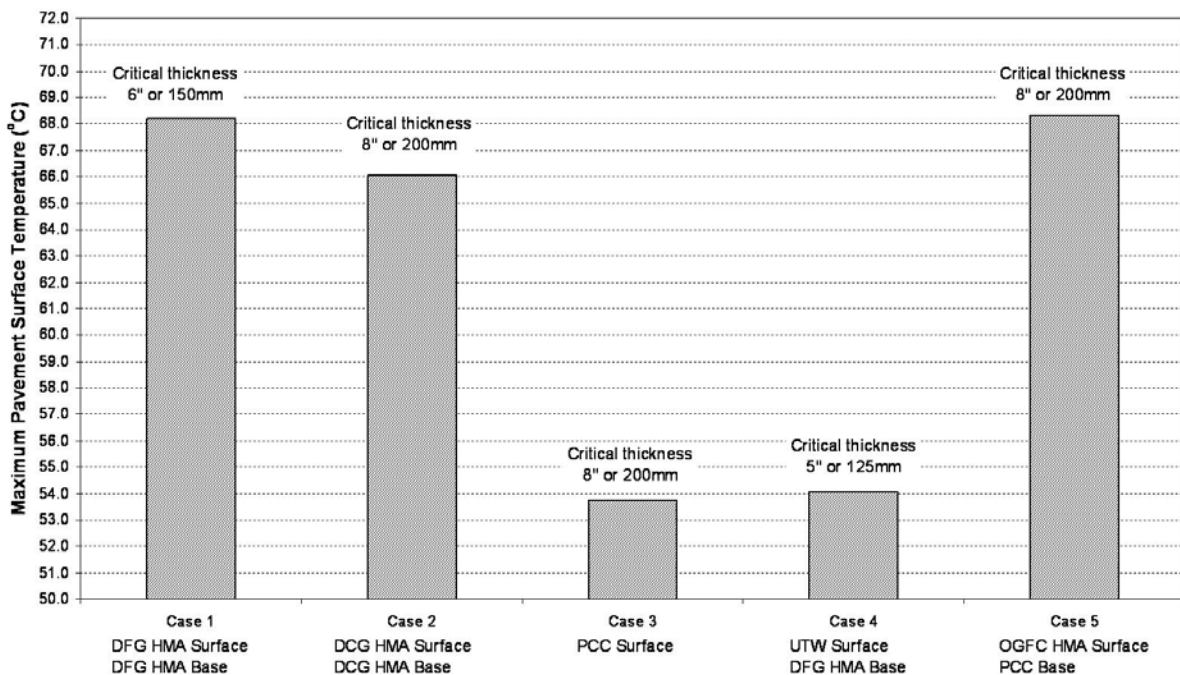
Figure 70 Lowest maximum temperatures at the respective critical thicknesses for each type of pavement
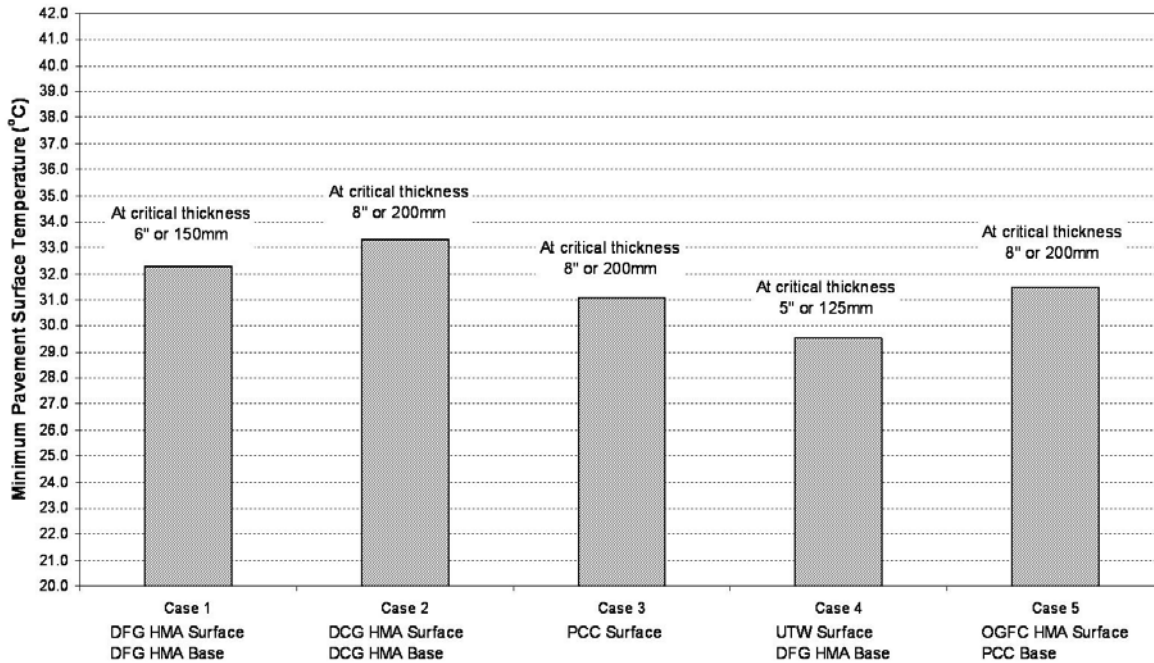
Figure 71 Corresponding minimum temperatures at the respective critical thicknesses for each type of pavement

It can be observed that pavements with light-colored surface, PCC or UTW surfaces will have the lowest maximum and minimum surface temperatures when compared to those with darker color (the HMA surfaces). This is due to the change in albedo (Gui *et al*., 2006). Nevertheless, it is also vital to consider the critical thickness, $L \approx \delta = \sqrt{\alpha t}$, in order to achieve the minimum surface temperature. Where not constrained by strength or other considerations, the pavement thickness should be made as close to the thermal penetration depth as possible, in order to minimize the surface temperature.

Chapter 4: Evaluating Impact on Energy and Safety

Roadway visibility is one of the most critical issues related to safety of drivers and pedestrians. Years of research have been devoted to enhancing the technologies that improve the visibility and response time of drivers. Advances in headlights, street lighting systems, lane markings, pedestrian clothing, and placement of signs are a few of the many safety measures that have resulted from the focus on visibility and safety. The visibility is particularly important at night when the driver's perception of their surroundings is limited to the areas illuminated by their headlights, street lights, retroreflective devices in the roads or the lights of other vehicles on the road. Even with these advances in safety, night time safety still remains a primary concern for transportation officials.

Providing these safety measures for citizens costs municipalities, building owners, and the federal government millions of dollars a year for installation, operation, and maintenance. The annual costs include street lighting systems required to maintain adequate visibility on highways, streets, and parking lots. Even minor improvements in lighting effectiveness and energy efficiency will result in major savings for government and private organizations.

This report has focused on the importance of high albedo (solar reflectance) pavement materials for reducing pavement surface temperatures and mitigating the Urban Heat Island effect. While visible light (sensible by the human eye) only makes up 43% of the total solar spectrum it can be assumed that a high albedo correlates reasonably well with a surface that also reflects visible light. This is certainly the case with PCC, which has relatively higher initial albedo (>0.30) and appears as a light grey to the human eye. Luminance, similar to albedo, is the ratio of total visible light reflected from the pavement towards the observer. It is measured in candela per meter squared (cdm^{-2}) and is closely related to the brightness that our eyes perceive.

A pavement with a greater luminance could provide more to the surrounding area, increasing the amount of light near the road surface at night and thereby improve the driver's ability to see objects near the road. This also opens the possibility to use fewer or less intense lighting systems which can save money in energy and installation costs.

This section of the report discusses the luminance characteristics of concrete pavements and evaluates the reduction in energy use made possible by the specification and use of high albedo pavement materials. The section begins by defining key terms, presents measured luminance values for concrete pavements, quantify the benefits of high albedo (high luminance) pavements based on modeling results, and concludes with recommendations for roadway lighting design.

Luminance

The ratio of the light reflected at a specific point to the total light striking an object is referred to as the luminance coefficient, q, and is dependant on the position of observer and the light source, the nature of the surface itself and several other variables. Luminance, Q, is the ratio of total light average reflected in a hemisphere from a surface to a light source (illuminance) horizontal to the surface. This is represented mathematically as;

$$Q = \frac{\int \Omega_e q d\Omega}{\int \Omega_e d\Omega}$$

Where, Ω_e is the solid angle defined by the hemisphere above the surface. The International Commission on Illumination (CIE) developed a classification system for luminance of pavements. These are provided below.

Table 16 Classification of road surfaces based on luminance (Q) (from ANSI RP-8)

Class	Q	Description
R1	0.1	Portland Cement Concrete
R2	0.07	Asphalt with a minimum of 60% gravel
R3	0.07	Asphalt with a dark aggregate
R4	0.08	Asphalt with avery smooth texture

In one study, the luminance for 150 pavement samples (Adrian and Jobanputra 2005) were measured. They found a mean PCC luminance of 0.1138 cdm^{-2} with a standard deviation of 0.0216 cdm^{-2}. For the asphalt samples they found a mean luminance of 0.0793 cdm^{-2} with a standard deviation of 0.0164 cdm^{-2}. It is apparent that PCC will provide a higher luminance value than asphalt in almost all cases.

Spectral Reflectance

The spectral reflectance (wavelength specific) measurements of PCC and asphalt concrete follow a similar trend with the exception that the PCC is 2.34 times more reflective over the same wavelengths. Different types of light sources provide light in different wavelengths. PCC and asphalt reflect the greatest amount of light in longer wavelengths ranges. It is important to choose light sources that produce light in the similar range as the surfaces being illuminated to achieve the greatest luminance. High Pressure Sodium (HPS) lights produce light closer to the reflectance range of concrete and asphalt than Metal Halide (MH).

Visibility

There are generally three factors that determine visibility; contrast, ambient luminance and size. Contrast is the difference in luminance between an object and its surroundings and can be represented as;

$$C = \frac{L_{object} - L_{background}}{L_{background}}$$

Where L_{object} is the luminance of the object and $L_{background}$ is the luminance of the surfaces behind the object.

Ambient luminance is that overall luminance of the background behind in the object being viewed. The ambient luminance is much greater during the day than at night making contrast even more important at night.

The size of the object is important to visibility and is measured in terms of angular size (Ziedman 2005). For example a six foot person viewed at 200 feet will appear to be the same size as a three foot person at 100 feet. Because the size, other than signs, is not under the control of designers,

they are limited to using street lightning and roadway reflectivity as their only means of improving night time visibility.

Improving Night Time Safety

It is well known that street lights lower accident rates by illuminating the roadway beyond the reach of the vehicle headlights and by reducing the glare from oncoming headlights. In areas where there are no street lighting, roadway reflectivity can increase size of the visible portion of the roadway. Reflective surfaces can also increase the background and ambient lighting which creates more contrast between the object and it background. In additions to increasing ambient luminance, reflective roadways enhance the reflection of headlamps generating more illumination on objects in front of the moving vehicle. In general, roadway reflectivity can provide many of the same safety benefits that are normally provided strictly by streetlights (Ziedman 2005).

Reducing Energy Demand and Installation Costs

There have been several studies that analyzed the impact of pavement reflectance on lighting source requirement (Starks 1986; Pomertantz 2000a; Adrian and Jobanputra 2005). Starks was among the first to publish on this subject, analyzing the luminance levels of different pavement types in 1986. Energy savings were estimated during a study conducted in California (Pomerantz et al. 2000a). They found that by using more reflective pavement materials will increase illumination and designers could save energy and costs by using fewer or less powerful street lamps. They estimated a 20% reduction in the required strength of the light sources by changing the pavement reflectivity from 10% to 30%.

A typical lighting situation for a parking lot can be modeled using software tools such as Lumen Micro 7.5. When modeling roadway lighting scenarios there are many variables that can contribute to the results including pole height, luminaire tilt, and geometry of lighting installation. These variables should be held constant in order to focus on the effects of the surface material types specifically.

In a detailed analysis using Lumen Micro 7.5 software, Adrian and Jobanputra modeled a parking lot (50m x 100m) with luminaire pole heights of 10 meters, having a horizontal tilt and bracket arm length of 0.5 meters. The luminaire used was the McGraw-Edison CS7265 HPS. Maintaining a constant configuration of light poles over the modeled section four standard luminaire wattage types (400, 250, 150 and 100 Watts) were modeled. The analysis produced two interesting results. First, they found that when using a luminaire that uses 400 Watts the average luminance in the asphalt lot was 3.4 cdm^{-2} while the PCC had an average luminance of 6.03 cdm^{-2} under identical conditions. The PCC lot was able to produce the same luminance as the asphalt parking lot by using the 250W luminaires. This equates to an energy savings of 41% by simply using a PCC parking lot surface. Besides the fact that the PCC surface reflected more of the light it also produced a more uniform light distribution which is an additional aesthetic benefit. Considering the systems will operate for 5 hours a day, in one year, the asphalt parking lot would require 6,026 kW-hr more energy than the PCC lot while maintaining equal luminance. More reflective pavements can also allow for a reduction in the total number of street lamps required for roads and street light. Using the same model and parking lot configuration, Adrian was able to show that the PCC lot would be able to provide the same lighting levels with only 14

luminaires compared to the 22 required for the asphalt lot. By using 8 less luminaires for the PCC lot the property owner could save approximately 5,844 kW-hr over one year of operation. This is a savings of 57 % between the two designs. These findings show that reflective pavements can improve nigh time visibility, enhance safety, and lower initial and operational costs related to lighting.

Summary

A review of pavement lighting studies have shown that high albedo (high reflectivity) pavements such as PCC have several advantages over darker pavements beyond reduction in temperatures. PCC provides nearly twice the luminance of asphalt concrete pavements. This increase in luminance can reduce demand for lighting by 41% to 57% when compared to conventional asphalt pavements. These savings in electrical energy and installation costs are evidence that when considering energy demand and safety, high albedo pavements should be preferred over darker pavements.

Chapter 5: Summary

Task 15 of the 2005 ACPA Concrete Pavement Research and Development program addresses the need to quantify the reflectance, absorption and emittance – of different concrete pavement surface materials, including the effects of color and texture over time, as a means of mitigating the Urban Heat Island (UHI) effect. In an effort to mitigate the effect of UHI, the US Environmental Protection Agency and the US Green Building Council through its Leadership in Environmental and Energy Design, LEED™ Rating Systems are working to develop a variety of techniques and processes through which temperature reductions can be achieved and the overall impact of heat absorption and transfer can be reduced. Little however has been done to consider or evaluate the impact and opportunities of design, material selection and innovation related to pavement surfaces.

The main objective of this research study was to provide understanding, supporting documentation, and tools on how pavement designs and materials selection contribute to surface and subsurface temperature fluctuations. This objective was achieved through two focus areas that outlined the scope of work of this research: thermal properties and reflectance evaluation, and heat absorption and transfer modeling.

In the first focus area, the reflectance "albedo" characteristics of various concrete pavement surfaces / mix types were identified. Surface and in-depth pavement temperatures of several field sections were collected to help validate modeling efforts in the second focus area of this study. Perhaps one of the most notable accomplishments in this area was the development of a simplified laboratory test procedure to measure the thermal conductivity of paving materials. Laboratory tests were also conducted to measure key thermal properties of the different paving materials. These properties were used in the second focus area of this study by provide input parameters for the pavement heat absorption and transfer model.

In the second focus area, a pavement heat absorption and transfer model was developed and validated. This fundamental model accounts for the surface rates of solar radiation absorption and heat transmission (re-radiation) of various pavements designs. It can be used for comparative evaluation and what-if-scenarios for the different pavements designs and types.

This research project serves to increase the body of knowledge centered on the economic, environmental, and social implications and benefits of concrete pavements. The outcome of the two focus areas outlined above will assist future decision makers and designers when choosing appropriate pavement materials for their particular application. It will provide further awareness of urban heat island, and drives further municipal ordinances and building codes that incorporate environmentally appropriate materials into development and rehabilitation projects.

Thermal Properties Data Collection

While the engineering performance of many common pavement variations has been well documented through past research, the thermal and radiative characteristics have not. In this report, the results of several studies and pavement test sections were presented; they quantified the albedo, temperature behavior, and thermal properties of several common pavement types.

In addition, there have been limited research investigations that have monitored the surface to deep ground temperature gradients under pavements in the field. The research team set out to

provide years worth of subsurface temperature data from near surface to 3m (10 ft) below the surface of various urban materials. This marks the first pavement focused effort of its kind. Experimental data from these actual pavement test sections were used in calibrating the theoretical predictive model developed in the second focus area of the study.

Laboratory Testing

The thermal and physical properties of concrete pavement materials were measured for several different samples. Material samples were obtained from a variety of sources including concrete suppliers, construction projects, and laboratory prepared.

Development of a New Thermal Conductivity Test Procedure

The standard procedure for measuring thermal conductivity is ASTM C 177-04. This method requires the temperature at steady state to determine k and mandates slab specimen geometries. These large dimensions present several difficulties in the fabrication of laboratory pavement samples. In addition, obtaining this size of pavement specimen from in-service pavement would disturb a large section of the pavement and entail additional costs to traditional materials sampling techniques.

Perhaps the most notable accomplishment task of this study was the development of a test method for accurately measuring the thermal conductivity of pavement materials. The method utilizes a cylindrical geometry common among field and laboratory samples prepared for mechanical testing of Portland cement concrete and asphalt mixtures. Theoretical analysis using fundamental heat transfer theory was applied to determine the appropriate design parameters for an experimental apparatus. An experimental apparatus was developed, constructed and evaluated using the propagation of uncertainty method. The experimental results fell within known values and previous estimates reported in the literature, and the confidence intervals found were determined to be within acceptable limits of accuracy.

Development of a Pavement Heat Absorption and Transfer Model

A one-dimensional mathematical model was developed to calculate the pavement near-surface temperatures using the hourly measured solar radiation, air temperature, dew-point temperature and wind velocity data. This model was based on the fundamental energy balance, and takes into account convection and radiation at the surface, as well as conduction to and from the ground. The model was validated against measured temperature data collected from pavement test sections using embedded thermocouples and climatic field equipment. The model was then used to identify the influence of the pavement thermophysical and geometry properties on the surface temperatures. This allowed ascertaining the optimal properties that would lower these temperatures, and consequently mitigate the UHI effects. It would also give insight on how future pavements could be constructed for mitigating such effects, while still maintaining satisfactory performance and lifetime.

A unique aspect of this model is that it is a stand-alone tool that can be used to evaluate different scenarios of pavement heat absorption and transfer. Other similar models (like the EICM) are usually integrated and used within a comprehensive pavement design analysis program. The

model validation results showed good accuracy in predicting near-surface pavement maximum and minimum temperatures.

The model was also used to vary the material thermal properties independently to evaluate the effects of each pavement property on the surface temperatures. The thermophysical properties variations included *thermal conductivity, volumetric heat capacity, thermal diffusivity, albedo* and *emissivity*. The results showed that the factor with the highest impact on pavement maximum temperatures is the albedo, followed by thermal diffusivity, thermal conductivity, emissivity and volumetric heat capacity. The reduction in the pavement minimum temperature was mostly affected by emissivity and albedo.

In a comparative analysis across a variety of different pavement types, the analysis showed that the light-colored surface, found in conventional and thin whitetopping concrete pavement designs, will have the lowest maximum surface temperatures. In fact, a thin whitetopping concrete pavement design would achieve the lowest minimum and maximum surface temperatures because of the combined albedo and reduced thickness effects.

Evaluating Impact on Energy and Safety

A review of pavement lighting studies have shown that high albedo (high reflectivity) pavements such as PCC have several advantages over darker pavements beyond reduction in temperatures. PCC provides nearly twice the luminance of asphalt concrete pavements. This increase in luminance can reduce demand for lighting by 41% to 57% when compared to conventional asphalt pavements. These savings in electrical energy and installation costs are evidence that when considering energy demand and safety, high albedo pavements should be preferred over darker pavements.

References

Adrian, W. and R. Jobanputra. "Influence of Pavement Reflectance on Lighting for Parking Lots." PCA R&D Serial No. 2458. Portland Cement Association 2005

Akbari, H., "Cooling Our Communities: An Overview of Heat Island Project Activities," Annual Report, Heat Island Group, Lawrence Berkeley National Laboratory, Berkeley, 1995

Akbari H. *et. al.*, "Cool Surfaces and Shade Trees to Reduce Energy Use and Improve Air Quality in Urban Area", *Solar Energy*, Vol.70, No.3, pp.295-210, 2001

Akbari, H., Pomerantz, M., and Taha, H., "Policies to Reduce Heat Islands: Magnitudes of Benefits and Incentives to Achieve Them", Proceedings of 1996 LBL-38679, *ACEEE Summer Study on Energy Efficiency in Buildings*, Vol.9, pp.177, 1996

American National Standard Practice for Roadway Lighting, ANSI/IESNA RP-8-00, Illuminating Society of North America, 1999; Approved 6/27/2000 by American National Standards Institute, Reaffirmed 2005. (ISBN 0-87995-160-5)

Asaeda, T., and Thanh, V, "Characteristics of permeable pavement during hot summer weather and impact on the thermal environment", Building and Environmental Report No.35, pp.363-375, 2000

ASHRAE, Handbook of Fundamentals, 2004

ASTM International Test C 177 - 04, "Standard Test Method for Steady-State Heat Flux Measurements and Thermal Transmission Properties by Means of the Guarded-Hot-Plate Apparatus," *Annual Book of ASTM Standards*, West Conshohocken, PA, 2006.

ASTM C 351-92b (1999) Standard Test Method for Mean Specific Heat Capacity of Thermal Insulation

Barnes, K., Morgan, J., and Roberge, M., "Impervious Surfaces and the Quality of Natural and Built Environment", Department of Geography and Environmental Planning, Towson University, Baltimore, Maryland, 2001.

Bentx D.P., "Sorptivity-based Service Life Predictions for Concrete Pavements", Building and Fire Research Laboratory, National Institute of Standards and Technology, Gaithersburg, Maryland, Sept 2001

Best, M.J., "A Model To Predict Surface Temperatures", *Boundary-Layer Meteorology*, pp.279-306, 1998

Bhardwaj, R., P. Phelan, J. Golden, and K. Kaloush. "An urban energy balance for the Phoenix, Arizona, USA Metropolitan Area." Proceedings of the IMECE2006. ASME International

Mechanical Engineering Congress and Exposition., November 5-10, 2006, Chicago, Illinois, USA, 2006.

Boedecker Plastics, Inc. 904 West 6th Street, Shiner, Texas 77984 USA <http://www.boedeker.com/polye_p.htm> August 7, 2007

Boriboonsomsin, K. & Reza, F. (2007) *Mix Design and Benefit Evaluation of High Solar Reflectance Concrete for Pavements.* Proceedings of the Transportation Research Board's 86th Annual Meeting. Washington D.C., January, 2007

Caltrans, Maintenance Technical Advisory Guide (TAG), State of California Department of Transport, Chap.8, Oct 2003

Cengel, Yunus A.; Boles, Michael A. *Thermodynamics - An Engineering Approach*. McGraw Hill, 2002.

Çengel, Y., *Heat Transfer. A Practical Approach*, 2nd edition, McGraw-Hill, New York, pp.368-375, pp.2, 23, 83 & 578, 2003

Chadbourn B. *et. al*., "An Asphalt Paving Tool for Adverse Condition", University of Minnesota, Department of Civil Engineering, June 1998

Chen, J.S., Lin, K.Y. and Chang, M.K., "Influence of Coarse Aggregate Shape on the Strength of Asphalt Concrete Mixtures", *Journal of the Eastern Asia Society for Transportation Studies*, Vol.6, pp.1062-1075, 2005

Corlew, J.S., and Dickson, P.F. (1968). "Methods for Calculating Temperature Profiles of Hot-Mix Asphalt Concrete as Related to the Construction of Asphalt Pavements", *Asphalt Paving Technology 1968, Proceedings: Association of Asphalt Paving Technologists Technical Sessions*, Vol.37, pp.101-140, 1968

Delatte, N., D. Miller, D., and Mikajic, A. (2007) *Portland Cement Pervious Concrete Pavement: Field Performance Investigation on Parking Lot and Roadway Pavements.* Report to the Ready Mixed Concrete Research & Education Foundation. December 1, 2007.

Dempsey, D. V., and Thompson, M. R. "A heat transfer model for evaluating frost action and temperature related effects in multi-layered pavement system." *Transportation Research Record 342*, Transportation Research Board, Washington, D.C., 39–56, 1970.

Federal Highway Administration. Fly Ash Facts for Highway Engineers. http://www.fhwa.dot.gov/pavement/recycling/fach01.cfm.

FHWA, "The Effects of Higher Strength and Associated Concrete Properties on Pavement Performanace", U.S. Department of Transportation, Federal Highway Administration, Publication No.FHWA-RD-00-161, Jun 2001

Figliola, R. and D. Beasley. Theory and Design for Mechanical Measurements, Fourth Edition. John Wiley & Sons, Inc. pp 110-141, 2006.

Golden, J.S., "The Built Environment Induced Urban Heat Island Effect in Rapidly Urbanizing Arid Regions - A Sustainable Urban Engineering Complexity", *Environmental Sciences*, Vol.1, No.4, pp.321-349, 2004.

Golden, J.S., and Kaloush K., "Mesoscale and Microscale Evaluation of Surface Pavement Impacts on the Urban Heat Island Effects", *International Journal of Pavement Engineering*, 2005.

Golden, J., P. Guthrie, K. Kaloush, and R. Britter. "Summertime urban heat island hysteresis lag complexity." *ICE Proceedings, Engineering Sustainability*, 158(4), 197-210, 2005.

Gray, K.A., and Finster, M.E., "The Urban Heat Island Photochemical Smog, and Chicago: Local Features of the Problem and Solution", Department of Civil Engineering, Northwestern University, Evanston, Illinois, 2000.

Gui J. *et. al.*, "Impact of pavement thermophysical properties on surface temperatures", *ASCE Journal of Materials in Civil Engineering*, 2006.

Heath, M.T., *Scientific Computing, An Introductory Survey*, 2nd edition, Mcgraw-Hill, New York, pp.460-461, 2002

Highter, W. H., and Wall, D. J. "Thermal properties of some asphaltic concrete mixes." *Transportation Research Record 968*, Transportation Research Board, Washington, D.C., 38–45, 1984.

Jordan, P. G., and Thomas, M. E. "Prediction of cooling curves for hot-mix paving materials by a computer program." Transportation and Road Research Lab. Rep. No. *729*, Crowthorne, Berkshire, England, 1976.

Kanit, T., S. Forest, I. Galliet, V. Mounoury, D. Jeulin. "Determination of the size of the representative volume element for random composites: statistical and numerical approach." *International Journal of Solids and Structures*, Vol 40, Issue 13-14, ppg 3647-3679, 2003.

Kavianipour, A., and Beck, J. V. "Thermal property estimation utilizing the Laplace transform with application to asphaltic pavement." *Int. J. Heat Mass Transfer*, 20(3), 259–267, 1977.

Khan, M.I. "Factors affecting the thermal properties of concrete and applicability of its prediction models." *Building and Environment*, 37, pp 607 – 614, 2002.

Kinouchi, T., Yoshinaka, T., Fukae, N., and Kanda, M., "Development of cool pavement with dark colour high albedo coating", Tokyo Institute of Technology, Tokyo, Japan, 2004

Kline, S. J., and F.A. McClintock, "Describing uncertainties in single-sample experiments." *Mechanical Engineering* 75:3-8, January 1953.

Illuminating Engineering Society of North America. "Lighting for Parking Facilities: RP-20-98". 1998.

Lapujade, P.G., (1994). "On site roof reflectance measurement methodology: theory and limitations.' FSEC-RR-28-94.

Lawrence Berkeley National Laboratory (LBNL). Urban Heat Island Group. <http://eetd.lbl.gov/HeatIsland/>

Levinson, R. & Akbari, H. (2002) Effect of composition and exposure on the solar reflectance of portland cement concrete. Cement and Concrete Research. 32 p1679-1698.

Luca, J. and D. Mrawira. "New Measurement of Thermal Properties of Superpave Asphalt Concrete." *Journal of Materials in Civil Engineering*, Vol. 17, No. 1, January/February 2005, pp. 72-79.

Lumen Micro 7.5™, Light Technologies, Inc.

Mamlouk, M.S. and Zaniewski, J. P. *Materials for Civil and Construction Engineers*. Second Edition, Pearson Prentice Hall, New Jersey 07458, 2005.

MEPDG. "Guide for Mechanistic – Empirical Design of New and Rehabilitated Pavement Structures." NCHRP 1-37A Final Report, Transportation Research Board, National Research Council, Washington, D.C., 2004.

Mobasher B. et. al., "Laboratory Evaluation of ADOT's Thin Whitetopping PCC Test Sections – Cottonwood", Department of Civil and Environmental Engineering, Arizona State University, 2004.

Moffat, R.J (1982). Contributions to the Theory of Single Sample Uncertainty Analysis, R J Moffat, Department of Mechanical Engineering, Stanford University, Transactions of ASME, Vol.104

Moffat, R.J. (1985). Using Uncertainty Analysis in the Planning of an Experiment, R J Moffat, Department of Mechanical Engineering, Stanford University, Transactions of ASME, Vol.107 Cengel, Y. (1996) Heat Transfer – A Practical Approach. McGraw-Hill Higher Education.

Mrawira, D. and J. Luca. "Effect of aggregate type, gradation, and compaction level on thermal properties of hot-mix asphalts." *Canadian Journal of Civil Engineering*
2006, vol. 33, n°11, pp. 1410-1417, 2006.

National Slag Association. Blast Furnace Slag: the Construction Material of Choice., http://www.nationalslagassoc.org/PDF_files/NSABlastFurn.PDF

NAPA, "HMA Pavement Mix Type Selection Guide", National Asphalt Pavement Association and U.S. Department of Transportation, Federal Highway Administration, 2001

NCHRP 1-37A., "Guide for Mechanistic-Empirical Design of New and Rehabilitated Pavement Structures", Final Report, Part 2. Design Inputs, Chapter 3. Environmental Effects, National Cooperative Highway Research Program, Transportation Research Board, National Research Council, 2004

Oke, T.R., *Boundary Layer Climate*, 2nd edition, Routledge, London, 1968

O'Hanlon J.F. , Allen R. W., et al., Driver's Visibility Requirements for Roadway Delineation, FHWA Report RD-77-165, November 1977, Vol. 1, Effects of Contrast and Configuration on Driver Performance and Behavior, Washington, DC.

Phukan, A. *Frozen ground engineering*, Prentice–Hall, Englewood Cliffs, N.J., 1985.

Pomerantz, M., H. Akbari and J.T. Harvey.. Durability and Visibility Benefits of Cooler Reflective Pavements. LBNL – 43443. Lawrence Berkeley National Laboratory. 2000a

Pomerantz, M., B. Pon, H. Akbari, and S.C. Change "The Effect of Pavements' Temperatures on Air Temperatures in Large Cities." Heat Island Group. LBNL-43442. Lawrence Berkeley National Laboratory, Berkeley, CA., 2000b.

Sailor, D., K. Resh and D. Segura. "Field measurement of albedo for limited extent test surfaces." *Solar Energy*, 80(5), 589-599, 2006.

Samonsen, E., Janoo, V. C., and Isaacson, U. "Prediction of temperature and moisture changes in pavement structures." *J. Cold Region Engineering*, 11(4), 291–307, 1997.

San Diego Plastics, Inc. 2220 Mckinley Ave., National City, CA 91950
<http://www.sdplastics.com/polyeth.html> August 7, 2007

Schindler, A.K., Ruiz, J.M., Rasmussen, R.O., Chang, G.K., and Wathne, L.G., "Concrete pavement temperature prediction and case studies with the FHWA HIPERPAV models", *Cement and Concrete Composites*, Vol.26, No.5, pp.463-471, 2004

Scott, K. *et. al.*, "Effects of Tree Cover on Parking Lot Microclimate and Vehicle Emission", *Journal of Arboriculture*, Vol. 25, pp.129-142, May 1999

Smith G.B. *et. al.*, "Coloured paints based on iron oxide and silicon oxide coated flakes of aluminium as the pigment for energy efficient paint: optical and thermal experiments", Solar Energy Materials & Solar Cells, Vol. 79, pp.179-197, 2003

Souza, L., Rodrigues, D., and Mendes, J., "Sky View Factors Estimation using a 3D-GIS Extension", São Paulo State University, Bauru, Brazil, 2003

Stark, R.E. 1986. "Road Surfaces Reflectance Influences Lighting Design." Lighting Design + Applications April.

Taha, H., Akbari, H., Rosenfeld, A., and Huang, J., "Residential Cooling Loads and the Urban Heat Island – the Effects of Albedo", *Building and Environment*, Vol.23. No.4, pp.271-283, 1988

Takeda, K. Laboratory Work in Chemistry I (Calibration of Beckmann Differential Thermometer) Tan, S., Low, B., and Fwa, T. "Determination of thermal conductivity and diffusivity by transient heating of a thin slab." *Building Environment*, 27(1), 71–76, 1992.

Tan, S., Fwa, T., Chuai, C., and Low, B. "Determination of thermal properties of pavement materials and unbound aggregates by transient heat conduction." *J. Test. Eval.*, 25(1), 15–22, 1997.

Tomosawa, F. and Noguchi, T., "Relationship Between Compressive Strength and Modulus of Elasticity of High-Strength Concrete", University of Tokyo, Japan, 2000

United Nation Population Fund, "Global Population Hits 6 Billion", *The State of World Population*, 1999

U.S. Army Corp of Engineers, "Arctic and Sub-arctic Construction Calculation Methods for Determination of Depths of Freeze and Thaw in Soils", Technical Manual TM 5-852-6/AFR88-19, Vol.6, pp.2-1 & 2-6, 1988

U.S. Department of Energy, "Tomorrow's Energy Today for Cities and Counties: Cooling our Cities", National Renewable Energy Laboratory, Technical Information Program DOE/CH10093-211, Nov 1993

U.S. Environmental Protection Agency "Cooling our Communities: A Guidebook on Tree Planting and Light-Colored Surfacing,", January 1992, 22P-2001

U.S. Green Building Council (2006). LEED New Construction v2.2 Reference Guide. United States Green Building Council. Washington, DC.

Witczak, M. W., Kaloush, K., Pellinen, T., El-Basyouny, M., and Von Quintus, H. "Simple Performance Test for Superpave Mix Design", NCHRP Report 465, Transportation Research Board-National Research Council, Washington, D.C., 2002.

Wolfe, R. K., Heath, G. L., and Colony, D. C. "University of Toledo time–temperature model laboratory field validation." *Rep. No. FHWA/OH-80/006*, Dept. of Industrial Engineering, Univ. of Toledo, Toledo, Ohio, 1980.

Ziedman, K. "Roadway Reflectivity and Visibility. Report prepared for the Granite Rock Company", Watsonville, CA. 2005

Zubeck H. and Bethard T., "Polymer-Modified Asphalt Emissions", University of Alaska Anchorage, March 2001
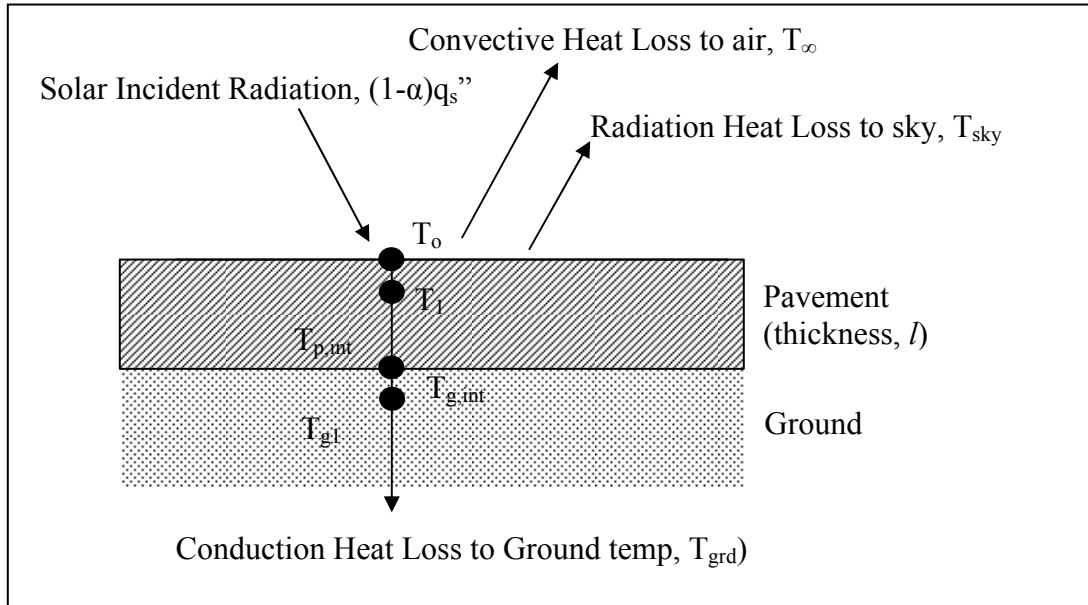
APPENDICES

APPENDIX A - DETAILED WORKINGS OF PAVEMENT THERMAL MODEL (EXPLICIT FINITE DIFFERENCE METHOD)

APPENDIX B - PAVEMENT THERMAL MODEL OPERATING PROCEDURES

APPENDIX A

DETAILS OF THE PAVEMENT THERMAL MODEL

(EXPLICIT FINITE DIFFERENCE METHOD)

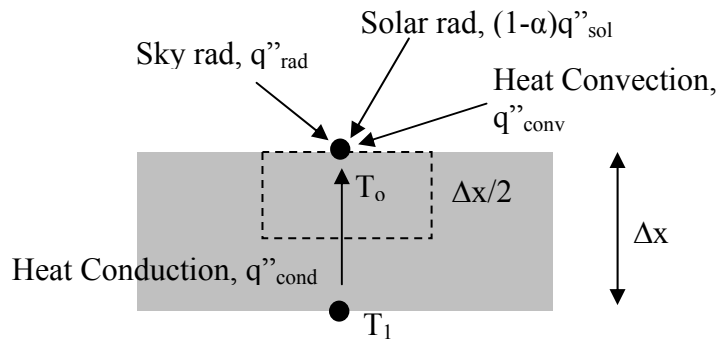# DETAILED WORKINGS OF PAVEMENT THERMAL MODEL (EXPLICIT FINITE DIFFERENCE METHOD)

Modes of heat transfer occurring in pavement

(Note: The distance between each temperature nodes is assumed at a constant Δx)

i. *Consider pavement surface, T_o*

Using Energy Balance on surface Node:

$$E_{st} = E_{in} + E_{gen}$$

Governing Equation using finite difference method

$$\rho_{pave} c_{pave} A \frac{\Delta x}{2} \left(\frac{T_o^{p+1} - T_o^p}{\Delta t} \right) = \psi_{sol}(1-\alpha) q_s'' A + h_\infty A(T_\infty^p - T_o^p) + h_{rad} A(T_{sky}^p - T_o^p) + k_{pave} A \frac{T_1^p - T_o^p}{\Delta x}$$

| Energy Stored | Solar Radiation | Atmospheric Heat Convection | Sky Radiation | Heat Conduction to Ground |

- [A1]

109

Rearranging [A1],

$$\frac{\rho_{pave}c_{pave}\Delta x}{2\Delta t}T_o^{p+1} = \left(\frac{\rho_{pave}c_{pave}\Delta x}{2\Delta t} - h_{rad} - h_\infty - \frac{k_{pave}}{\Delta x}\right)T_o^p + \left(\psi_{sol}(1-\alpha)q_s'' + h_\infty T_\infty^p + h_{rad}T_{sky}^p + \frac{k_{pave}}{\Delta x}T_1^p\right)$$

$$\boxed{T_o^{p+1} = \left(1 - \frac{2\Delta t}{\rho_{pave}c_{pave}\Delta x}\left[h_{rad} + h_\infty + \frac{k_{pave}}{\Delta x}\right]\right)T_o^p + \frac{2\Delta t}{\rho_{pave}c_{pave}\Delta x}\left(\psi_{sol}(1-\alpha)q_s'' + h_\infty T_\infty^p + h_{rad}T_{sky}^p + \frac{k_{pave}}{\Delta x}T_1^p\right)}$$

- [A2]

For Explicit FD method, Courant–Friedrichs–Lewy (CFL) stability condition needs to be satisfied:

$$\left(1 - \frac{2\Delta t}{\rho_{pave}c_{pave}\Delta x}\left[h_{rad} + h_\infty + \frac{k_{pave}}{\Delta x}\right]\right) \geq 0, \text{ or } \boxed{\Delta t \leq \left(\frac{\rho_{pave}c_{pave}\Delta x^2}{2\left(h_{rad}\Delta x + h_\infty \Delta x + k_{pave}\right)}\right)}$$
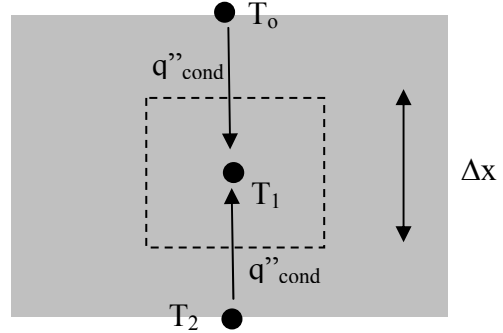
- [A3]

ii. *Consider pavement interior, T_m*

Using Energy Balance on pavement interior Node:

$$E_{st} = E_{in} + E_{gen}$$

Governing Equation using finite difference method

$$\rho_{pave}c_{pave}A\Delta x\left(\frac{T_m^{p+1} - T_m^p}{\Delta t}\right) = k_{pave}A\frac{T_{m-1}^p - T_m^p}{\Delta x} + k_{pave}A\frac{T_{m+1}^p - T_m^p}{\Delta x}$$

- [A4]

Rearranging [A4],

$$\boxed{T_m^{p+1} = \left(1 - \frac{2\Delta t}{\rho_{pave}c_{pave}\Delta x}\left[\frac{k_{pave}}{\Delta x}\right]\right)T_m^p + \frac{\Delta t}{\rho_{pave}c_{pave}\Delta x}\frac{k_{pave}}{\Delta x}\left(T_{m-1}^p + T_{m+1}^p\right)}$$
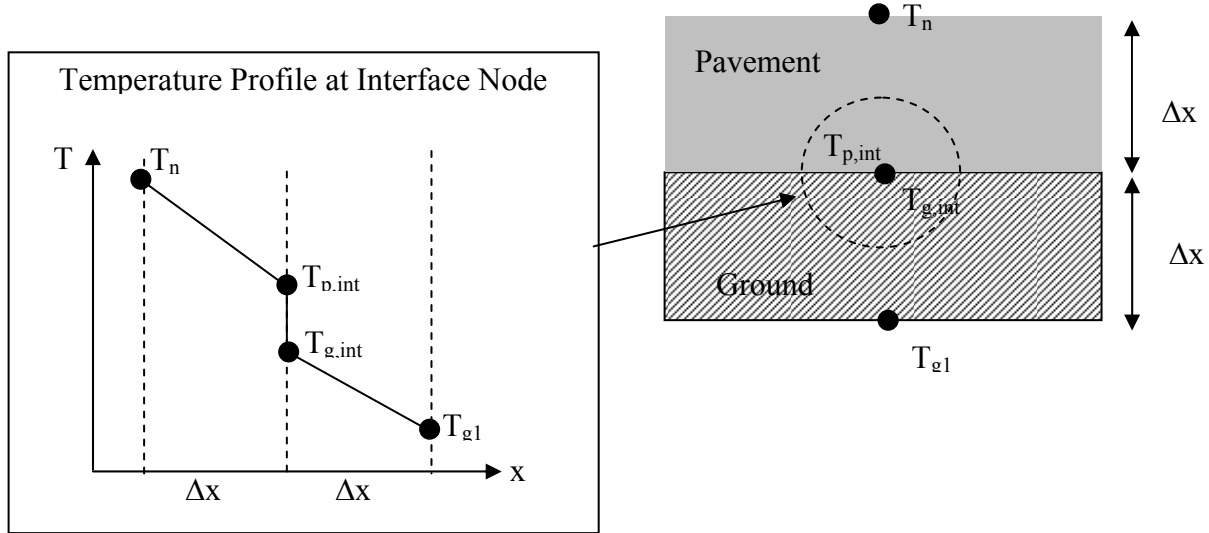
- [A5]

CFL stability condition:

$$\left(1 - \frac{2\Delta t}{\rho_{pave} c_{pave} \Delta x}\left[\frac{k_{pave}}{\Delta x}\right]\right) \geq 0 \quad \text{or} \quad \boxed{\Delta t \leq \frac{\rho_{pave} c_{pave} \Delta x^2}{2k_{pave}}} \qquad \text{- [A6]}$$

iii. **Consider pavement/ground interface, $T_{p,\text{int}}$ and $T_{g,\text{int}}$**

(or pavement multi-layer interfaces)

Assume a temperature node in both the pavement and ground each, located δ away from the

"interface" such that $\delta \ll \Delta x$, $T_{p,\text{int}}$ and $T_{g,\text{int}}$ (*Note that $T_{p,\text{int}} \neq T_{g,\text{int}}$*)

a. <u>Consider the temperature, $T_{p,\text{int}}$</u>

By Surface Energy Balance: $q''_{pave} = q''_{grd}$

Hence, by approximation:

$$k_{pave} \frac{dT_{pave}}{dx} = k_{grd} \frac{dT_{grd}}{dx}$$

$$k_{pave} \frac{T_n - T_{p,int}}{\Delta x} = k_{grd} \frac{T_{g,int} - T_{g1}}{\Delta x}$$

$$T_n - T_{p,int} = \frac{k_{grd}}{k_{pave}} \left(T_{g,int} - T_{g1} \right)$$

$$T_{p,int} = T_n - \frac{k_{grd}}{k_{pave}} T_{g,int} + \frac{k_{grd}}{k_{pave}} T_{g1} \qquad\qquad\qquad \text{- [A7]}$$

Let the heat transfer between $T_{p,int}$ and $T_{g,int}$ be q''_{int} such that

$$q''_{int} = h_c \left(T_{p,int} - T_{g,int} \right)$$

where h_c is the surface conductance (W/m^{2}K)

$$T_{g,int} = T_{p,int} - \frac{q''_{int}}{h_c}$$

$$T_{g,int} = T_{p,int} - R_c q''_{int} \qquad\qquad\qquad\qquad \text{- [A8]}$$

where Rc is the contact resistance ($R_c = \dfrac{1}{h_c}$ m^{2}K/W)

(8) into (7)

$$T_{p,int} = T_n - \frac{k_{grd}}{k_{pave}} \left(T_{p,int} - R_c q''_{int} \right) + \frac{k_{grd}}{k_{pave}} T_{g1}$$

$$\left(1 + \frac{k_{grd}}{k_{pave}} \right) T_{p,int} = T_n + \frac{k_{grd}}{k_{pave}} R_c q''_{int} + \frac{k_{grd}}{k_{pave}} T_{g1}$$

Since $q''_{int} = q''_{pave} = q''_{grd}$,

Hence $q''_{int} = k_{pave} \dfrac{T_n - T_{p,int}}{\Delta x}$

Therefore, $$T_{p,\text{int}} = \frac{\left(1 + \dfrac{k_{grd}R_c}{\Delta x}\right)T_n + \left(\dfrac{k_{grd}}{k_{pave}}\right)T_{g1}}{\left(1 + \dfrac{k_{grd}}{k_{pave}} + \dfrac{k_{grd}R_c}{\Delta x}\right)}$$

$$\boxed{T_{p,\text{int}} = \frac{\left(k_{pave}\Delta x + k_{pave}k_{grd}R_c\right)T_n + k_{grd}\Delta x T_{g1}}{\left(k_{pave}\Delta x + k_{grd}\Delta x + k_{pave}k_{grd}R_c\right)}}$$ - [A9]

b. *Consider the temperature,* $T_{g,\text{int}}$

From [A7], $$T_{g,\text{int}} = T_{g1} + \frac{k_{pave}}{k_{grd}}T_n - \frac{k_{pave}}{k_{grd}}T_{p,\text{int}}$$ - [A10]

From [A8] $$T_{p,\text{int}} = T_{g,\text{int}} + R_c q''_{\text{int}}$$ - [A11]

where Rc is the contact resistance ($R_c = \dfrac{1}{h_c}$ m^{2}K/W)

[A11] into [A10]

$$\left(1 + \frac{k_{pave}}{k_{grd}}\right)T_{g,\text{int}} = T_{g1} - \frac{k_{pave}}{k_{grd}}R_c q''_{\text{int}} + \frac{k_{pave}}{k_{grd}}T_n$$

Since $q''_{\text{int}} = q''_{pave} = q''_{grd}$

Hence $$q''_{\text{int}} = k_{grd}\frac{T_{g,\text{int}} - T_{g1}}{\Delta x}$$

Therefore, $$T_{g,\text{int}} = \frac{\left(1 + \dfrac{k_{pave}R_c}{\Delta x}\right)T_{g1} + \left(\dfrac{k_{pave}}{k_{grd}}\right)T_n}{\left(1 + \dfrac{k_{pave}}{k_{grd}} + \dfrac{k_{pave}R_c}{\Delta x}\right)}$$

$$\boxed{T_{g,\text{int}} = \frac{\left(k_{grd}\Delta x + k_{pave}k_{grd}R_c\right)T_{g1} + k_{pave}\Delta x T_n}{\left(k_{grd}\Delta x + k_{pave}\Delta x + k_{pave}k_{grd}R_c\right)}}$$ - [A12]

c.   _Verification of_ $T_{p,\text{int}}$ _and_ $T_{g,\text{int}}$

Assuming that there is no contact resistance, i.e. $R_c = 0$

From [A9]
$$T_{p,\text{int}} = \frac{k_{pave}\Delta x T_n + k_{grd}\Delta x T_{g1}}{k_{pave}\Delta x + k_{grd}\Delta x}$$

From [A12]
$$T_{g,\text{int}} = \frac{k_{grd}\Delta x T_{g1} + k_{pave}\Delta x T_n}{k_{grd}\Delta x + k_{pave}\Delta x}$$
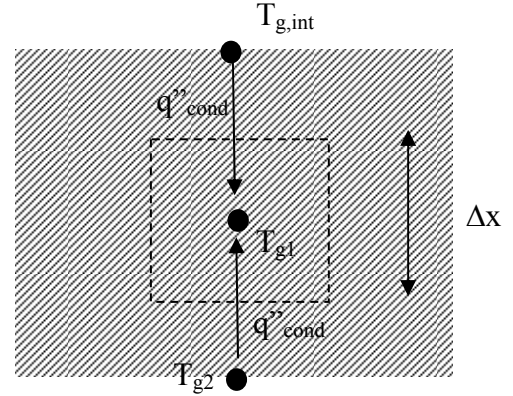
Therefore $T_{p,\text{int}} = T_{g,\text{int}}$ for **$R_c = 0$**

(Note:

iv.   *Consider ground interior, T_n*

Using Energy Balance on ground interior Node:

$E_{st} = E_{in} + E_{gen}$

Governing Equation using finite difference method

$$\rho_{grd} c_{grd} A\Delta x\left(\frac{T_n^{p+1} - T_n^p}{\Delta t}\right) = k_{grd} A\frac{T_{n-1}^p - T_n^p}{\Delta x} + k_{grd} A\frac{T_{n+1}^p - T_n^p}{\Delta x}$$
- [A13]

Rearranging [A13]

$$\boxed{T_n^{p+1} = \left(1 - \frac{2\Delta t}{\rho_{grd} c_{grd}\Delta x}\left[\frac{k_{grd}}{\Delta x}\right]\right)T_n^p + \frac{\Delta t}{\rho_{grd} c_{grd}\Delta x}\frac{k_{grd}}{\Delta x}\left(T_{n-1}^p + T_{n+1}^p\right)}$$
- [A14]

Similarly, to satisfy CFL stability condition:

$$\left(1 - \frac{2\Delta t}{\rho_{grd} c_{grd}\Delta x}\left[\frac{k_{grd}}{\Delta x}\right]\right) \geq 0, \text{ or } \boxed{\Delta t \leq \frac{\rho_{grd} c_{grd}\Delta x^2}{2k_{grd}}}$$
- [A15]

114

### v.	*Courant-Friedrichs-Lewy (CFL) Stability Criterion*

From the CFL stability equations established for the pavement surface node, pavement interior node and ground interior node (Eq.[A3], [A6] and [A15]), it is important to determine the stability criteria that will suit all 3 conditions. From the equations expressions, it is determined that Eq.[A3] has the most stringent criteria, i.e.

$$\Delta t \le \left(\frac{\rho_{pave} c_{pave} \Delta x^2}{2(h_{rad} \Delta x + h_\infty \Delta x + k_{pave})} \right)$$

Hence for the thermal model with Δx assumed at half-inch interval (i.e. 0.0127m), given the known range of pavement and ground properties, in order to satisfy the CFL stability criterion , Δt has to be $\le$ 180s ((i.e. time-step interval must be lower than 3 mins). However due to the fact that Eq.[A3] is also dependent on the variables of h_{rad} and h_∞, it is critical that the time-step Δt is relatively small enough to allow for any changes of these variables, which might reduce the Δt requirement of less than 3 mins. Therefore the thermal model is programmed with the time-step, Δt taken as 120s (i.e. 2 mins) interval, in order to safely meet the stability criterion.

### vi.	*Simplification of Equations*

With both x and t determined, we can now proceed to simplify the time-step equations so as to allow the easy computation of the temperature distribution while marching out-in-time.

Eq.[A2] --- *Pavement Surface Node*

$$T_o^{p+1} = \left(1 - \frac{2\Delta t}{\rho_{pave} c_{pave} \Delta x} \left[h_{rad} + h_\infty + \frac{k_{pave}}{\Delta x} \right] \right) T_o^p + \frac{2\Delta t}{\rho_{pave} c_{pave} \Delta x} \left(\psi_{sol}(1-\alpha)q_s'' + h_\infty T_\infty^p + h_{rad} T_{sky}^p + \frac{k_{pave}}{\Delta x} T_1^p \right)$$

115

Let
$$\delta_1 = \frac{2\Delta t}{\rho_{pave} c_{pave} \Delta x}$$

$$A_{surface} = \left(1 - \delta_1 \left[h_{rad} + h_\infty + \frac{k_{pave}}{\Delta x} \right] \right)$$

$$B_{surface} = \delta_1 \frac{k_{pave}}{\Delta x}$$

$$C_{surface} = \delta_1 \left(\psi_{sol} (1-\alpha) q_s'' + h_\infty T_\infty^p + h_{rad} T_{sky}^p \right)$$

Therefore
$$\underline{T_o^{p+1} = A_{surface} T_o^p + B_{surface} T_1^p + C_{surface}} \qquad \text{- [A16]}$$

Eq.[A5] --- Pavement Interior Node

$$T_m^{p+1} = \left(1 - \frac{2\Delta t}{\rho_{pave} c_{pave} \Delta x} \left[\frac{k_{pave}}{\Delta x} \right] \right) T_m^p + \frac{\Delta t}{\rho_{pave} c_{pave} \Delta x} \frac{k_{pave}}{\Delta x} \left(T_{m-1}^p + T_{m+1}^p \right)$$

$$T_m^{p+1} = \left(1 - \delta_1 \left[\frac{k_{pave}}{\Delta x} \right] \right) T_m^p + \frac{1}{2} \delta_1 \left(\frac{k_{pave}}{\Delta x} \right) \left(T_{m-1}^p + T_{m+1}^p \right)$$

Let
$$A_{pave} = \left(1 - \delta_1 \left[\frac{k_{pave}}{\Delta x} \right] \right)$$

$$B_{pave} = \delta_1 \frac{k_{pave}}{2\Delta x}$$

Therefore
$$\underline{T_m^{p+1} = A_{pave} T_m^p + B_{pave} \left(T_{m-1}^p + T_{m+1}^p \right)} \qquad \text{- [A17]}$$

Eq.[A9 & [A12] --- Pavement/Ground Interface Nodes (or Pavement Multi-layers Interface Nodes)

$$T_{p,\text{int}} = \frac{\left(k_{pave}\Delta x + k_{pave}k_{grd}R_c\right)T_n + k_{grd}\Delta x T_{g1}}{\left(k_{pave}\Delta x + k_{grd}\Delta x + k_{pave}k_{grd}R_c\right)}$$ - [A18]

$$T_{g,\text{int}} = \frac{\left(k_{grd}\Delta x + k_{pave}k_{grd}R_c\right)T_{g1} + k_{pave}\Delta x T_n}{\left(k_{grd}\Delta x + k_{pave}\Delta x + k_{pave}k_{grd}R_c\right)}$$ - [A19]

Eq.[A14] --- Ground Interior Node (or Different Pavement Layer Interior Node)

$$T_n^{p+1} = \left(1 - \frac{2\Delta t}{\rho_{grd}c_{grd}\Delta x}\left[\frac{k_{grd}}{\Delta x}\right]\right)T_n^p + \frac{\Delta t}{\rho_{grd}c_{grd}\Delta x}\frac{k_{grd}}{\Delta x}\left(T_{n-1}^p + T_{n+1}^p\right)$$

Let
$$\delta_2 = \frac{2\Delta t}{\rho_{grd}c_{grd}\Delta x}$$

$$A_{grd} = \left(1 - \delta_2\left[\frac{k_{grd}}{\Delta x}\right]\right)$$

$$B_{grd} = \delta_2\frac{k_{grd}}{2\Delta x}$$

Therefore
$$T_n^{p+1} = A_{grd}T_n^p + B_{grd}\left(T_{n-1}^p + T_{n+1}^p\right)$$ - [A20]

117

APPENDIX B

PAVEMENT THERMAL MODEL OPERATING PROCEDURES

PAVEMENT THERMAL MODEL
OPERATING PROCEDURES

The pavement temperature simulation model is developed using MS Excel© spreadsheet

with the explicit finite difference equations derived for the heat transfer occurring at and

within the pavement (see Appendix A). The step-by-step procedure to operating the

simulation program is as follows:

Step 1: Open the file: FD Model_Pave 3days.xls

Go to worksheet: Day1 Data
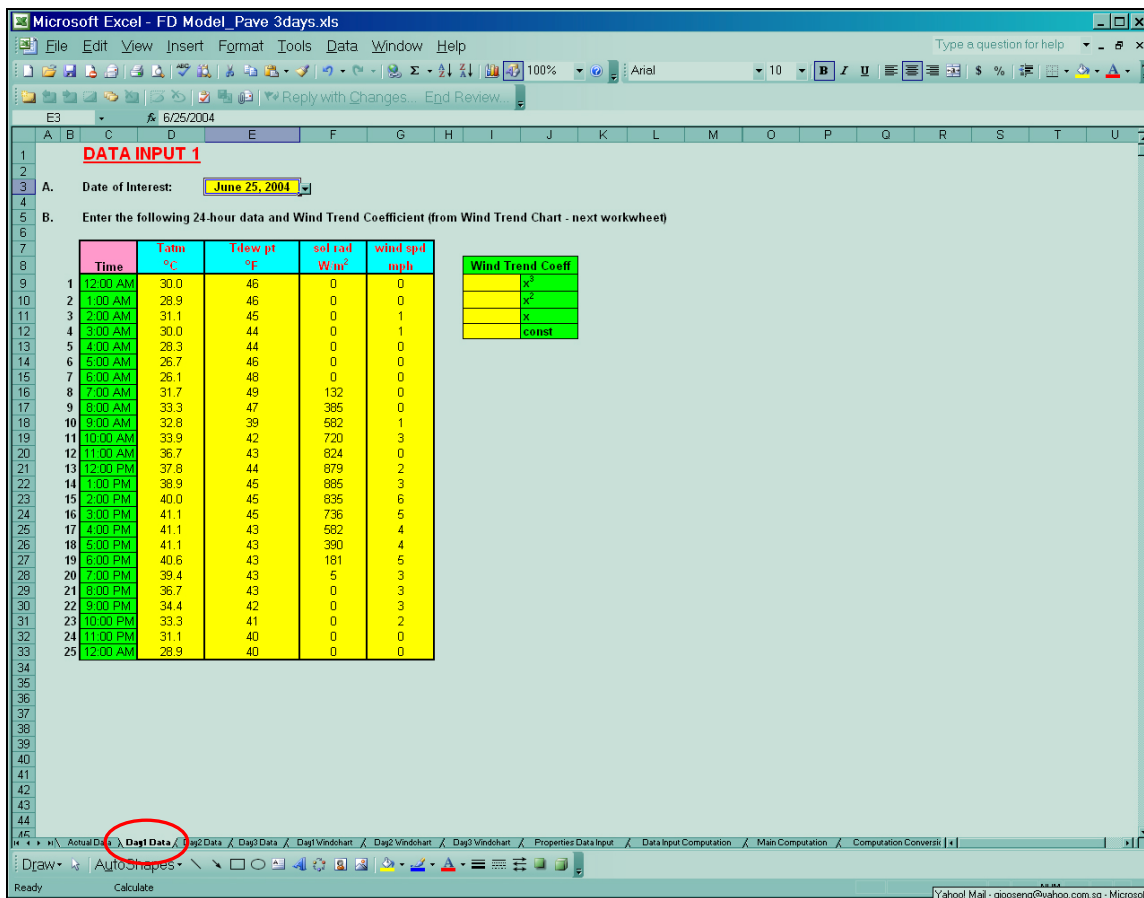
Select the Date of Interest from the drop-down list, followed by the input of the

hourly data for the atmospheric temperature (Tatm in °C), dew point temperature (Tdew pt in

^{o}F), solar radiation (`sol rad` in W/m^2) and wind speed (`wind spd` in mph) for that day.

These data are readily available at http://ag.arizona.edu/azmet/azdata.htm.

Step 2: Go to worksheet: `Day1 Windchart`
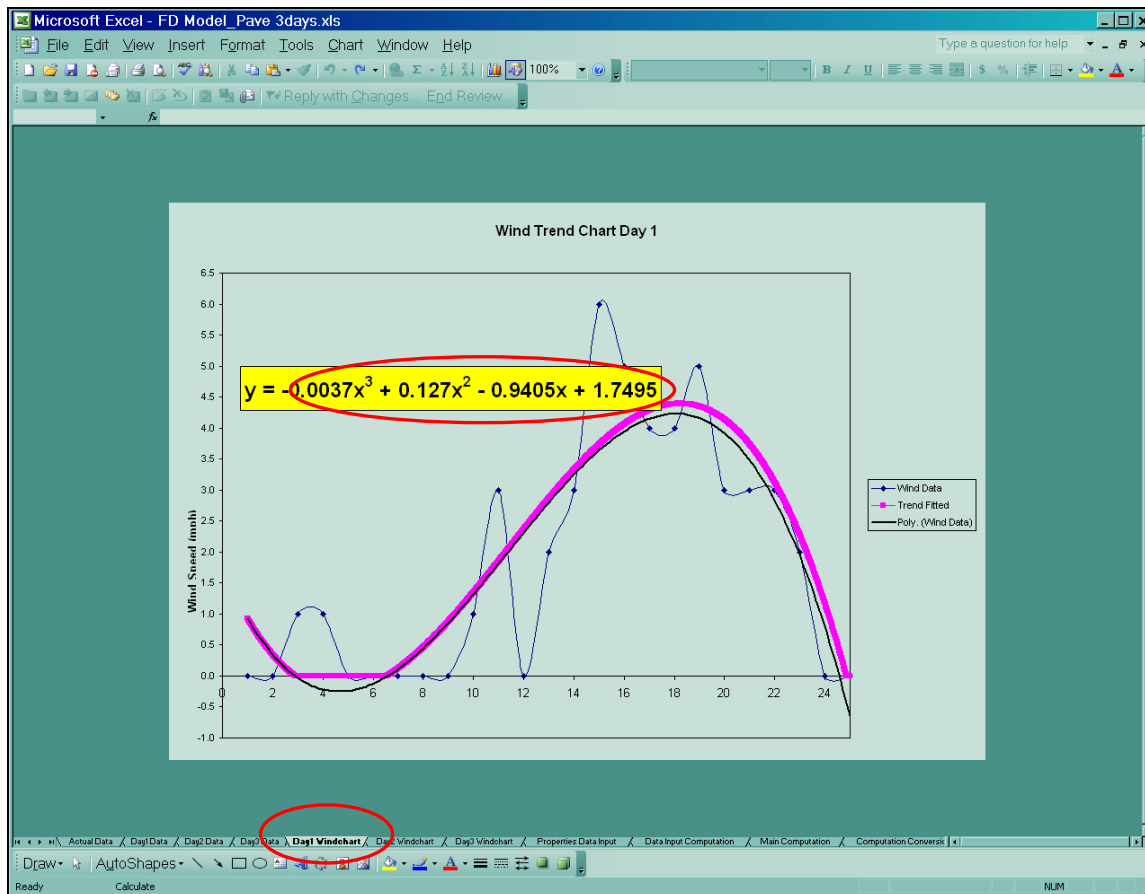
Note the coefficients and input them back to the worksheet: `Day1 Data`
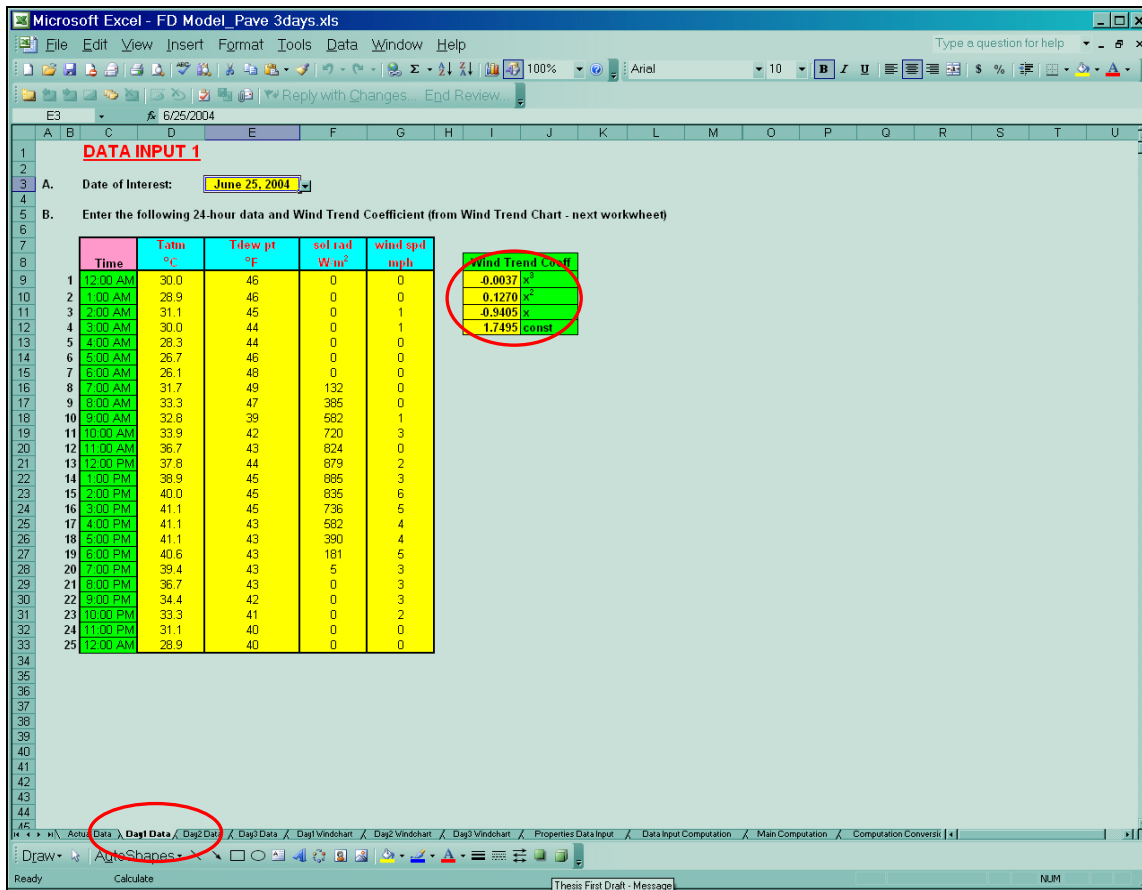
Step 3: Repeat Steps 1 and 2 for worksheets: `Day2 Data` & `Day3 Data`.

Step 4: Once completed, proceed to worksheet: `Properties Data Input`
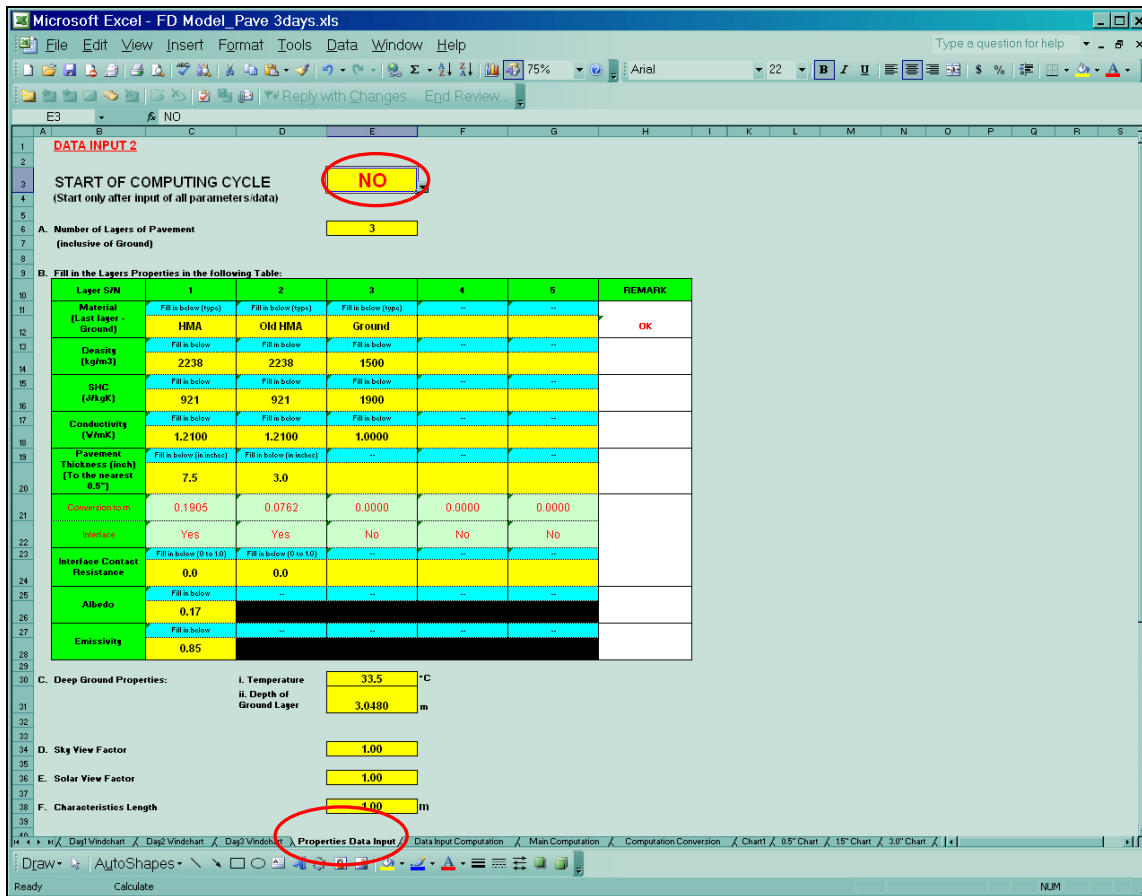
Ensure that the START OF COMPUTING CYCLE is set to NO.

Press function key, F9 to reset the program.

Step 5: Input the pavement material properties and boundary conditions within the worksheet

(i.e. input data in yellow cells of the worksheet). Ensure all data are correctly placed and entered.

Step 6: Select the START OF COMPUTING CYCLE to YES

Press function key, F9 to begin the iterative cycles of the program. Note the iteration,

which should stop after 10 cycles.
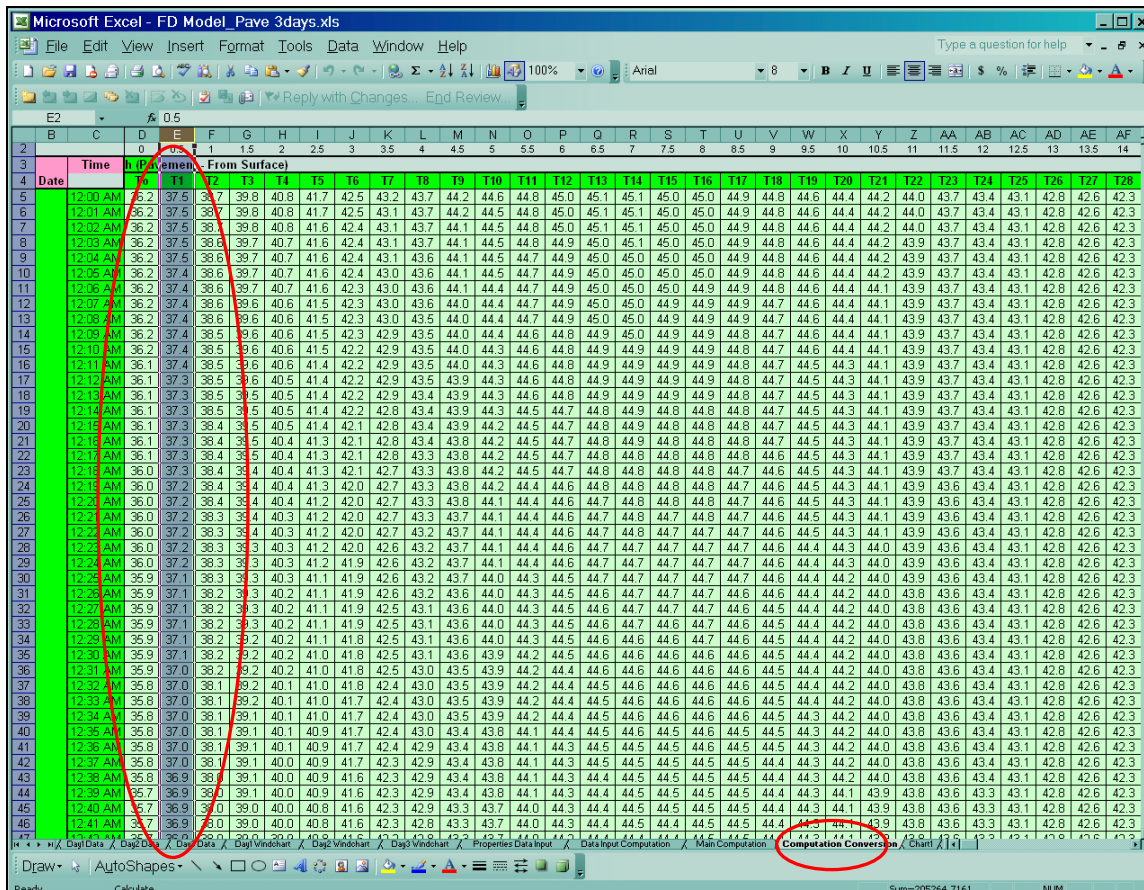
Step 7: Go to worksheet: `Computation Conversion`

Each column in this worksheet shows the respective temperatures at different depth within the pavement. For this research, the column representing the 0.5" depth is the main focus as the interest lies in the near surface pavement temperatures.

Step 8: Select both Columns C and E from the worksheet: `Computation Conversion` and copy the data onto a new file. Remember to paste the data as `Value` in the `Paste Special…` under the `Edit` tab in the tool bar of the `Windows`.
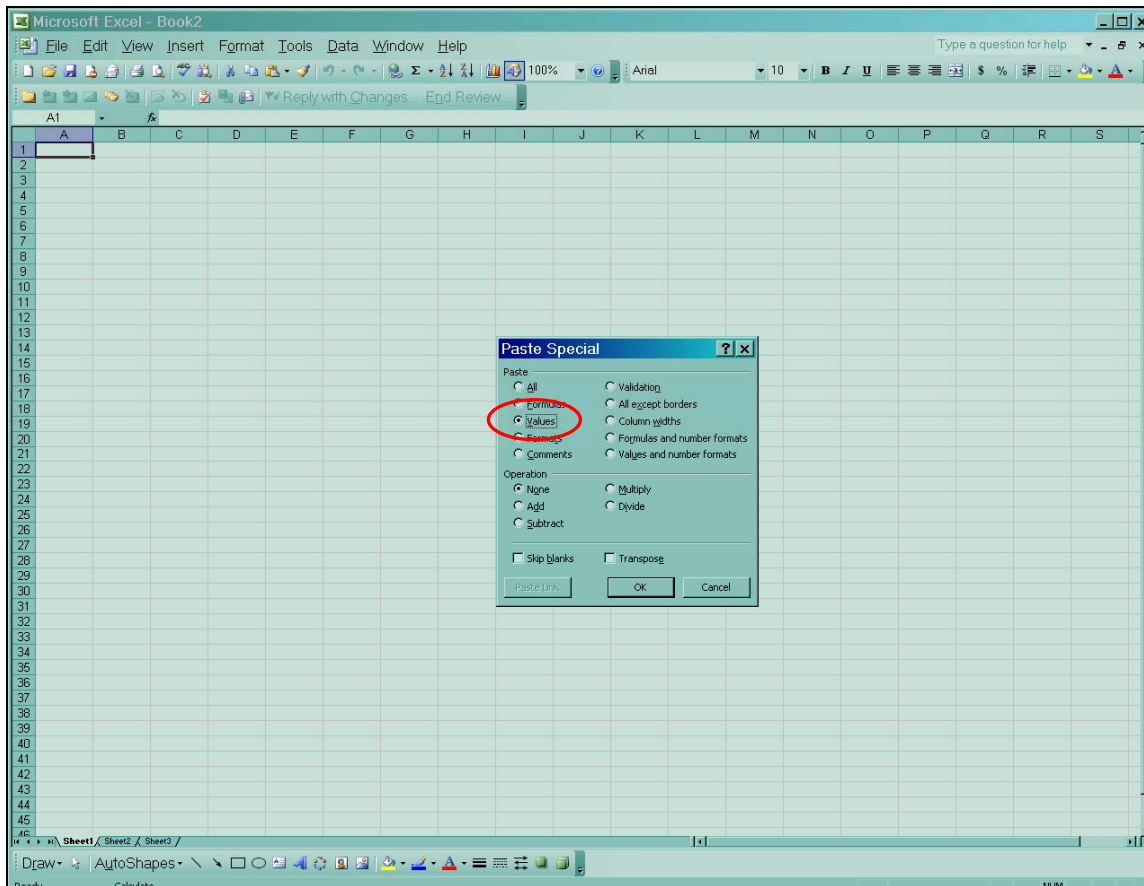
Step 9: Plot the 3-day diurnal cycles of the near surface pavement temperatures under the new spreadsheet.

Step 10:   Save the new file.